SIMULATION STUDIES ON MICRODROPLET GENERATION AND TRAPPING IN T-JUNCTION DEVICES

Thesis

Submitted in partial fulfilment of the requirements for the degree of

DOCTOR OF PHILOSOPHY

IN

PHYSICS

by

SRIPADARAJA.K.

(135031PH13P04)

DEPARTMENT OF PHYSICS

NATIONAL INSTITUTE OF TECHNOLOGY KARNATAKA,

SURATHKAL, MANGALORE-575025

JULY 2022

SIMULATION STUDIES ON MICRODROPLET GENERATION AND TRAPPING IN T-JUNCTION DEVICES

Thesis

submitted in partial fulfilment of the requirements for the degree of

DOCTOR OF PHILOSOPHY

IN

PHYSICS

by

SRIPADARAJA.K.

(135031PH13P04)

Under the Guidance of

Prof. M.N. Satyanarayan

&

Prof. G. Umesh

DEPARTMENT OF PHYSICS

NATIONAL INSTITUTE OF TECHNOLOGY KARNATAKA,

SURATHKAL, MANGALORE-575025

JULY 2022

DECLARATION

By the Ph. D Research Scholar

I hereby *declare* that the Research Thesis entitled **"Simulation studies on microdroplet generation and trapping in T-Junction devices"** which is which is being submitted to the **National Institute of Technology Karnataka, Surathkal** in partial fulfilment of the requirements for the award of the Degree of **Doctor of Philosophy** in **Physics** is a *bonafide report of the research work carried out by me*. The material contained in this Research Thesis has not been submitted to any University or Institution for the award of any degree.

Sripadaraja.K
Reg No. 135031PH13P04
Department of Physics

Place: NITK, Surathkal
Dt: 22 July 2022

CERTIFICATE

This is to certify that the Research Thesis entitled "**Simulation Studies on microdroplet generation and trapping in T-Junction devices**" submitted by Sripadaraja. K (Reg No. 135031PH13P04) as the record of the research work carried out by him, is accepted as the Research Thesis submission in partial fulfilment of the requirements for the award of the degree of **Doctor of Philosophy**.

Research Guide(s)

Prof. M.N. Satyanarayan Prof. G. Umesh

Chairman – DRPC

I DEDICATE THIS TO

ALL MY

TEACHERS

AND

MY DEAR WIFE

SRIDEVI. K

ACKNOWLEDGEMENT

It has been a great learning experience pursuing research at National Institute of Technology, Karnataka (NITK) Surathkal. I thank the institute for all the support provided. The support and help provided by all the individuals who helped me to achieve what I have up to this point are deeply appreciated. Few of them requires special mention here.

I convey my gratitude to my research supervisors Prof. M.N. Satyanarayan and Prof. G. Umesh for their guidance, encouragement, and support. Throughout the doctoral work, the learning experience that I gained through their sound advice at every stage helped me to handle failures. Their continued support throughout the course of my research work has been made my thesis appear in the present form.

I convey my gratitude to Mr. J. Guru Dutt, Director, SriDutt Technologies Pvt Ltd, Bangalore who encouraged me to take-up research activity and provided all the necessary support required.

I am greatly thankful to RPAC members, Prof. B.D. Prasanna, Associate Professor and Head of Dept, Dept of Chemical Engineering and Prof. Ajith.K.M, Associate Professor and Head of Dept, Dept of Physics for their continued guidance during all my seminars which helped to shape my research work.

I would like to express my special thanks to my friends and colleagues Dr. Nimith. K.M, Mr. Achyuta. K, Dr. Makesh. M and Dr. Sourie Ranjana who helped and supported me in many ways.

Lastly, I earnestly yearn to thank my family, my parents Mr. Krishna Murthy Rao. K. V and Mrs. Shashikala. K, my dear wife Sridevi. K, our daughters Saanvi and Sarayu, and lastly my sisters Shilpa. K and Sheela. K for their love and sacrifice that motivated me to achieve this goal.

Sripadaraja. K

ABSTRACT

In this thesis we present results of simulation studies on the generation of microdroplets due to the flow of two immiscible liquids in microfluidic T-junction devices and their trapping in Microwells built into the devices. We have studied devices, of the Slip-Chip type, having a single T-junction and double T-junction. We have used ANSYS Fluent Solver, which employs the Volume of Fluid (VOF) method, for the numerical simulations. The generation of water droplets in mineral oil has been studied for the case of steady flow of the two liquids as well as for the case of pulsed flow of water, the dispersed phase liquid. Droplet generation has been investigated in two different regimes - viz., squeezing and squeezing to dripping transition regime. The effect of fluid flow rates and surfactant concentration (Span 80 in mineral oil, the continuous phase liquid) on the droplet generation has been investigated. The scaling of the droplet length with the flow rate of either of the two liquids has been shown to be similar to results reported in the literature. It is seen that addition of a surfactant leads to formation of smaller droplets and an increase in the frequency of droplet generation. To understand droplet generation, we have plotted the pressure, within the two liquids, close to the T-junction as a function of time. These plots have given us a good insight into the process of droplet generation. Droplets generation by pulsed flow of water, keeping the flowrate of oil constant, revealed very interesting behaviour. In the absence of a surfactant, only single droplets are generated during each pulse duration. However, when the surfactant concentration exceeds a certain value, a pair of smaller droplets are generated for each pulse. The generation of droplet pairs happens at a higher surfactant concentration if the width of the side-channel, carrying the dispersed phase liquid, is reduced. Further, if the pulse width is reduced, only one, relatively small, droplet is generated per pulse, irrespective of the surfactant concentration. In many applications, merging of two (or more) droplets is required. To explore the merging of two droplets, we studied droplet generation in a double T-junction device. Depending on the geometry of the device, it is seen that the generated droplets either merge at the junction or travel further without merging. Merging of the droplets happens for relatively smaller width of the side-channel. With gradual increase in capillary number, droplets are generated in alternate regime. Our studies on droplet trapping in microwells indicate

that inclusion of additional structures, such as a shallow circular pit or a pinhole, in the main channel of the device, enhances the chance of trapping. It is seen that the droplets traveling faster than a critical trapping velocity (U_{cr}) do not get trapped in the microwell. The addition of a surfactant is seen to lead to a significant reduction in U_{cr} for droplet trapping. The trapping of droplets traveling at velocities close to U_{cr} depends strongly on the alignment of the microwell and the pit or pinhole in the two plates of the Slip-Chip device. Dependence of droplet trapping on the dimensions of the pit or pinhole, the liquid flowrates and the surfactant concentration has been investigated. It is seen that droplet trapping does not happen if the surfactant concentration exceeds a certain value depending on the flowrates of the two liquids. The investigations reported in this thesis clearly indicate that extensive numerical simulations are required for arriving at an optimum design for a Microfluidic device for any application.

Keywords: Droplet Microfluidics, Two-phase flow, Volume of Fluid Method (VOF), Droplet Trapping.

Table of Contents

CHAPTER 1 **1**

INTRODUCTION **1**
1.1 Droplet Microfluidics 1
1.2 Literature Review 2
1.3 Droplet Microfluidic Devices. 12
1.4 Dimensionless parameters 15
1.5 Surface Tension and Interfacial tension 18
1.6 Surface Wetting 19
1.7 Surfactant and its influence on droplets. 20
1.8 Scope of the thesis 21
1.9 Objectives of the thesis 23
2.10 Organisation of Thesis 23

CHAPTER 2 **26**

NUMERICAL SIMULATION STRATEGY AND TOOLS EMPLOYED **26**
2.1 Introduction 26
2.2 Fluid equations for simulations 28
2.3 Discretization Scheme for Computation 30
2.4. Model for Simulation using VOF solver 32
2.5 Simulation Parameters for the liquids and the devices 33
2.6 Parameters for Single T-junction device 33
2.7 Parameters for Double T-junction device 36
2.8 Parameters for Droplet Trapping 37
2.9 Simulation Settings using ANSYS Software 38

CHAPTER 3 **41**

MICRODROPLET GENERATION AND TRAPPING BY STEADY FLOW OF TWO IMMISCIBLE LIQUIDS IN T-JUNCTION MICROFLUIDIC DEVICES. **41**
3.1 Introduction 41
3.2. Effect of Surfactant on Droplet Generation: 45
3.3 Droplet Trapping 52
3.4. Conclusion 56

CHAPTER 4 **58**

MICRODROPLET GENERATION AND TRAPPING BY PULSED FLOW OF DISPERSED PHASE LIQUID IN T-JUNCTION MICROFLUIDIC DEVICES. **58**
4.1. Introduction 58

4.2. Droplet generation – Steady flow rate of the two liquids 60
4.3 Droplet generation – Pulsed flow of dispersed phase liquid 62
4.4 Droplet Trapping 70
4.5 Conclusion 71

CHAPTER 5 **73**

MICRODROPLET GENERATION IN DOUBLE T-JUNCTION MICROFLUIDIC DEVICES. **73**
5.1 Introduction 73
5.2 Validation of simulation results 76
5.3 Effect of increase in width of side-channel on droplet generation. 77
5.4 Effect of increase in width of the main channel on droplet generation. 82
5.5 Effect of Surfactant on Alternate droplet formation. 85
5.6 Conclusion 89

CHAPTER 6 **91**

SUMMARY AND CONCLUSIONS **91**
6.1 Summary 91
6.2 Conclusions 95
6.3 Scope and Future work 97

REFERENCES **98**

PUBLICATIONS **107**

List of Figures

Fig 1.1 Schematic of various Crossflow devices a) with $\theta = 90^o$, called T-junction, b) device with $0^o < \theta < 90^o$. c) device with $0^o < \theta < 180^o$ called Y-junction, d) K-junction. e) V-junction, f) Head-on geometry, g) Two parallel T-junction that produces droplet pairs. h) Double T-junction generating droplet pairs. Image Source : (Zhu and Wang 2017) 13

Fig 1.2 Schematic representation of Flow focusing device. Image Source : (Anna and Mayer 2006) 14

Fig 1.3 Schematic representation of Co-flow device. Image Source: (Cramer et al. 2004) 15

Fig 1.4: Simplified cartoon of molecules near the interface of a liquid with a gas. The liquid-air interface is shown as a red line. Image Source : ("Fundamentals of Capillarity" 2012) 18

Fig 1.5 Schematic representation of various wetting regimes. a) Total Wetting. b) Partial Wetting and c) Non-wetting. (Blue Colour: water and Brown Colour: Solid surface). γ_{LG}, γ_{SG}, and γ_{SL} are the surface tension between liquid-gas, solid-gas, and solid-liquid. Image Source : ("Minimal Energy and Stability Rubrics" 2012) 19

Fig 1.6 a) Dispersion of surfactant molecules in bulk liquid, b) distribution of surfactant molecules at the interface across a droplet of oil in water (the oil drop is shown in blue colour), c) Arrangements of surfactant molecules below and above critical micelle concentration (CMC). The display for the case above CMC shows one micelle. Image Source: a & b) Wikipedia, and c) (Steven Abbott 2018) 21

Fig 2.1 a) Small part of a 2-dimensional Cartesian grid, b) The shape and position of the two-fluid interface in each cell of the domain. The number in each cell indicates the volume fraction of the dispersed phase fluid shown in blue color. The white color represents the continuous phase fluid. Image Source (ANSYS FLUENT Technical reference document) 30

Fig 2.2: Schematic of the microfluidic device showing (a) the broadside view and (b) the top view of the device with the micro-well and the Pit. Schematic of a second device showing (c) the broadside view and (d) the top view of the device with the micro-well and the Pinhole 34

Fig 2.3: a) Schematic view of T-junction device. (b) The waveform for pulsed flow rate 34

Fig 2.4: Schematic view of microfluidic double T-junction device showing a) the side view of the device, and b) the top view of the device. c) Droplet generation mechanism in Double T-junction device. 36

Fig 3.1: Location of pressure measuring points P_d and P_c in dispersed phase and continuous phase liquids respectively. 46

Fig 3.2: Droplet generation for different flow rate of continuous phase liquid without the surfactant at fixed value of Qd = 0.2µl/min. a) Qc= 0.25µL/min. b) Qc= 0.5µL/min c) Q_c = 1µL/min, (d-f) Pressure versus time at point P_c for Q_c values as in a-c respectively.....46

Fig 3.3: Droplet generation sequence and pressure versus time plots for various surfactant concentration (weight %) at a fixed value of Q_d at 0.2µl/min and changing Q_c a) Q_c = 1µL/min. b) Q_c = 0.5µL/min c) Q_c = 0.25µL/min, for a total flow time of 0.5Sec.; Pressure versus time at point P_c and P_d , respectively, for (d,e) Q_c = 1µL/min; (f,g) Q_c = 0.5µL/min and (h,i) Q_c = 0.25µL/min. 47

Fig 3.4: a) Droplet length versus flow rate of oil (for fixed Q_d = 0.2µl/min). b) Dimensionless droplet length (L/w) versus flow rate ratio. c) Surfactant concentration profile (in moles/litre) at the front pole of the droplet (oil is shown in red and water in blue colour). d-f) interface of the droplet for concentration 0.2%, 1% and 4% respectively. 50

Fig 3.5: Influence of surfactant at various concentration on velocity vector profile in the dispersed phase liquid during the droplet formation process at a fixed value of Q_d at 0.2µl/min and Q_c = 0.25µL/min. 51

Fig 3.6: Top view of the microchannel geometry with the micro-well shown as a full circle and the Pit with the channel. The different extents of alignment of the micro-well and the Pit are, a) 100% alignment b) 75% Alignment c) 50% alignment d) 25% alignment and e) total misalignment; f) Top view of the droplet in the channel; g) Broadside view of the droplet in the channel. 53

Fig 3.7: a-e) Shape of the droplet of different lengths just before entering the micro-well, for different Pit-Micro-well alignments. f-h) Top View of droplet motion (length 200µm) in microchannel before entering the Micro-well, f) 100% alignment, g) 75% Alignment h) 50% alignment. (i-m) The shape of the droplet (length = 100µm) just before entering the micro-well, for different Pit-Micro-well alignments. n-p) Top View of droplet motion (length 100µm) in microchannel before entering the micro-well, n) 100% alignment o) 50% alignment p) 0% alignment.....54

Fig 3.8: Flowrate versus trapping for various Pit-well alignment (%). a) for droplet length 200µm and b) for droplet length 100µm.....57

Fig 4.1: a) Dimensionless length of the droplets (L/w) plotted as a function of the ratio of flow rates (Q_d/Q_c) of fluids a) when Q_d is fixed and Q_c is varied, and b) when Qc is fixed and Q_d is varied.....62

Fig 4.2: Generation of droplets for various flow rates of Q_c and Q_d for both D1 and D2. a) Droplet length versus flow rate of oil at a fixed flow rate of water, b) Dimensionless length of the droplets (L/w) plotted as a function of the ratio of flow rates of fluids, c) Droplet length versus flow rate of water at a fixed flow rate of oil, d) Dimensionless length of the droplets (L/w) plotted as a function of the ratio of flow rates of fluids, ...62

Fig 4.3: Sequence of droplet generation with and without surfactant for D1; Q_c = 0.2µL/Sec and Q_d = 0.1µL/Sec. a-e) ΔT_1 = 6.5msec and ΔT_2 = 6.5msec, a) 0%, b) 0.2%, c) 1% d) 2%, e) 4%, and (f-j) ΔT_1 = 3.25msec and ΔT_2 = 6.5msec, f) 0%, g) 0.2%, h) 1% i) 2%, j) 4%.....64

Fig 4.4: Pressure Vs time at point P_d for D1 with and without surfactant. a,b) $\Delta T_1 = \Delta T_2$ = 6.5msec, c,d) ΔT_1 = 6.5msec and ΔT_2 = 13 msec, e,f) ΔT_1 = 3.25msec and ΔT_2 = 6.5msec, g,h) ΔT_1 = 3.25msec and ΔT_2 = 13msec. Operating flow rates are Q_d = 0.1µL/s (ON State), 0µL/s(OFF State) and Q_c = 0.2µL/s 65

Fig 4.5: Sequence of droplet generation with and without surfactant for D2; Q_c = 0.2µL/Sec and Q_d = 0.1µL/Sec. a-e) ΔT_1 = 6.5msec and ΔT_2 = 6.5msec, a) 0%, b) 0.2%, c) 1% d) 2%, e) 4%, and (f-j) ΔT_1 = 3.25msec and ΔT_2 = 6.5msec, f) 0%, g) 0.2%, h) 1% i) 2%, j) 4%.....67

Fig 4.6: Pressure Vs time at point P_d for D2 with and without surfactant. a,b) $\Delta T_1 = \Delta T_2$ = 6.5msec, c,d) ΔT_1 = 6.5msec and ΔT_2 = 13 msec, e,f) ΔT_1 = 3.25msec and ΔT_2 = 6.5msec, g,h) ΔT_1 = 3.25msec and ΔT_2 = 13msec. Operating flow rates are Q_d = 0.1µL/s(ON State), 0µL/s(OFF State) and Q_c = 0.2µL/s 69

Fig 5.1: Droplet generation in single and double T-junction device. (a) Droplet length versus flowrate of oil at a fixed flowrate of water (0.2 µl/min) in single T-junction device: Comparative study with the experimental results reported by Bashir et al 2014 at 4% surfactant concentration, (b) Double T-junction device, experimental results from the work of Zheng et al. 2004a, (c) Computational results of the present study. (Q = W_f = water fraction). Λ = 1 and $\lambda_d = \lambda_c$ = 16 mPa.s. 76

Fig 5.2: Effects of increase in the width of side-channel in single T-junction device a-f) Droplet generation showing the transition from dripping to the jetting regime ("x" represents the droplet length), g) Droplet length and frequency in single T-junction device, h) Pressure at point P_c and P_d in a single T-junction device.....78

Fig 5.3: a) Capillary number in both single and double T-junction devices, b) Pressure at point P_1, P_2, and P_c in double T-junction device. 79

Fig 5.4: a-f) Droplet generation in double T-junction device for change in width of SC2 from 100µm to 50µm while SC1 is at 100µm. g) Representation of double T-junction device into two sections and deformation of dispersed phase liquid during alternate droplet generation. h-i) Sequence of droplet formation – Transition from merging to the alternate regime,.....80

Fig 5.5: a-c) Pressure difference (ΔP) Vs time at point P_1 and P_2 for SC2 = 90µm, 70µm, 50µm, respectively. 81

Fig 5.6: Effects of increase in the width of the main channel in single T-junction device a-f) The sequence of droplet generation, ("x" represents the droplet length) g) Droplet length and frequency, h) Pressure at point P_c and P_d. 83

Fig 5.7: a) Capillary No. in both single and double T-junction device, b) Pressure at point P_d and P_c in double T-junction device.....83

Fig 5.8: a-f) Droplet generation in double T-junction device for change in the width of the main channel between 50 µm to 100 µm. g) The sequence of droplet formation in the alternate regime, for the width of the main channel at 70 µm, h) ΔP Vs time at points P_1 and P_2 showing the transition from merging regime to the alternate regime (width of MC = 70 µm). 84

Fig 5.9: a) Droplet generation in merging regime. b) Sequence of Droplet generation in merging regime c) Pressure at the dispersed phase liquid inlet Vs Time for surfactant concentration.....86

Fig 5.10: Pressure Vs time for various surfactant concentration, a) Difference of pressure ($\Delta P=P_1-P_2$) Vs time for surfactant concentration of 0.2%, 0.4% and 0.8%, b-e) for 1%, 2%, 3%, 4% of surfactant concentration respectively. 88

List of Tables

Table 1.1 : Different regimes of droplet generation.....17

Table 2.1: Physical parameters of the liquids used in the simulations.....33

Table 2.2: Dimensions of microchannel investigated with a steady flow of two liquids (see Fig 2.3a) 34

Table 2.3: Steady flow rates of two liquids used in the simulation (see Fig 2.3a).....35

Table 2.4: Flow rates of the two liquids used in the simulations (see Fig 2.3a).....35

Table 2.5: Dimensions of T-junction devices investigated with the pulsed flow of dispersed phase liquid (see Fig 2.3a) 35

Table 2.6: Pulsed parameters used in the simulations (see Fig 2.3b) 35

Table 2.7: Steady flow rates of two liquids used in the simulation (see Fig 2.4).....36

Table 2.8: Dimensions of double T-junction device investigated with a steady flow of both liquids (see Fig 2.4). 37

Table 2.9: Diameter of droplet and Pit chosen for droplet trapping (See Fig 2.2a and 2.2b).....37

Table 2.10: Length of the droplet and pinhole chosen for droplet trapping (See Fig 2.2c and 2.2d) 38

Table 3.1: Droplet release time based on the flow rate of oil (Q_c) at fixed Qd = 0.2µL/min.....48

Table 3.2: Effect of surfactant concentration on droplet length & maximum pressure at points P_d and P_c.....49

Table 4.1: Trapping status of the droplet (length 80µm) based on the flow rate of oil (Depth of pinhole is 40µm) 71

NOMENCLATURE

Abbreviations

ADF	Alternate Droplet Formation
CMC	Critical Micelle Concentration
DoD	Droplet on Demand
FC	Fluorocarbon
HLB	Hydrophilic-Lipophilic Balance
LBM	Lattice Boltzmann Method
PDMS	Polydimethylsiloxane
PMMA	Poly (methyl methacrylate)
PRESTO	Pressure Staggering Option
SDS	Sodium dodecyl sulfate
SLIC	Simple Line Interface Calculation
VOF	Volume of Fluid
MC	Width of Main Channel in double T-junction
SC1 and SC2	Width of two side channels in double T-junction respectively

SYMBOLS AND UNITS

A	Area
B_o	Bond Number
C_a	capillary Number
θ	contact angle
cSt	centistokes
Kg/m^3	Kilogram/cubic meters
ρ_{avg}	Density (averaged) of the two immiscible liquids
ρ_o	Density of oil
ρ_w	Density of water
D_c	Diffusion Coefficient
$Ergs/cm^2$	Energy per unit area
V_o	Fractional volume of oil
V_w	Fractional volume of water
Q_c	Flowrate of Continuous phase liquid
Q_d	Flowrate of Dispersed phase liquid
Q (Q_d/Q_c)	Flowrate Ratio
$\lvert\vec{n}\rvert$	Gradient of fractional volume
H	Height
γ	Interfacial Tension
$\overrightarrow{F'}$	Interfacial tension force
KPa	Kilopascal
L	Length
msec	millisecond
mPa.s	milliPascal Second
mN/m	Milli Newton per meter
μm	micrometre
μl/hr	Microliter per hour
μl/min	Microliter per minute
μl/sec	Microliter per second

$\hat{n}$	Normal Component to the droplet surface
O/W	Oil droplets in water
O/W/O	Oil-in-water-in-oil
P	Pressure
P_1 & P_2	Pressure at two different points inside channel
P_c	Pressure at point in the main channel
P_d	Pressure at point in the side channel
Pa	Pascal
Pa.s	Pascal Second
R_e	Reynold's number
R_n	Radius of curvature of droplet
Λ	ratios of widths of side channel to main channel
E	Surface energy
γ_{LG},	Surface tension between liquid and gas
γ_{SG}	Surface tension between solid and gas
γ_{SL}	Surface tension between solid and liquid
α	Surfactant Concentration
$\hat{n}_w$	Unit vectors normal to the wall
$\hat{m}_w$	Unit vectors tangential to the wall
$\overrightarrow{U^i}$	Velocity of the liquid
μ_d	Viscosity of dispersed phase liquid
μ_c	Viscosity of continuous phase liquid
λ	Viscosity Ratio (μ_d/μ_c)
η_{avg}	Viscosity (averaged) of the two immiscible liquids
W	Width
W_e	Weber Number
W/O	Water droplets in Oil
W/O/W	Water-in-oil-in-water
U_c	Velocity of Continuous phase liquid
U_{cr}	Critical velocity of droplet
wt/wt %	weight/weight percentage

CHAPTER 1

INTRODUCTION

1.1 Droplet Microfluidics

A microdroplet is a liquid drop of volume less than 1 nano-litre, which corresponds to a spherical droplet of radius 100μm. Thus, such droplets are much smaller than a typical raindrop or a drop falling from a water tap. The structure and dynamics of such small droplets are dominated by fluid pressure, viscosity, and surface tension, and the inertial forces, such as gravitational force, may be neglected. In microfluidics, processes such like evaporation, interfacial tension and adsorption at the surfaces become important (Rowan et al. 1995, 1997). Producing and handling large numbers of microdroplets for specific applications has been a major challenge (Solvas and deMello 2011). Generation of microdroplets in a controlled manner has been achieved by either spraying a liquid through a fine nozzle into a gaseous atmosphere or by the flow of one liquid into another immiscible liquid. The generation of droplets of a specific volume, which is termed mono-disperse droplets, is a major challenge (Sohrabi et al. 2020). These techniques are implemented in devices called *microfluidic devices*, which consist of channels of micrometre dimensions for the liquids to flow. Microfluidic devices of various geometries have been designed and studied over the last two decades. The type of device depends on the exact mechanism selected for generating the droplets. Collecting the generated droplets in the desired manner is an additional challenge. Some major advantages of microfluidics are:

- The use of very small quantities of liquids leads to the highly efficient use of expensive liquids (Stone et al. 2004).
- Parallel chemical/physical analysis of a very large number of droplets. This has led to the development of micro-chips for chemical/biological studies.
- Synthesis of exotic new materials using micro-droplets.
- Synthesis of emulsions and foams with novel properties.
- Single bio-cell analysis and similar applications (Clausell-Tormos et al. 2008).

In this thesis, microdroplet generation by a simultaneous flow of two immiscible liquids has been examined. We have specifically studied T-junction devices for droplet generation and have carried out simulation studies to arrive at optimum design parameters for the T-junction microfluidic devices.

1.2 Literature Review

A very simple technique to generate microdroplets on large scale was demonstrated using the ultra-sonication method by Haynes et al. (1988). These droplets carried drug particles and were shown to function as excellent anaesthetics. Using chemical manipulation techniques, liquid and gel-based microdroplets were generated for cancer diagnosis and treatment, clinical microbiology, and food safety (Weaver et al. 1991). Stabilisation of microdroplets of silicone oil in water was demonstrated by adding and polymerising vinyl monomer to prepare skin care compositions (Kopolow et al. 1992). Microfluidizers were also used to generate droplets in nanolitre volumes using high-pressure pumps (Tomas et al. 1994; Dalgleish et al. 1997). It was then found that a larger scope and market potential in producing microdroplets and hence, several optical studies such as the determination of refractive index and dispersion (Huckaby and Ray 1995), Raman scattering (Pasternack et al. 1996), and photochemical reactions (Ray and Bhanti 1997). Rothschild and Forte (1995) developed a silicon-based microchannel using the microfabrication process that can be used to generate microdroplets using two immiscible liquids. The flow of the liquids in the microchannel is dominated by viscosity which makes the flow laminar (Brody et al. 1996). Microfluidic devices made of Polydimethylsiloxane (PDMS) were used for generating water droplets of picolitre volume (Hosokawa et al. 1999b). They studied the efficiency of merging microdroplets by fluorescence imaging (Hosokawa et al. 1999a, 2000). Triolein microdroplets were produced in microfluidic devices with a trapezoidal cross-section (Kawakatsu et al. 2000).

There have been several investigations over two decades to understand the dynamics involved in droplet formation process for various applications. Effect of flowrates, viscosity ratio, channel dimensions on droplet size are some of the studies reported in

the past. The length of the water droplet was seen to decrease with the increase in the flow rate of oil in a device made of PMMA (Nisisako et al. 2002). The same device failed to produce oil droplets in water as PMMA (Polymethyl methacrylate) is hydrophobic and oil wets its surface. Droplets of identical size were produced in a microchannel device by He et al. (2004). Droplets of 1,6 Hexanediol diacrylate (a monomer) were generated in Polyvinyl alcohol (PVA) aqueous solution in different microfluidic devices such as T-junction and two Y-junctions in tandem made of quartz-glass (Nisisako et al. 2004). In the case of a T-junction device, monodisperse droplets could be generated when the flow rate of continuous phase liquid (Q_c) is more than five times the flow rate of dispersed phase liquid (Q_d). However, for a fixed Q_c, as Q_d increases, droplets of different sizes were generated and beyond a certain value of Q_d droplet generation did not occur. They also demonstrated the merging of two droplets using Y-junction devices. A mathematical model was developed to predict the droplet generation in the squeezing, transition, and dripping regime (Xu et al. 2008). The study also showed that droplets generated in the squeezing and dripping regimes are dominated by pressure and interfacial tension respectively. This was also observed in the simulation studies using the phase-field model (Menech et al. 2008) and the Lattice Boltzmann method (LBM) (Gupta et al. 2009; Liu and Zhang 2009).

Train of droplets are generated with the steady flow of the two liquids. However, many applications require droplets of constant volume to be generated at a prescribed rate, which ensures optimum use of liquids, thereby reducing the costs. Such techniques are called Droplet on Demand (DoD). One way of achieving DoD is by pulsing the flow of dispersed phase liquid, while the continuous phase liquid flow rate is kept constant. In DoD devices, the flow of the dispersed phase liquid is controlled by using commercially available microvalves at the inlet of the side channel through which it flows into the device. In the first DoD device, demonstrated by Lin et al in 2008, the generation of droplets of different volumes was achieved by controlling the inlet pressure of the dispersed phase liquid and the duration for which the valve was kept open (Lin and Su 2008). In such devices, both pneumatic and electromagnetic microvalves were used (Churski et al. 2010). Piezoelectric microvalves have been used to produce droplets of nanolitre to picolitre volumes at frequencies ranging from 20Hz to 400 Hz (Jakiela et

al. 2014). Simulation studies have been carried out on a microfluidic device with multiple T-junctions to optimize their performance (Tangen et al. 2015). These studies have shown that the droplet volume and the generation frequency may be controlled by the proper choice of the pulse waveform to operate the microvalves. The microvalves are usually operated in the pulsed mode by adopting standard pulse waveforms such as rectangular, triangular, and sinusoidal functions of time. In a recent study, it has been shown that the use of rectangular voltage waveforms for operating the microvalves leads to better control of the droplet volume (Qian et al. 2019). Hence, we adopt rectangular waveforms in one of our studies.

Swapping the channel inlets of a cross-junction device, it can also be used as a double T-junction device. The mechanism of alternate droplet generation happens as follows: when the dispersed phase liquid from one of the side channels enters the main channel, it blocks the continuous phase liquid as it grows at the junction. Due to this, there is an increase in pressure upstream. Dispersed phase liquid is passed through the two side channels whereas the continuous phase liquid is passed through the main channel. The droplet generation in double T-junction transits from merging to an alternate regime with an increase in capillary number. The first study on a double T-junction device was carried out by Zheng et al. (2004) to produce alternate droplets in different regimes namely “merging regime” (the two droplets merge at the junction itself), “alternating regime” (the two droplets are generated one after the other and move on without merging) and “alternate-jetting regime”, which is similar to alternating regime except that the droplets are generated well away from the T junctions for capillary number ranging from 0.001 to 0.05. A modified geometry was proposed to demonstrate droplet generation in various regimes for synthesising CdS nanoparticles (Hung et al. 2006). In this device, droplets of different volumes were produced from each side channel by controlling the flow rate of the dispersed phase liquid independently in the two side channels. Picolitre aqueous droplets were generated in a double T-junction device in an alternate regime (Fidalgo et al. 2007). In this device, a portion of the microchannel wall was made hydrophilic. Pairs of droplets generated were merged when they reach the hydrophilic region in the microchannel and finally get trapped. A device with two T-junctions in tandem was developed to synthesis poly (lactide-*co*-glycolide) commonly

known as PLGA (Hung et al. 2010). In this device silicone oil was use as continuous phase liquid and a side channel carried water and another side channel carried PLGA. This method was adopted to deposit multilayers of polyelectrolyte (positively and negatively charged) (Lee et al. 2010). It was shown that the flow rate ratio ($Q = Q_d/Q_c$) is the key parameter to control the droplet length, frequency, and distance between the droplets. It was recommended to maintain it below 0.4 as the polyelectrolyte droplets can easily aggregate together due to electrostatic interaction if the distance between the two droplets is too close. A small volume of dispersed phase liquid breaks off to form the droplet. The dispersed phase liquid recoils back into the side channel and in the process, the dispersed phase from another side-channel enters the main channel to form the droplet and this cycle continues (Yesiloz et al. 2015).

An important application of droplet microfluidic devices is the generation of multiple droplets and merging them at the desired stage. This is of relevance to studies on chemical/biochemical reactions. In a device having two T-junctions, two droplets can be generated separately, each having different reagents. One such device was developed to produce two droplets containing DNA and DNA markers to perform fluorescence imaging on the merged droplet (Guo et al. 2010). Similar experiments were carried out to perform mass spectroscopy on merged droplets of myoglobin and pepsin (Sun et al. 2013). A device with four T-junctions was fabricated and used to produce four droplets of different reagents in the same device (Zec et al. 2012). The velocity vector fields during the merging process in straight and diverging microchannels were studied. The merging happens along with the flow and not at the junction. In this device, droplets were generated in double T-junction and Y-junction (side-channel is at 45^o to the main channel) (Jin and Yoo 2012). The inclination of side channel at 45^o (Jin and Yoo 2012) and 90^o (Surya et al. 2015) to the main channel can also produce droplets in the alternate regime. Devices with side channels inclined at 45^o (Jin and Yoo 2012) and 90^o (Surya et al. 2015) with the main channel have been used to produce droplets in the alternate regime. Further, the study showed that the droplets were generated in merging regime for $Ca < 0.027$ and $Q = 0.13$ to 0.9 and alternate regime for Ca ranging between 0.028 to 0.13 while Q was at 0.75 to 0.13. The droplet generation mechanism was understood through simulations using the Volume of Fluid (VOF) Method and the results were

found to match with less than 15% of the error margin. A numerical study using a double T-junction device shows that, for side channels of different widths, the minimum capillary number for generating droplets in the alternate regime varied from 0.02 to 0.05 (Ngo et al. 2015). Further, analysis of the temporal variation of pressure in the main channel, revealed that the droplet generation mechanism changes from the merging to the alternate regime in a symmetric double T-junction device. Applications such as the production of artificial lipid bilayers (Schlicht and Zagnoni 2015) and the formation of synthetic lipid bilayers between the droplet interface (Elani et al. 2016; Nguyen and Sarles 2016 p.) have been demonstrated in the past. Droplet formation in the alternate regime was demonstrated experimentally and supported with matching simulation results using a double T-junction device having symmetric tapered side channels (Saqib et al. 2018). Experiments on single-cell pairing were carried out using multiple droplets with mineral oil as the continuous phase liquid (Babahosseini et al. 2019). The merging efficiency of two different reagents with hydrogel droplets showed 90% efficiency while Q was maintained between 0.1 to 0.6. Using simulation, it was shown that the droplet generation in the merging regime in a double T-junction device can be understood by plotting pressure versus time (Han and Chen 2019a). In this study, pressure change with time shows that blocking time and breaking time of dispersed phase liquid increases with interfacial tension from 3mN/m to 12mN/m. Further, it was shown that the average pressure increases with the viscosity of continuous phase liquid from 0.2 mPa.s to 4 mPa.s and the frequency of droplet generation and average pressure increases with an increase in the flow rate of continuous phase liquid from 0.2μL/hr to 0.8μL/hr. They continued and presented the study on droplet merging by varying the angle between the side channel and the main channel between 30^o to 150^o (Han and Chen 2019b). The study showed that increased droplet generation frequency and smaller diameters of droplets were found when the angle between the side and main channel is at 60^o, channel height to width ratio.

The interfacial tension between the two immiscible liquids and the viscosity of the two liquids are two important factors that contribute to droplet generation. For practical applications, the generated droplets are collected in a vial and pipetted out manually for further investigations. To prevent droplets from coalescing in the vial, surfactants are

added to one of the two liquids based on their solubility. This reduces the interfacial tension (Tadros 2013). Surfactants stabilize the droplets and increase its durability. The studies related to surfactants takes us to the early works on the dynamics of droplets in fluids can be traced to the classic work, both experimental and theoretical, by G.I.Taylor (Taylor 1932, 1934). The primary interest then was on the buoyancy-driven motion of spherical drops and bubbles in static fluids, including the effects of surfactants on the motion. This topic has been discussed very well in the excellent treatise on Physicochemical Hydrodynamics by V.G.Levich (Veniamin Grigor′evich Levich 1962). In later studies, the deformation and breakup of drops moving in flowing fluids were investigated. Much of this work has been reviewed by A.Acrivos (Acrivos 1983) and by J.M.Rallison (Rallison 1984). The breakup of drops at low Reynolds Number was studied more extensively at various flow conditions by Stone and co-workers (Stone et al. 1986; Stone and Leal 1989). In these studies, the role of spatial gradients in the interfacial tension was ignored. Such gradients were later shown to cause large deformation of spherical drops and their eventual breakup especially in the presence of surfactants. A combined analytical and numerical study on the effect of surfactants on finite deformation of droplets in flowing fluids was reported by Stone and Leal (Stone and Leal 1990; Borhan and Mao 1992). They showed that a nonuniform distribution of surfactant occurs at the surface of the drop which leads to large deformation of the initially spherical drop. The breakup of the drop was seen to depend on the capillary number. He et al. (1991) studied the effect of surfactants on the hydrodynamics drag on spherical droplets due to the Marangoni effect. A continuum model was developed to calculate the interfacial tension (Brackbill et al. 1992). The influence of an insoluble surfactant on droplet breaking and deformation was studied for different values of viscosity ratio ($\lambda = \mu_d/\mu_c$) such as 0.1, 1, and 10 (Milliken et al. 1993); here μ_d and μ_c are the viscosity of dispersed and continuous phase liquids, respectively. The influence of the surfactant was seen to be dominant for $\lambda = 0.1$.

In a pioneering work, Thorsen et al. (2001) investigated the generation of microdroplets of water in oil using T-Junction devices made of urethane acrylate. They studied the generation of water droplets in various oils such as decane, tetradecane, and hexadecane and also the influence of a surfactant (Span 80) on droplet size. Water droplets were

generated in tetradecane with the addition of span 80 (Dreyfus et al. 2003). In this study, it was shown that the contact angle of water increased with surfactant concentration. Further, it was concluded that to achieve stable droplet formation the concentration of surfactant should be above critical micelles concentration. Double emulsions such as water-in-oil-in-water (W/O/W) and oil-in-water-in-oil (O/W/O) were produced using corn oil and water in a device made of glass (Nisisako et al. 2005). Lipophilic and hydrophilic surfactants were mixed in oil and water, respectively, to avoid the coalescence of droplets. The oil droplets were generated continuously, as the glass is hydrophilic, but water droplets were produced with a hydrophobic coating. The recirculation flow field inside the droplet was demonstrated using the velocity field vectors (Nguyen et al. 2006). (Garstecki et al. 2006) studied the dependence of droplet size on Q_c and Q_d for $C_a \leq 0.1$. The scaling equation proposed by Garstecki et al. 2006 is inconsistent for higher C_a and this was demonstrated by producing water droplets in hexadecane + 1% Span 80 (wt/wt %) (Adzima and Velankar 2006). Further, it was shown that the pressure in the droplet generating channel (main channel in Fig 1.1) increases with the droplet size. The increase in the flow rate of Q_c decreases the size of n-octane droplets (H. Xu et al. 2006). This study was repeated with and without the presence of surfactant (sodium dodecyl sulfate) on a device made of PMMA (Xu et al. 2006). The droplet length was reduced with an increase in Q_c. The addition of surfactant altered the wetting conditions of the microchannel as the surfactant molecules adsorb with their polar heads in the water phase and the tail on the wall surface. The size of the droplet reduces with the increase in the surfactant concentration. This was demonstrated with surfactants like SDS and tween 20 (Wang et al. 2009a). The reduction in droplet size was not seen at concentrations greater than Critical Miscille Concentration (CMC) (for SDS it is 10mmol/L and Tween 20 it is 0.03mmol/L). The droplet generation mechanism also depends on the channel geometry and dimensions (Gupta and Kumar 2010a; Steijn et al. 2010).

Due to the addition of surfactant interfacial tension reduces and in-turn, reduces the pressure difference ΔP between the pressure in dispersed phase liquid and that in the continuous phase liquid. Apart from this, the droplet size decreases, and the rate of droplet generation increases for a constant flow rate of the dispersed phase liquid (Peng

et al. 2011). Dispersed phase liquids from two side channels in a double T-junction device can be merged. This stands as an improved alternative for mixing different reagents for investigating protein-protein interaction and cell-based assay (Um et al. 2008). This was demonstrated by producing water droplets in mineral oil. A surfactant such as Span 80 was mixed at 0.5% concentration (wt/wt). The study shows that, in the case of a straight channel, the rear droplet merges with the front droplet without generating any noticeable vortex motion while in the diverging channel a strong backflow occurs in the middle region of the front droplet, and the vortex motion in the rear droplet. In a similar device, water droplets were generated in mineral oil with different concentrations (0% to 5%) of Span 80 (Surfactant) (Liu and Qin 2013). In applications involving cell encapsulation, the encapsulated cell may slip to continuous phase liquid. In order to avoid this, droplets of water and air bubbles were generated to clearly locate the cell which are encapsulated (O'Brien et al. 2012). Monodispersed water-in-oil-in-water (W/O/W) emulsion droplets were generated in decane. Various surfactants such as Span 80, Span 85, and SY Glyster CRC-75 were used as a surfactant at 1% concentration (wt/wt) (Hirama and Torii 2015) added to decane. One device contained both, a double T-junction and a Y-junction. First droplets were generated in an alternate regime. During this process, fluorescence microbeads were mixed in water (DMEM) and passed through one of the side channels. This generated a droplet pair (one droplet from each side channel constitutes droplet pair). The aqueous droplet pair generated at the double T-junction was again encapsulated in oil in a Y-junction. The droplet pair merged after being encapsulated in organic liquid when the surfactant's hydrophile-lipophile balance (HLB) value was between 3 or 4.3.

Merging efficiency was reduced with an increase in surfactant concentration up to 3% and no merging was seen at 5% of surfactant concentration. It was demonstrated that droplets can also be merged with two T-junctions (two side channels are parallel) for synthesizing inorganic-organic block copolymer (Hoang and Dien 2014). Bashir et al. 2011 showed that the role of contact angle and interfacial tension on the droplet is more significant for λ 0.8 than for 0.1. The length of the droplet is higher for $\lambda = 0.8$ than for $\lambda = 0.1$ for a fixed flow rate ratio and interfacial tension. The pinch-off time of the droplet decreases as there is an increase in contact angle from 120^{o} to 180^{o}. The

interfacial tension was evaluated for silicone oil having four different viscosities (10cSt, 20cSt, 50cSt, 100cSt) with two different dispersed phase media, viz. aluminium oxide suspensions in water and FC43 (Glawdel and Ren 2012). In the experiments performed, it was observed that the droplet length remained almost constant for capillary numbers ranging from 0.0028 to 0.008. In the work reported by (Wang 2013), Fe_2O_3 nanoparticles were introduced into individual droplets. Simulations were carried our using the VOF model. In each simulation nanoparticles of particular size were employed. The nanoparticle size was taken to range from 10nm to 100nm. Variation of droplet size with concentration of nanoparticles of known size was determined. The droplet size was seen to reduce with increase in the concentration of nanoparticles. The effect of the concentration of surfactants like SDS or Tween 20 added to silicon oil has been experimentally studied, wherein the interfacial tension was evaluated by recording the droplet generation using a high-speed camera (Wehking et al. 2014). Further based on their study an analytical model was formulated to determine the interfacial tension due to increased surfactant concentration. Most of these experimental studies assume a uniform distribution of surfactant molecules at the droplet interface and focus on the influence of surfactant on both the droplet size and frequency of droplet generation in various regimes. Numerical simulations have been carried out to understand the influence of surfactant concentration at the droplet/bubble interface (Bastani et al. 2018). The influence of surfactant (Span 80 mixed with octane) on droplet generation was numerically investigated using Lattice Boltzmann Method (Riaud et al. 2018). This study uses two computational models to investigate the uniform and non-uniform distribution of surfactant molecules at the interface. The model adopted for the non-uniform distribution of surfactant accounts for the droplet generation mechanism, which was experimentally demonstrated (Wang et al. 2016).

Very recently, the generation of water droplets in FC-40, using surfactants such as 1H,1H,2H,2H-perfluoro-1decanol, and PEG-Krytox was studied. It was observed that the flow velocity of the droplet increased by 25% which was exploited to control the distance between the droplets and also for an on-demand merging of two droplets (Ferraro et al. 2018). The use of surfactants such as Picosurf-1 in a DoD device has been shown to stabilize the generated droplets and improve the wetting of the main

channel walls of the DoD device (Totlani et al. 2020). The surfactant adsorption first appears at the front end of the droplet as it expands into the main channel and gradually covers the entire droplet before it is released. The profile of the velocity vectors inside the droplet indicates liquid circulation which stops as the droplet is about to be released. It was also observed that the frequency of droplet generation increases for capillary number ranging from 0.01 to 0.1. Such increase in frequency was demonstrated using numerical simulation (Gupta and Kumar 2010b; Han and Chen 2019a; Menech et al. 2008).

In order to perform optical studies on microdroplets for a longer duration, a trapping mechanism was developed. The results of this investigation were used for preparing precursors for advanced ceramics (Lankers et al. 1994). Different mechanisms exploited for trapping involve manipulation of surface energy (Dangla et al. 2011), hydrodynamics-based trapping (Wang et al. 2009b), and Laplace pressure(Simon et al. 2012). Surface energy-based trapping is achieved by proper choice of the geometry of the device and the micro-wells(Abbyad et al. 2011; Dangla et al. 2011). The effect of surface energy change leading to trapping was numerically studied by Nagel et al. (2014). Further, the change in Laplace pressure of droplets entering the well was also determined. It was seen that droplet trapping occurred at a critical value of the capillary number (Amselem et al. 2015). The anchoring of droplet to micro-well was studied using Lattice Boltzmann Method(Liu and Zhang 2017). This study demonstrated that the anchoring efficiency increases with increase in the diameter of the well. To capture individual microdroplets for further analysis, trapping the generated droplets in an array of micro-wells is convenient. We have investigated droplet generation and trapping in a Slip-Chip type device in the T-junction geometry. This device consists of two separate plates, one having a cylindrical well and the second plate having a shallow Pit with a circular opening along the main channel. The second plate is placed on the plate containing the wells such that the Pit lies over the well.

1.3 Droplet Microfluidic Devices.

Microdroplets can be generated by two different techniques, viz. active and passive methods (Zhu and Wang 2017). In the case of the active method, different types of energy, such as electrical, magnetic, centrifugal, optical, thermal, and mechanical, are applied to the microfluidic device externally. In passive methods, no external forces are applied and the droplets are generated simply due to the flow of two immiscible liquids in the devices at appropriately controlled flow rates (Squires and Quake 2005). Of the two liquids, one is used in larger quantities and is called the continuous phase liquid. It has viscosity μ_c and its flow rate is denoted as Q_c. The other liquid, used in much smaller quantities, is called the dispersed phase liquid and has a viscosity of μ_d and its flow rate is denoted as Q_d. The continuous phase liquid wets the channel wall and also carries the generated microdroplets as it flows along the channel. The microdroplets are separated from the channel wall by a thin layer of the continuous phase liquid. The droplets have a high surface-to-volume ratio. The choice of liquids depends on the intended application. Droplets of various volumes can be generated by controlling the flow rate of the two liquids and depending on the channel dimensions, the droplets may be spherical or may acquire an elongated shape termed to be 'Plug'.

The three main types of passive devices employed for generating microdroplets experimentally are T-junction (Thorsen et al. 2001), Cross Junction (Anna and Mayer 2006), and Co-flow (Cramer et al. 2004) devices. In what follows, we briefly discuss each of these devices.

1.3.1. **Cross-flow Devices**

Various types of cross-flow devices are shown in Fig.1.1. The two liquids used for droplet generation are immiscible. The continuous phase liquid meets the dispersed phase liquid at angles in the range $0^o < \theta < 180^o$. At the junction, where the two liquids meet, the shear force due to the continuous phase liquid pushes the dispersed phase liquid column along its flow direction. This interaction leads to squeezing of the interface between the two liquids at the junction resulting in a pinching-off of a droplet.

Once the droplet is released, the dispersed phase liquid retracts back into the side channel. This process keeps repeating as the two liquids flow continuously in the device and a train of droplets are produced. Among the various configurations in cross-flow devices, the T-junction type has been widely used (Fig 1.1a). In this device, the continuous and dispersed phase liquid meet at an angle $\theta = 90^o$ at the junction. It has been shown that a T-junction device with $\theta < 90^o$ (Fig.1.1b) leads to the generation of droplet pairs (Ménétrier-Deremble and Tabeling 2006). The generation of droplets in the Y-junction devices (Fig 1.1c) was reported by Steegmans et al. (2009). Applications involving the use of assays and microfluidic chips require a generation of droplets on demand (DoD). In such cases, the volume, frequency, and composition of the droplets can be controlled by regulating the flow rate of the dispersed phase liquid.

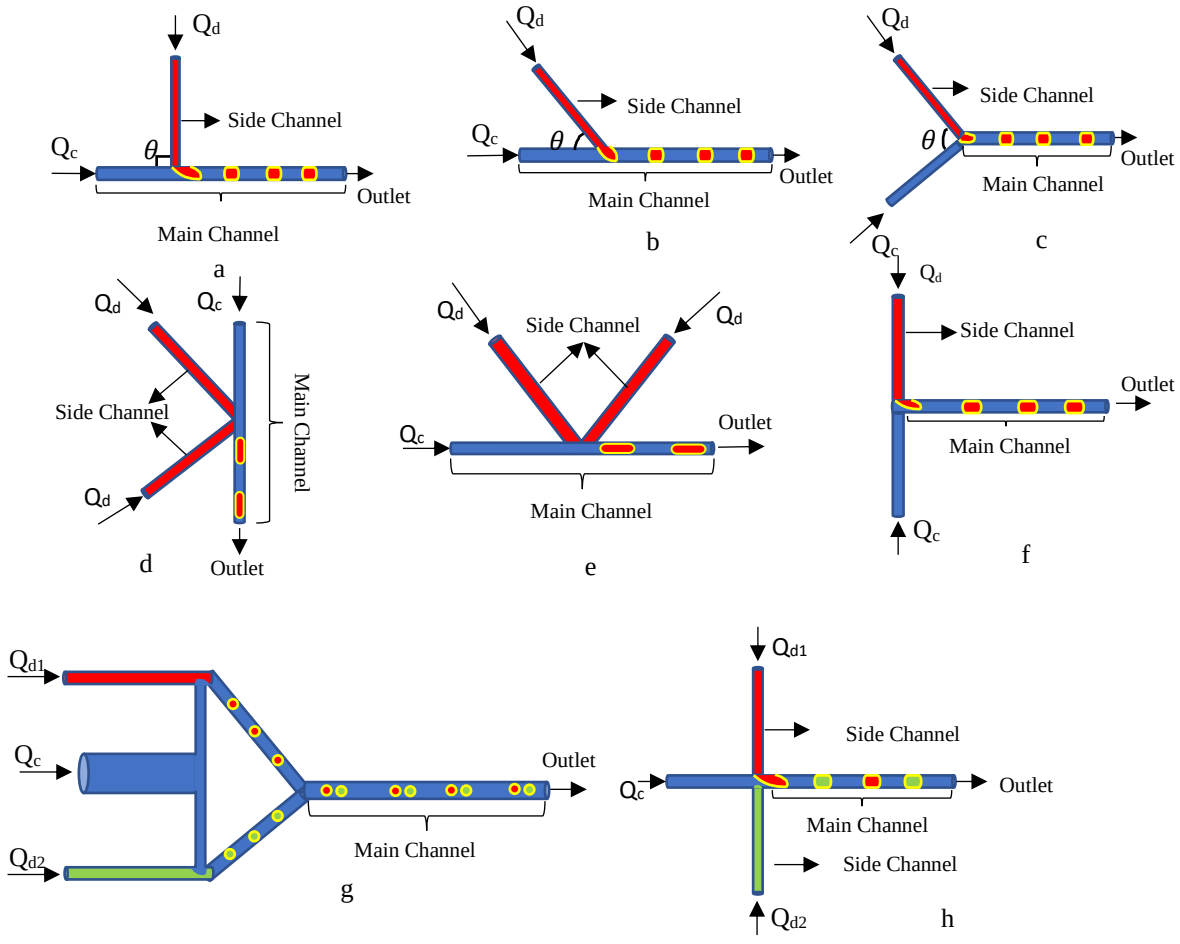

Fig 1.1 Schematic of various Crossflow devices a) with $\theta = 90^o$, called T-junction, b) device with $0^o < \theta < 90^o$. c) device with $0^o < \theta < 180^o$ called Y-junction, d) K-junction. e) V-junction, f) Head-on geometry, g) Two parallel T-junction that produces droplet pairs. h) Double T-junction generating droplet pairs. Image Source : (Zhu and Wang 2017)

This mechanism was achieved using K-junction (Fig 1.1d) (Lin et al. 2012) and V-junction (Fig 1.1e) (Tangen et al. 2015). In the "Head-on geometry" shown in Fi.g1.1f, the two liquids enter the junction from opposite directions to generate the droplets (Shui et al. 2009). Devices containing two T-junctions, which are parallel to each other (Fig 1.1g), was proposed to generate droplet pair of two different dispersed phase liquids (Lee et al. 2016). A double T-junction was designed to produce droplets alternatively from the two side channels (Fig 1.1h) (Zheng et al. 2004b).

1.3.2. **Flow Focusing Devices**

This device is similar in structure to that shown in Fig.1.1h. However, here the dispersed phase liquid is passed through the main channel whereas the continuous phase liquid is passed through the two side channels, as shown in Fig 1.2.

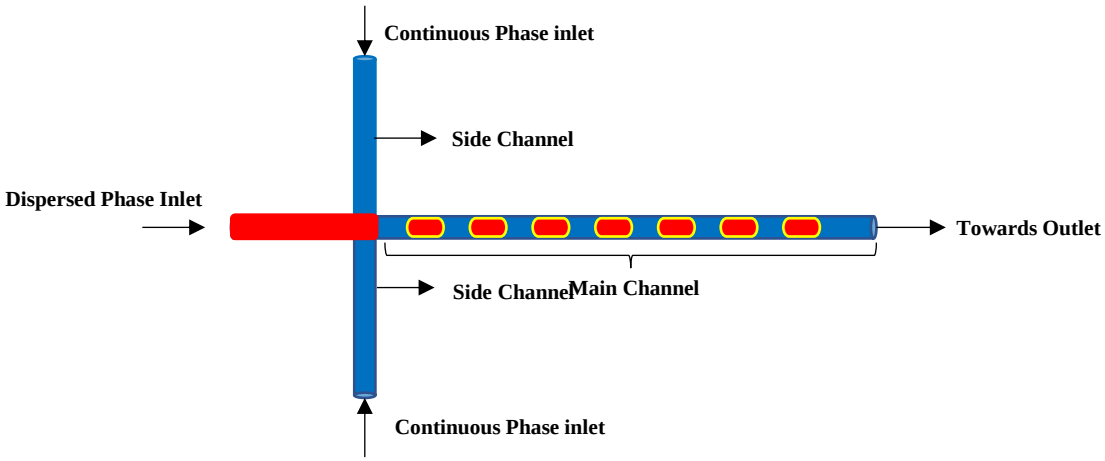

Fig 1.2 Schematic representation of Flow focusing device. Image Source : (Anna and Mayer 2006)

Due to the shear force of the continuous phase liquid from the two side channels, it constricts the dispersed phase liquid column as it enters the main channel resulting in the formation of droplets. A train of monodispersed droplets can be generated with a steady flow of the two liquids (Anna and Mayer 2006). The droplet can be formed in the main channel either at the junction or away from the junction depending on the flow rates of the two liquids.

1.3.3. **Co-flow Device**

In this device, the two liquids flow in the same direction and the dispersed phase liquid, flowing in the inner tube, is released into the continuous phase liquid flowing in the main channel (outer tube) as shown in Fig 1.3. Such devices have been fabricated using the soft lithography process (Anderson et al. 2000). As the dispersed phase liquid stream flows into the main channel, the viscous drag of the continuous phase liquid, which flows at a higher velocity, pulls the dispersed phase liquid until it breaks up into droplets. This was first reported by Umbanhowar et al. in 2000. Droplets can either be generated at the junction or away from it by controlling the flow rate of the two liquids (Cramer et al. 2004).

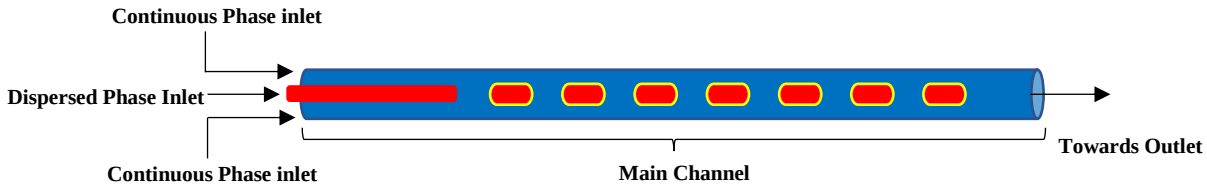

Fig 1.3 Schematic representation of Co-flow device. Image Source: (Cramer et al. 2004)

1.4 Dimensionless parameters

Droplet generation and its motion in the microfluidic devices are analysed in terms of several dimensionless parameters such as Reynolds number (R_e), Bond number (B_o), Weber number (W_e), and capillary number (C_a) (Zhu and Wang 2017). We define these parameters below.

The Reynolds number (R_e) is the ratio of inertial forces to viscous forces acting on the flowing liquid and is defined as

$$R_e = \frac{\rho U L}{\mu} \tag{1.1}$$

where ρ is the density of the liquid, U is the characteristic velocity of the liquid, L is the characteristic length for the device geometry, and μ is the dynamic viscosity of the

liquid. For liquids flowing in microfluidic devices, R_e is invariably < 1.0 and, hence, the flow is laminar.

The dominance of gravitational forces over surface tension forces for the liquid is estimated through the Bond number (B_o) given by,

$$B_o = \frac{\Delta\rho g L^2}{\gamma} \tag{1.3}$$

where Δρ is the difference in density of the two immiscible liquids, g is the acceleration due to gravity, L is the characteristic length for the device and γ is the interfacial tension between the two liquids. In microflows, the gravitational force is invariably negligible due to the small mass of the droplets, and therefore Bo << 1.

The interface (more details in Sec 1.4) between the two liquid phases can be analysed through the Weber number (W_e) which is defined as the ratio of inertial force to surface tension and is given by

$$W_e = \frac{\rho U^2 L}{\gamma} \tag{1.4}$$

where ρ is the density of the liquid, U is the liquid velocity, L is the characteristic length for the device and γ is the interfacial tension between the two liquids. Typically, for liquid flow in microfluidic devices W_e < 1.0.

The droplet generation mechanism is governed by the capillary number (C_a), which is defined as the ratio of viscous forces to interfacial forces and is given by,

$$C_a = \frac{\mu U}{\gamma} \tag{1.2}$$

where μ is the dynamic viscosity of the liquid, U is the characteristic liquid velocity and γ is the interfacial tension between the two liquids. Depending on the magnitude of this parameter the droplets may be generated by either dripping or squeezing or jetting mechanism (Table 1.1). Further, the breakup of droplets also depends on the value of C_a.

In the squeezing regime, the dispersed phase liquid flows into the main channel, forms an interface with the continuous phase liquid, and expands into the main channel, partially blocking the flow of the continuous phase liquid in the main channel. The continuous phase liquid exerts excess pressure on the interface of the two liquids. As a result of this pressure, the interface is squeezed at the junction forming a neck in the stream of the dispersed phase liquid. The neck gets narrower with increasing pressure and, eventually, a droplet of the dispersed phase liquid is pinched off. In the case of the dripping regime, the generation of the droplet is dominated by the shear force of the continuous phase liquid on dispersed phase liquid. The droplet is generated, even before the dispersed phase liquid stream can completely block the flow of the continuous phase liquid in the main channel. In this case, the increase in the pressure at the junction is not significant in comparison with the viscous drag force. A gradual change happens between the squeezing and dripping regime and the intermediate state is known as the transition regime. When the droplet generation happens far downstream from the junction, it is termed to be the jetting regime. Beyond this regime, with a further increase in the flow rate of dispersed phase liquid, the two liquids flow parallel to each other in two separate streams. In the parallel flow of the two streams, droplets are not produced. The range of capillary numbers for each regime is given in Table 1.1 (Xu et al. 2008).

Table 1.1 : Different regimes of droplet generation

Capillary Number (C_a)	**Regime**
10^{-4} to 0.002	Squeezing
0.002 to 0.01	Transition
0.01 to 0.3	Dripping
Above 0.3	Jetting

The droplet volume decreases with the increase in C_a. Other factors that are involved in droplet generation are the channel dimensions (Gupta and Kumar 2010a; Zhang et al. 2014), flow rate ratio ($Q = Q_d/Q_c$) (Garstecki et al. 2006), viscosity ratio ($\lambda = \mu_d/\mu_c$).

1.5 Surface Tension and Interfacial tension

A liquid is a condensed phase of matter and is characterised by the strong intermolecular attraction which is called cohesive force. At the surface of the liquid surrounded by air, the liquid molecules experience attractive force from both the molecules within the liquid as well as the air (Fig.1.4). The cohesive force on the liquid molecules at the surface due to the air molecules is much weaker due to the very low density of air. Hence, the liquid molecules at the surface are subjected to a net force acting inwards into the liquid. This force acts to minimize the surface area of the liquid and is described as Surface Tension γ which is a positive quantity. Surface tension can be looked upon as either force per unit length (dynes/cm) or energy per unit area (ergs/cm^2).

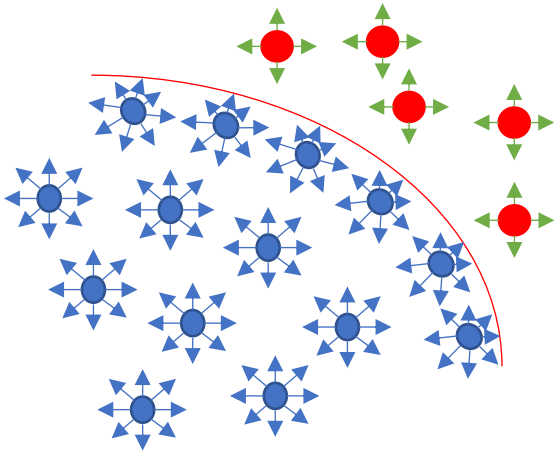

Fig 1.4: Simplified cartoon of molecules near the interface of a liquid with a gas. The liquid-air interface is shown as a red line. Image Source : ("Fundamentals of Capillarity" 2012)

If one liquid is surrounded by another liquid, then the value of γ may be positive or negative depending on the nature of the liquids. In this case, we shall call the cohesive force "Interfacial tension". If γ is positive then it implies that the two liquids are immiscible. In any case, interfacial tension is much smaller than the surface tension for individual liquids. At the interface of the two liquids, the total surface energy is given by $E = \gamma A$, where A is the interfacial surface area. The interfacial tension is proportional to the pressure difference between the two liquid phases. This pressure difference is given by the Young-Laplace equation (Vowell 2009)

$$\Delta P = \gamma \left(\frac{1}{R_1} + \frac{1}{R_2} \right) \tag{1.5}$$

where R_1 and R_2 are the radii of curvature of the interface of a spheroidal liquid drop; for spherical droplets $R_1 = R_2$ and in such a case we have

$$\Delta P = \left(\frac{2\gamma}{R} \right) \tag{1.6}$$

When the droplet is in motion, the Laplace pressure (Young Laplace equation) is dependent on both interfacial tension and the contact angle (θ) of the droplet with the channel wall. It is given by,

$$\Delta P = \left(\frac{4\gamma Cos\theta}{d} \right) \tag{1.7}$$

where d is the width of the microchannel.

1.6 Surface Wetting

When a drop of a liquid is placed on the surface of a solid, then depending on the intermolecular interactions at the interface, it may sit on the solid surface as a drop or spread out on the surface, which is referred to as wetting of the surface. The wetting or the contact angle is quantified in degrees (θ) which is determined by the force balance between the adhesive and cohesive forces acting on the liquid surface. The interaction of the two fluid phases (liquid and gas) with the surface of the solid plate can be categorised into three types: "total wetting", "partial wetting" and "nonwetting". This is shown schematically in Fig.1.5.

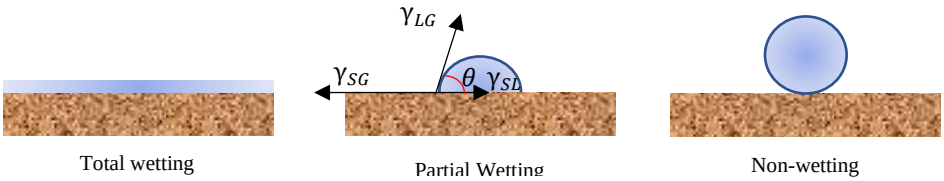

Fig 1.5 Schematic representation of various wetting regimes. a) Total Wetting. b) Partial Wetting and c) Non-wetting. (Blue Colour: water and Brown Colour: Solid surface). γ_{LG}, γ_{SG}, and γ_{SL} are the surface tension between liquid-gas, solid-gas, and solid-liquid. Image Source : ("Minimal Energy and Stability Rubrics" 2012)

When the liquid spreads out on the entire solid surface, it is termed "total wetting" and when the liquid spreads over a limited part of the solid surface, forming a convex-shaped bubble, it is termed "partial wetting". In the latter case, when $\theta > 90^o$ the surface

of the solid is called hydrophobic, and when $\theta < 90^o$ the surface is called hydrophilic if the liquid used is water (Vowell 2009).

1.7 Surfactant and its influence on droplets.

Droplets of water in oil (W/O) or oil in water (O/W) are thermodynamically unstable. They always tend to coalesce. To prevent coalescence of droplets surfactants are used. "Surfactant" is a short form for "Surface active agent". Surfactant molecules have a hydrophilic head and a hydrophobic tail. When surfactants are added to water, the surfactant molecules naturally move to the water-air (or water-oil) interface and orient themselves such that the head is inside the water whereas the tail out of the surface into the air. Since the head of the molecule carries an electric charge, the molecules spread out on the water-air surface. As the concentration of the surfactant is increased, the surface density of the surfactant molecules keeps increasing till a saturation level is reached. If the surfactant concentration is increased further, the surface cannot accommodate any more surfactant molecules and, hence, the molecules start forming ball-shaped clusters, in which the tails point towards the center and the heads are at the surface of the ball. These clusters are called micelles. The concentration of the surfactant at which the micelles start forming is called Critical Micelle Concentration (CMC).

Typically, in a system generating water droplets in an oil medium, the surfactant should be soluble in oil and for generating oil droplets in water, the surfactant should be soluble in water. The choice of surfactant is based on hydrophilic-lipophilic balance (HLB) (Griffin 1949).

$$HLB = 7 + \Sigma(No.of\ hydrophilic\ groups) - \Sigma(No.of\ hydrophobic\ groups) \qquad (1.8)$$

When the HLB values are in the range of 8-18 the surfactant is hydrophilic and in the range of 3-6, it is hydrophobic (Griffin 1954). The surfactant molecules at the surface of the liquid stay at the surface due to their amphiphilic nature, which results in

lowering the surface tension of the liquid. The distribution of surfactant molecules in a liquid is shown schematically in Fig 1.6.

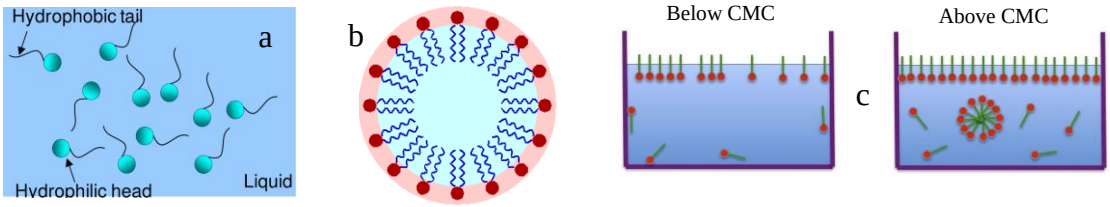

Fig 1.6 a) Dispersion of surfactant molecules in bulk liquid, b) distribution of surfactant molecules at the interface across a droplet of oil in water (the oil drop is shown in blue colour), c) Arrangements of surfactant molecules below and above critical micelle concentration (CMC). The display for the case above CMC shows one micelle. Image Source: a & b) Wikipedia, and c) (Steven Abbott 2018)

Surface or Interfacial tension can be characterised by the pendant drop method (Yakhshi-Tafti et al. 2011). The surfactants are divided into four types, non-ionic (no charge), anionic (negative charge), cationic (positive charge), and amphoteric (carry both a positive and a negative charge) (Schramm et al. 2003).

1.8 Scope of the thesis

Our literature survey has revealed that the controlled generation of microdroplets, of the required volume, at the desired rate depends on the physical properties of the two liquids, their flow rates, the use of surfactants, and the device geometry and dimensions. T-junction devices have been widely used for producing droplets on demand. In a T-junction device, the droplets can be produced by either a steady flow of the two liquids or by pulsing the flow rate of the dispersed phase liquid. It is seen that the droplet size and frequency of droplet generation can also be controlled by using a surfactant. An appropriate surfactant may be dissolved into either of the two liquids depending on the intended application of the device. The trapping of droplets in micro-wells can be facilitated by the inclusion of pits or pinholes in the main channel of the device further downstream from the T-junction.

The research progress reported so far indicates the need for investigating droplet generation due to the variation of physical parameters of the two immiscible liquids as well as for various device geometry. This is necessary to arrive at an optimized design

for the microfluidic device. Thus, droplet generation is required to be studied at several flow rates of the two liquids and for different surfactant concentrations. The investigations need to be extended to the pulsed flow of one of the two liquids using pulses of different pulse widths. Droplet generation in microfluidic devices with different channel widths is also required. Trapping of the droplets is required to be studied for different surfactant concentrations and over a range of flow rates. The role of additional structures, such as a shallow circular Pit or a Pinhole, built into the microfluidic device, is another factor to be investigated. Some applications require the merging of two, or more, droplets. Hence, studies on droplet generation in devices designed for generating two or more droplets become necessary. Thus, a large number of investigations are required to be done for each type of device before fabricating a microfluidic device suitable for a specific application. A practical approach towards this is to first carry out detailed simulation studies on any device.

Numerical simulations may be carried out using methods such as the interface tracking method (Hirt and Nichols 1981a), the level set method (Osher and Sethian 1988), and the phase-field method (Anderson et al. 1998). Among these methods, the interface tracking (or volume of fluid) method is widely used and has also been incorporated into commercially available software packages. Hence, we have carried out a numerical simulation of droplet generation and trapping in T-junction devices using ANSYS Fluent v18.1 software which contains the Volume of Fluid (VoF) method. We have investigated the role of surfactants on droplet generation and trapping. This study has been carried out for different fluid flow rates, different device geometries, and different surfactant concentrations. We have studied both the steady flow case as well as the pulsed fluid flow case. The microfluidic device is of the “Slip Chip” type, consisting of two plates, which is used in many experiments.

1.9 Objectives of the thesis

In light of the discussions of Sec.1.8.1, we have carried out the following investigations by numerical simulations:

- Study of droplet generation for the case of the steady flow rate of two immiscible liquids, water, and mineral oil. The effect of a surfactant (Span 80 in mineral oil) on droplet generation in the squeezing and squeezing-to-dripping transition regime is investigated.
- Study of droplet generation due to the pulsed flow of the dispersed phase liquid (water). This is done for different parameters of the rectangular waveform used. The studies are carried out for a range of flow rates and surfactant concentrations.
- Analyse droplet formation by generating plots of pressure versus time at points within the two liquids. This study is seen to give a good insight into the droplet formation dynamics.
- Study of droplet trapping in the T-junction devices for various flow velocities of the continuous phase liquid for various surfactant concentrations. The role of a shallow circular Pit or a Pinhole in facilitating the trapping of droplets has also been studied.
- Study of generation of droplet pairs in a double T-junction device for different flow rates and surfactant concentrations. The study is carried out for a symmetric device as well as for an asymmetric device. The conditions under which the two droplets merge are also investigated.

2.10 Organisation of Thesis

The research work presented in this thesis is divided into 6 chapters. The outline of the chapters is as follows:

Chapter 1 presents a brief introduction to the field of droplet microfluidics and its development over the past two decades. The mechanisms leading to the generation of microdroplets due to two-phase fluid flow in microchannels are discussed. Details about commonly used microdroplet generating devices are presented. The droplet generation mechanisms in T-junction devices, including the use of surfactants, are

discussed. A review of past literature on micro-droplet generation in T-junction devices and their applications is presented. The outstanding issues investigated in this thesis are mentioned. A summary of each chapter in the thesis is presented at the end.

Chapter 2: This chapter describes the details of the numerical method used in the present research work. The first section provides the details of the various solver schemes and optimisation techniques used in the volume of fluid (VOF) method. The details of the simulation settings, fluid properties, boundary conditions, flow rates of the two liquids for droplet generation, and varying concentrations of surfactants are mentioned. The device geometries of the various device types investigated in the thesis are presented.

Chapter 3: This chapter presents simulation results on droplet generation and trapping in a T-junction device due to the steady flow of the two liquids. Initially, we present the results on the scaling of droplet size with the ratio of the flow rates of the two liquids. Following this, we discuss the effect of a surfactant on droplet generation in the squeezing to dripping transition. Further, we present the results of the simulation of trapping a droplet in a micro-well by varying the diameter of the Pit in the channel plate and the alignment of the Pit with the micro-well. The significance of critical velocity for trapping droplets is also discussed.

Chapter 4: The simulation results on droplet generation and trapping due to pulsed flow of the dispersed phase liquid are presented in this chapter. Results of droplet generation due to pulses of different widths and the duty cycle are presented. Analysis of the pressure versus time graphs for the point P_d is presented and its implications on droplet generation are discussed. We have investigated the role of a pinhole in the channel in the trapping of the droplet in a micro-well. The effect of a surfactant on droplet generation and trapping is discussed. It is shown that droplet trapping occurs at an optimum flow rate of the continuous phase liquid.

Chapter 5: In this chapter, the generation of droplets in double T-junction is discussed. Simulation results for both, symmetric and asymmetric T-junction configurations are presented. The conditions under which the two droplets merge into one larger droplet are

described. Further, conditions under which the droplets travel without merging are also discussed. The effect of addition of a surfactant to the continuous phase liquid on droplet generation is discussed.

Chapter 6: Summarizes the major conclusions drawn from the present research work which is followed by the scope for future research in this field. An appendix followed by a list of references and a brief profile with publications in international journals and conferences are presented at the end of the thesis

CHAPTER 2

NUMERICAL SIMULATION STRATEGY AND TOOLS EMPLOYED

2.1 Introduction

The work presented in this thesis is concerned with the generation and trapping of micro-droplets in a controlled manner by exploiting the flow of two immiscible liquids in T-junction devices. As mentioned in Chapter 1, we have carried out extensive numerical simulations to arrive at an optimum design for the microfluidic devices for use in actual applications. The simulations studies are focused on the following two aspects:

- Droplet generation in the T-junction devices. This has been investigated for various flow rates of the two liquids in devices and a range of surfactant concentrations. The studies have been carried out for steady flow rates of the two liquids as well as for the case of pulsed flow of the dispersed phase liquid, keeping the flow rate of the continuous phase liquid constant. Further, we have studied droplet generation in devices with two different geometries, viz. single T-junction and double T-junction.
- Droplet trapping in micro-wells. These studies have been carried out for a range of flow rates of the two liquids for different surfactant concentrations. We have also investigated the role of additional structures, viz. a shallow circular Pit and a Pinhole close to the micro-well, in facilitating droplet trapping. The objective of these studies was to explore the parameter range which is best suited for efficient trapping of the micro-droplets.

The basic task in the simulations is to solve the well-known Navier-Stokes fluid equations numerically for two-phase fluid flow. Since the two liquids in our problems are immiscible, the primary step is to generate the interface between the two liquids at the T-junction and follow its evolution in time. The competition between the interfacial tension, the fluid pressure, and the viscous drag force result in instability in the temporal evolution of the interface, which leads to the release of micro-droplets at the T-junction.

The software modules employed for our studies have been selected for carrying out such investigations.

The investigations on droplet trapping involve the calculation of deformation of the surface of the droplet due to the additional structures, viz. the Pit and the Pinhole, and also as it enters the micro-well. Most often, the droplet shape is elongated, like a cylindrical capsule, as it moves along the flow channel, and becomes spherical as it gets trapped in the micro-well since the volume of the droplet remains constant. This change in shape implies a change in the surface area of the droplet and, hence, a change in its surface energy. Further, the shear stress exerted by the continuous phase liquid on the trapped droplet also becomes important beyond a critical flow rate. The software modules have been selected to incorporate these physical aspects.

In addition to the points discussed above, the effect of surfactants on droplet generation and trapping has been included in the simulations. From the point of view of applications, the generation of pairs of droplets and their merger in the flow channel has also been studied using appropriate software modules.

In an early numerical study on two-fluid flow, DeBar (1974) developed the KRAKEN software code to investigate the evolution of the interface between the two fluids. This was improvised and a new code called Simple Line Interface Calculation (SLIC) was developed by incorporating a new concept called the fractional volume of fluid method (Noh and Woodward 1976). Initially, this was found to be a robust method to represent the free surface in two- and three-dimensional space, but later it was found that it did not generate a smooth interface between the two fluid phases. With further improvements, several numerical methods such as the Volume of Fluid (VOF) method (Hirt and Nichols 1981b), level-set method (LS) (Osher and Sethian 1988), and phase-field method (PF) (Anderson et al. 1998) have been developed. One common factor in all three methods is the definition of “indicator function”. This function is taken as a “volume fraction” in VOF, a “signed distance function” in the Level set method, and a “mass fraction function” in the phase-field method (Zhang and Liu 2012). The VOF method is seen to have greater control over mass conservation, while the LS method

focuses on surface tension forces. Hence, a combination of VOF and LS methods is better suited for our studies (Cerdeira et al. 2020). We have employed this combination in ANSYS Fluent software package for our simulation studies.

2.2 Fluid equations for simulations

The basic equations used in the simulation are listed below. The continuity equation for an incompressible fluid is given by (Batchelor 2000).

$$\nabla.\left(\rho_{avg}\overrightarrow{U'}\right) = 0 \tag{1}$$

Navier-Stokes equation of motion for the fluid is given by,

$$\frac{\partial\left(\rho_{avg}\overrightarrow{U'}\right)}{\partial t} + \nabla\cdot\left(\rho_{avg}\overrightarrow{U'U'}\right) = -\nabla P + \nabla\cdot\bar{\tau} + \overrightarrow{F'} \tag{2}$$

where $\overrightarrow{U'}$, P, ρ_{avg}, $\bar{\tau}$ and F is velocity, pressure, density (averaged), stress tensor, and surface tension, respectively for the fluid. For Newtonian liquids which are incompressible, the shear stress is relative and proportional to the rate of strain tensor which is represented as,

$$\bar{\tau} = \gamma\eta_{avg} = \eta_{avg}(\nabla\overrightarrow{U'} + \nabla\overrightarrow{U'}*) \tag{3}$$

where η_{avg} is the averaged viscosity. For the two-component fluid being considered, we define the density and viscosity of the volume (averaged) in terms of the fractional volume of the two immiscible fluids such as oil (V_o) and water (V_w) as follows (Vivek Ranade 2002a).

$$\rho_{avg} = V_0\rho_o + (1 - V_w)\rho_w \tag{4}$$

$$\eta_{avg} = V_0\eta_o + (1 - V_w)\eta_w \tag{5}$$

The fractional volume of the individual fluid phase is computed by resolving the following equation.

$$\frac{\partial V_f}{\partial t} + \overrightarrow{U'}\cdot\nabla V_f = 0 \tag{6}$$

"f" is the subscript that describes any of the two fluids. In each mesh element, the fractional volume of the two phases is conserved implying $\Sigma\, V_f = 1$. If $V_f = 0$, the specific mesh element is said to be empty of the f^{th} phase, and $V_f = 1$ indicates that the element

(cell) is loaded with the f^{th} phase. Thus, the two-phase interface is demarcated by the value of the fractional volume.

We adopt the model of continuum surface force (CSF) (Brackbill et al. 1992) and accordingly define the interfacial tension force ($\overrightarrow{F'}$) which is volumetric and is represented as

$$\overrightarrow{F'} = \sigma\left(\frac{\rho_{avg} R_n \nabla V_f}{0.5(\rho_0 + \rho_\omega)}\right) \tag{7}$$

where "σ" is the coefficient of interfacial tension among two liquids and R_n is the radius of curvature of the droplet which is expressed in terms as

$$R_n = -\nabla \cdot \hat{n} = \frac{1}{|\vec{n}|}\left[\left(\frac{\vec{n}}{|\vec{n}|} \cdot \nabla\right)|\vec{n}| - (\nabla \cdot \vec{n})\right] \tag{8}$$

where $\hat{n}$ is the component normal to the droplet surface. Considering the formulation VOF the surface normal $|\vec{n}|$ is expressed as the gradient of fractional volume phase at the interface which can be written as

$$\vec{n} = \nabla V_f \tag{9}$$

The force due to interfacial tension is implemented by piecewise linear interface calculation (Vivek Ranade 2002b). The change in the interfacial tension in our study is due to increased surfactant concentration. Hence the convection-diffusion equation is considered, which is given by (Wang 2013),

$$\frac{\partial \alpha}{\partial t} + U' \cdot (\vec{\nabla}\alpha) = \vec{\nabla} \cdot (D_c \vec{\nabla}\alpha) \tag{10}$$

where α is the surfactant concentration in the bulk fluid and D_c is the diffusion coefficient of surfactant in the bulk liquid.

The effects of wall adhesion are considered by providing the necessary value for the contact angle with the channel wall (Θ_w). Therefore, the surface normal at the reference cell next to the wall is given by,

$$\hat{n} = \hat{n}_w \cos\theta_w + \hat{m}_w \sin\theta_w \tag{11}$$

where $\hat{n}_w$ and $\hat{m}_w$ are the unit vectors which are normal and tangential to the wall, respectively.

2.3 Discretization Scheme for Computation

In finite volume method, the region in which the fluid flow is to be studied is divided into a very large number of small-sized 3-dimensional volume elements called “cells”. These cells are also called “control volumes”. A node point is assigned to the centre of each cell. These node points form a cartesian grid of points in space. For example, a small part of a 2-dimensional cartesian grid is shown in Fig 2.1a.

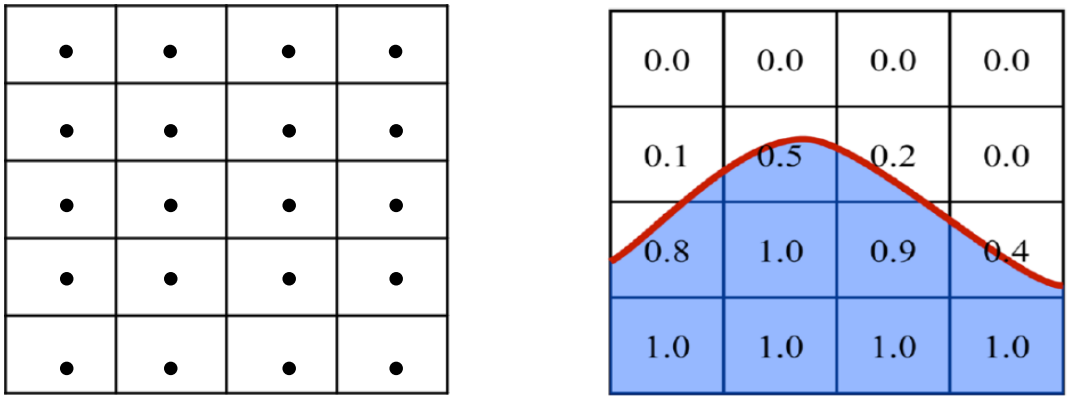

Fig 2.1 a) Small part of a 2-dimensional Cartesian grid, b) The shape and position of the two-fluid interface in each cell of the domain. The number in each cell indicates the volume fraction of the dispersed phase fluid shown in blue color. The white color represents the continuous phase fluid. Image Source (ANSYS FLUENT Technical reference document)

To simulate two-fluid flow, the fluid equations presented in Sec.2.2 have to be transformed into difference equations by adopting standard methods for numerical computations. The resulting algebraic equations are then employed to propagate a given fluid interface to the next set of node points, subject to the physically imposed boundary conditions. This process is iterated successively till the fluids reach the boundary at the end. The accuracy of the results depends on the choice of the size and geometry of each grid and the time step for propagating the fluid interface. Standard criteria for achieving a desired level of accuracy may be prescribed. The simulation results must closely match experimental results, failing which, the grid size and geometry will have to be modified. These steps have been incorporated in the software package ANSYS Fluent, which includes the Volume of fluid (VOF) package also.

The VOF method involves the following three steps for calculations:

1. An interface reconstruction algorithm is used to explicitly describe the interface in each cell depending on the volume fraction of the fluids for a given time step.

2. The advection algorithm is used to solve the advection equations, expressed in a different form, and calculate the distribution of volume fraction (V_f) at the next time instant.

3. The interfacial tension force model is used to account for interfacial tension effects at the interface of two immiscible liquids (Zhang and Liu 2012).

   In a two-phase fluid flow system, one of the two fluids is considered to be the primary phase fluid and the other is called the secondary phase fluid. The quantity of the two fluids present in any cell is expressed as two fractional numbers, which add up to unity. In particular, the volume fraction of the secondary phase fluid, shown in blue color in Fig.2.1b, is denoted by V_f, a variable for the cell. Thus, in each cell, the volume fraction of the primary phase fluid, shown in white color, is $(1-V_f)$. For example, in Fig.2.1b, the volume fraction of the dispersed phase fluid is 0.1, 0.5, 0.2, 0.0 in the first, second, third, and fourth cells, respectively, in the second row. This implies that the volume fraction of the continuous phase fluid in those four cells is 0.9, 0.5, 0.8, and 1.0, respectively.

   In such case, during the flow, we encounter three situations, i) $V_f = 0$ (No secondary fluid in the cell), ii) $V_f = 1$ (Secondary liquid occupies full cell), iii) $0 < V_f < 1$ (Secondary liquid occupies part of the cell reaming portion filled by primary phase). Depending on the local value of V_f in each cell, computation is carried out within the domain. Thus, VOF is a free surface modeling technique for computing the movement of dynamic surface in cells (in grid space) surrounding the interface during each time step. The channel dimensions have been mentioned in section 2.6 and 2.7.

2.4. Model for Simulation using VOF solver

We have used ANSYS Fluent solver v2020R2 “Pressure Implicit with Splitting of Operators (PISO)”, for simulating the droplet generation, taking into account the coupling between pressure and velocity in the momentum equation. Any false currents which may arise because of a mismatch between the pressure and interfacial tension forces are removed using the Pressure Staggering Option (PRESTO). The first order implicit scheme is solved with spatial derivatives. The convergence criterion for the solution of the continuity equation, the equations for X-momentum and Y-momentum, and the computation of the Level Set function were set as a residual of 0.001. Thus, if the residual in any computation drops below 0.001, then the solution is treated as having converged. The global Courant number, which is a dimensionless quantity, is maintained at less than 0.2; it varied between 0.08 to 0.17 throughout the simulations. This relates the time step increment used for solving the transport equations to the distinctive time of transportation of the fluid element across a control volume. The flow rate of the two liquids is prescribed at the respective inlets and a normal outflow condition is prescribed at the common outlet. The resultant droplet length is noted. Simulations are performed assuming that the inner surface of the channel is oleophilic and, hence, is completely wetted by the continuous phase liquid. No-slip boundary conditions were adopted for the continuous phase liquid. In the simulations, we take into account the effects due to the addition of a surfactant by varying both interfacial tension and contact angle in the range 7mN/m to 4mN/m and 152^{O} to 172^{O}, respectively (Bashir et al. 2014). Hexahedral mesh with an element size of 2µm is adopted for all the 2D simulations. The mesh convergence analysis was done to achieve a residual level less than 0.001as mentioned above. We carried out simulations to determine droplet length by taking mesh elements of sizes 4µm, 2µm, and 1µm. It was seen that the difference in droplet length for a mesh size of 2µm as against 1µm was less than 0.001. Hence, all the simulations were carried out for mesh elements of size 2µm which corresponded totally to about 130,000 elements in each simulation run. The main channel length is kept sufficiently long for the flow to become fully developed.

2.5 Simulation Parameters for the liquids and the devices

All the investigations were carried out taking mineral oil as the continuous phase liquid and pure water as the dispersed phase liquid. Span 80 was used as the surfactant mixed into mineral oil at concentrations varying from 0 to 4%. The essential physical parameters of these three liquids are displayed in Table 2.1.

Table 2.1: Physical parameters of the liquids used in the simulations.

Liquids Used	**Viscosity(mPa.s)**	**Density (kg/m^3)**
Continuous Phase Liquid (Mineral Oil)	24.7	840
Dispersed Phase Liquid (Water)	1	998
Surfactant (Span 80)	1000	990

The microfluidic device used in our study is a “Slip Chip” device (Li et al. 2010). A typical Slip Chip device comprises of two plates, one having the channels (called the Channel plate) for the liquids to flow, and the other, having the micro-wells (called the well plate) for trapping the droplets. In the device, the two plates are bonded together using a temporary sealant such that the channels and the micro-well face each other. In the channel plate, the continuous phase liquid flows into the device through the “main channel” inlet and the dispersed phase liquid flows into the device through the “side-channel” inlet. The droplets of water, generated at the junction, move downstream along with the oil and depending on its velocity, they may get trapped in the micro-well in the well plate.

2.6 Parameters for Single T-junction device

A schematic of the Slip Chip device is shown below in Fig.2.2. The Channel plate has a single T-junction channel and a shallow circular Pit at one place along the main channel. The well plate has only a cylindrical micro-well. The broad-side view and the top view of the device are shown in Fig 2.2a and 2.2b, respectively. In a second device, the Channel plate contains only the T-shaped flow channel, and the well plate contains

the micro-well with a small pinhole close to it. The broad-side view and top view of the device are shown in Fig 2.2c and 2.2d, respectively.

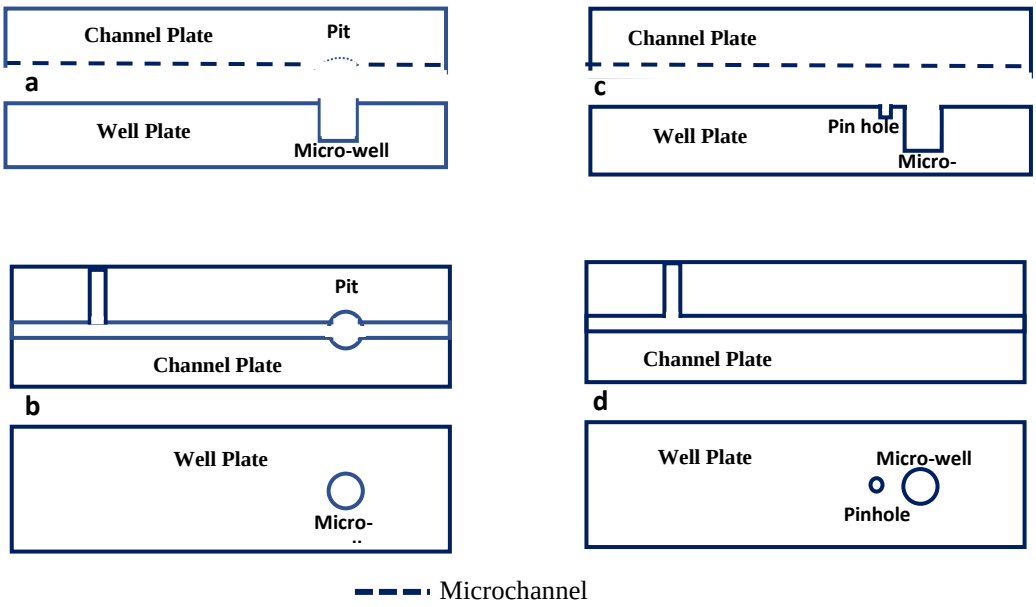

Fig 2.2: Schematic of the microfluidic device showing (a) the broadside view and (b) the top view of the device with the micro-well and the Pit. Schematic of a second device showing (c) the broadside view and (d) the top view of the device with the micro-well and the Pinhole.

The dimensions of the devices are displayed below in Table 2.2.

Table 2.2: Dimensions of microchannel investigated with a steady flow of two liquids (see Fig 2.3a)

Device	Microchannels	Width (W)	Length (L)	Height (H)
T-Junction	Side Channel	W_d = 100µm	L_d = 300µm	H = 50µm
	Main Channel	W_c = 100µm	L_c = 2000µm	

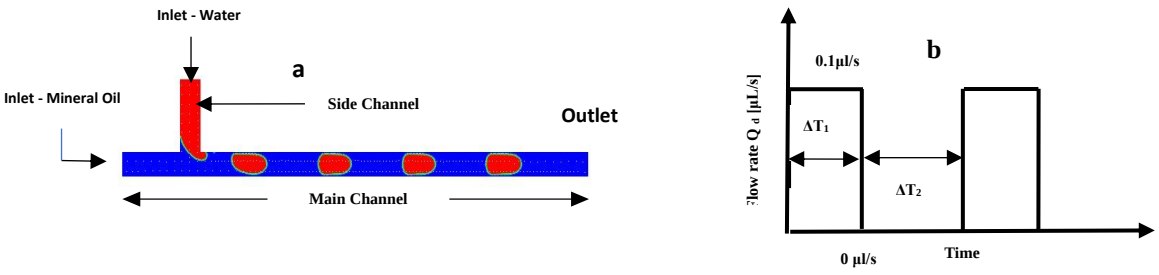

Fig 2.3: a) Schematic view of T-junction device. (b) The waveform for pulsed flow rate

Fig 2.3a shows the droplet pattern in a single T-junction device. Generation of droplets was investigated for (i) steady flow rates of the two liquids and (ii) for the steady flow of mineral oil but the pulsed flow of water. The pulsed waveform adopted for case (ii) is shown in Fig.2.3b. The flow rates employed in the simulations for case (i) are shown in Table 2.3 and that for case (ii) is shown in Table 2.4.

Table 2.3: Steady flow rates of two liquids used in the simulation (see Fig 2.3a)

Liquids Used	**Flow rate (µL/min)**
Continuous Phase Liquid (Mineral Oil)	0.25 - 1
Dispersed Phase Liquid (Water)	0.2

Table 2.4: Flow rates of the two liquids used in the simulations (see Fig 2.3a)

Liquids Used	**Flow rate (µL/sec)**
Continuous Phase Liquid (Mineral Oil)	Q_c = 0.2 (Steady flow)
Dispersed Phase Liquid (Water)	Q_d = 0.1 & 1 (Pulsed flow)

Table 2.5: Dimensions of T-junction devices investigated with the pulsed flow of dispersed phase liquid (see Fig 2.3a)

Device Types	**Microchannels**	**Width (W)**	**Length (L)**	**Height (H)**
Device 1 (D1)	Side Channel	W_d = 50µm	L_d = 300µm	H = 50µm
	Main Channel	W_c = 100µm	L_c = 2000µm	
Device 2 (D2)	Side Channel	W_d = 25µm	L_d = 300µm	
	Main Channel	W_c = 100µm	L_c = 2000µm	

Table 2.6: Pulsed parameters used in the simulations (see Fig 2.3b)

Pulse Parameters	**Duration (msec)**
ΔT_1	6.5 and 3.25
ΔT_2	6.5 and 13

The dimensions of the devices used for the simulation of droplet generation in the case of pulsed flow of water are displayed in Table 2.5 and these studies were carried out for pulse parameters shown in Table 2.6. The time duration mentioned in table 2.6 is

based on the droplet generation time for when the steady flow of Q_c = 0.2µl/sec and Q_d = 0.1µl/sec.

2.7 Parameters for Double T-junction device

Fig. 2.4 shows the schematic of the Double T-junction device. In this device, water enters the main channel (MC) through the two side channels SC1 and SC2. Mineral oil enters the main channel directly.

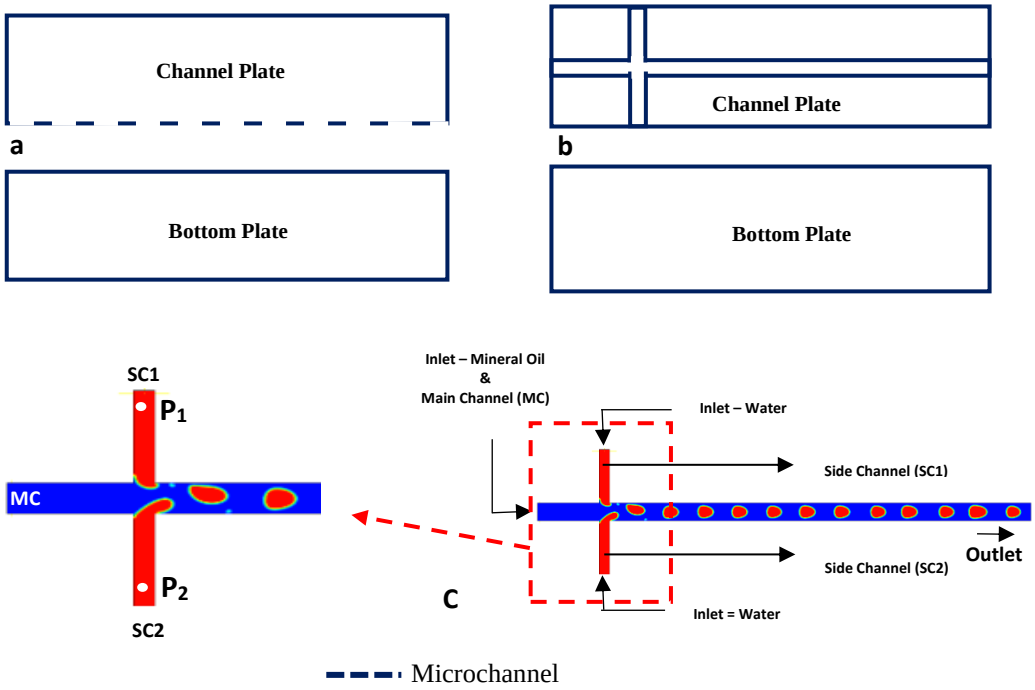

Fig 2.4: Schematic view of microfluidic double T-junction device showing a) the side view of the device, and b) the top view of the device. c) Droplet generation mechanism in Double T-junction device.

In this device, the micro-droplets are always generated in pairs due to the presence of the two side channels. The flow rates selected and dimensions of microchannels in the device are presented in Tables 2.7 and 2.8, respectively.

Table 2.7: Steady flow rates of two liquids used in the simulation (see Fig 2.4)

Liquids Used	Flow rate (µL/min)
Continuous Phase Liquid (Mineral Oil)	6
Dispersed Phase Liquid (Water)	3

Table 2.8: Dimensions of double T-junction device investigated with a steady flow of both liquids (see Fig 2.4).

Device Types	Microchannels	Width (W)	Length (L)	Height (H)
Device 1 (D1)	Side Channel	SC1 = 100μm	L_d = 300μm	H = 50μm
	Side Channel	SC2 = 50μm - 100 μm	L_d = 300μm	
	Main Channel	MC = 100 μm	L_c = 2000μm	
Device 2 (D2)	Side Channel	SC1 = 50 μm	L_d = 300μm	
	Side Channel	SC2= 50 μm	L_d = 300μm	
	Main Channel	MC = 50μm - 100 μm	L_c = 2000μm	

2.8 Parameters for Droplet Trapping

Simulation of the droplet generation, as well as its trapping in the same Program-run, requires large computation time. Hence, we studied the trapping mechanism separately by employing a 3D model for trapping. Trapping of microdroplets was investigated for devices of the geometry shown in Fig.2.2a and also Fig.2.2c. The Pit is aligned with the micro-well in the well plate. The diameter of the Pit and its alignment with the micro-well influence droplet trapping. The dimensions of the Pit and droplet length employed for the study are shown in Table 2.9.

Table 2.9: Diameter of droplet and Pit chosen for droplet trapping (See Fig 2.2a and 2.2b)

Pit Diameter (μm)	Droplet Length (μm)
20	200 and 100
40	
60	
80	
100	
140	
180	
200	

The dimensions of the pinhole and droplet length employed for the study are shown in Table 2.10.

Table 2.10: Length of the droplet and pinhole chosen for droplet trapping (See Fig 2.2c and 2.2d)

Pinhole Diameter (μm)	Droplet Length (μm)	Pinhole Diameter (μm)	Droplet Length (μm)
0	80	0	40
20		5	
30		10	
40		15	
45		20	
50		30	
55		40	
60			

2.9 Simulation Settings using ANSYS Software

The structure of the microfluidic device is created using the "Design Modeler" module with various rectangles and for the required dimensions. The completed design is then opened in the "Mesh" module. In this user interface, the mesh element size is set to 2μm, and various parts of the device are given user-defined names such as "inlet_oil, "inlet_water", "Outlet" and "Wall" which relate to the fluid inlets, outlet, and channel-wall, respectively. We choose hexahedral mesh as it is suitable for wall-bounded flow, and is computationally faster. These choices for the device design and mesh allow us to open the model through a fluent launcher for performing the simulation. In this launcher, we use parallel processing options with 2 cores, since the student version of the software used by us is restricted to 2 cores. The settings made on the fluent launcher open the fluent interface. In this interface, among the various options available, we chose the "pressure-based" solver, and time is kept "transient". Next, the multiphase solver model is chosen, and the volume of fluid (VOF) option is turned ON. In this window, we set "2" for the number of Eulerian phases, since we are dealing with two liquid phases in our problems. The implicit volume fraction is chosen with interfacial anti-diffusion to generate a sharp interface. The surface tension option is enabled. Further, we input the fluid properties such as viscosity and density for mineral oil and

water. We set mineral oil to be the primary phase and water to be the second phase. The boundary conditions are set as follows:

- The fluid velocity at the respective inlets is set for the flow rates mentioned in tables 2.3, 2.4, and 2.7. At the outlet, the normal outflow condition is selected.

- The surfactant concentration profile at the interface of the two liquids is generated by feeding in the appropriate value of surfactant concentration ranging from 0.2% - to 4%. The value provided relates to "α" in Eq.10 of Sec 2.2. We input the value of the diffusion coefficient of Span 80 in mineral oil from the available experimental data (Campanelli and Wang 1999). The change in the interfacial tension due to the increased surfactant concentration is taken into account through a user-defined function (UDF) written in C language. This generates the result of surfactant concentration across the interface in moles/liter.

- We use PISO (Ref Sec 2.3) scheme and, for the gradient behavior, we select the green gauss cell-based option. For the pressure and momentum selections, we choose PRESTO (Ref Sec 2.3) and second-order upwind, respectively. We initialise the simulation by considering first the mineral oil to pass through the device which wets the wall of the microchannel.

- The desired outputs such as velocity, pressure, and volume fraction are selected. The output data is saved at regular intervals of time. The time step for the computations is gradually reduced starting from 1msec till a global courant number below 0.2 is obtained. This was achieved for a time step size of 10μsec in our simulations. Depending on the required flow time, the number of time steps gets determined. The flow time of 0.5sec is achieved for 50000 number of time steps for the step size of 10μsec.

- The simulation runs approximately for 34 hours on the Laptop to achieve a flowtime of 0.5 sec using a dual-core processor (limitation of ANSYS Fluent student version). The

required results such as velocity vector, pressure, volume fractions, and associated graphs were plotted using the CFD post module.

CHAPTER 3

MICRODROPLET GENERATION AND TRAPPING BY STEADY FLOW OF TWO IMMISCIBLE LIQUIDS IN T-JUNCTION MICROFLUIDIC DEVICES.

3.1 Introduction

In this chapter, we present the results of simulation studies on droplet formation due to the continuous flow of two immiscible liquids in a T-junction microfluidic device. The two liquids employed for the studies are (i) mineral oil as the continuous phase liquid and (ii) water as the dispersed phase liquid. The two liquids flow with different but constant flow rates Q_c, for mineral oil, and Q_d, for water. Droplet generation is investigated for varying values of Q_c and Q_d to confirm the scaling law for normalised droplet length as a function of the flow rate ratio. The range of flow rates enables us to investigate the generation of droplets in (a) the squeezing regime, (b) the dripping regime, and (c) the squeezing-to-dripping transition regime. To understand the dynamics of the pinch-off process of the droplets at the T-junction, we have studied the variation of the pressure with time in both water and mineral oil at points close to the junction. We have carried out simulation studies on the role of surfactants in droplet generation by investigating (i) the variation of droplet length as a function of surfactant concentration and (ii) the temporal variation of pressure in the two liquids at different surfactant concentrations. The surfactant used in the studies was Span-80.

A second important study reported in this chapter is the trapping of the water droplets of different lengths in a micro-well. Trapping of droplets is investigated as a function of the flow rate of mineral oil, which is also the speed of the droplets in the flow channel. The effect of a Pit, as an additional structure in the flow channel, on the trapping process was studied. The effect of surfactant on the trapping process was also studied. A comparison of our results with some results reported earlier is included.

Microdroplet generation in microfluidic devices depends mainly on Capillary Number C_a defined as the ratio of viscous forces to interfacial forces. The capillary number also changes if the dimensions of the microchannel are changed (Gupta and Kumar 2010b).

The value of the capillary number determines the mechanism for droplet generation. The mechanism called squeezing occurs at low values of C_a. In this mechanism, the dispersed phase liquid, in our case it is water, flows in from the side channel into the main channel, thereby partially blocking the flow of the continuous phase liquid, i.e., mineral oil. When the dispersed phase liquid enters the main channel (in which continuous phase liquid already flowing), and it starts to grow until it blocks the junction. At this stage, the shear stress exerted by the continuous phase is not enough to produce a detachment of the drop. The blockage created by the plug increases the pressure upstream of the emerging droplet and leads to squeezing of the neck of the immiscible thread. Hence, this mechanism is called the Squeezing regime (Garstecki et al. 2006). The squeezing process continues till it leads to the generation of a droplet. This process repeats and train of droplets are produced.

If the value of C_a is increased, a new mechanism, called Dripping, causes the generation of the droplet. In this mechanism, he shear force exerted by the flowing mineral oil is sufficiently strong to overcome the interfacial tension and pull-out droplets from the water column at the junction. It may be noted that, in the dripping regime, the water column blocks the path of mineral oil to a very limited extent, whereas, in the squeezing regime the blocking process is significantly larger. The state between the squeezing and dripping regime is known as the Transition regime.

With further increase in Ca, the water droplets will be generated in what is called Jetting regime, wherein the water droplets are generated well away from the T-junction. In this mechanism, the formation of droplets from the protruding dispersed phase liquid occurs due to a capillary instability which is responsible breaking of the jet. Thus, the water column entering the main channel continues to flow as a continuous stream, parallel to the mineral oil stream, to quite some distance downstream before breaking into a train of microdroplets. These droplets then move further downstream.

Microdroplet generation in a T-junction device was first demonstrated by Thorsen et al. (2001). In the device, water droplets were produced in various oils such as decane, tetradecane, and hexadecane with the addition of surfactant (Span 80). The water

droplet length seems to decrease with an increase in the flow rate of oil in a device made of PMMA (Nisisako et al. 2002). The same device failed to produce oil droplets in water as PMMA (Polymethyl methacrylate) is hydrophobic and oil wets its surface. Water droplets were generated in tetradecane with the addition of Span 80 (Dreyfus et al. 2003). In this study, it was shown that the contact angle of water increased with surfactant concentration. The recirculation flow field inside the droplet was studied by (Nguyen et al. 2006). When the dispersed phase liquid enters the main channel in which continuous phase liquid is already flowing, it forms a plug in the main channel and keeps growing until it partially blocks the junction. This happens mainly due to the excess pressure in the side-channel through which the dispersed liquid flows in. During this process, growth of the plug is determined by (i) the fluid pressures in the main and side channels, (ii) interfacial tension and, (iii) the shear stress due to the flowing continuous fluid. As the plug grows, the shear stress becomes smaller and beyond a certain limit it can no longer balance the fluid pressure in the side channel. This leads to the formation of a "neck" at the T-junction. This mechanism is called Squeezing regime (Garstecki et al. 2006). The squeezing process continues till it leads to the generation of a droplet. This process repeats and train of droplets are produced. Further, it was shown that the pressure in the main channel increases with the droplet size. The droplet generation in the squeezing and dripping regimes depend on the competition between shear stress and interfacial tension. This was demonstrated through simulation studies using the phase-field model (Menech et al. 2008) and the Lattice Boltzmann method (LBM) (Gupta et al. 2009; Liu and Zhang 2009). It was observed that the size of the droplet reduced with the increase in the concentration of surfactants like SDS and tween 20 (Wang et al. 2009a). The droplet generation mechanism also depends on the channel geometry and dimensions (Gupta and Kumar 2010a; Steijn et al. 2010).

To gain a better understanding of the droplet generation mechanism the temporal variation of pressure during the droplet generation was studied in squeezing, dripping, and jetting regimes (Yan et al. 2012). Glawdel et al. (2012) investigated droplet formation in a squeezing to the dripping-transition regime. Further, they proposed a theoretical model for the estimation of the size of droplets produced in different regimes. This was shown to be in close agreement with their experimental results.

Experiments were also conducted to generate oil droplets in water using a T-junction device (Carrier et al. 2014). The influence of viscosity of both the immiscible liquids on droplet generation was studied (Nekouei and Vanapalli 2017) and a theoretical model was presented to predict the droplet length.

Depending on the solubility, surfactants are used in any one of the two liquids to avoid droplets from coalescing in the vial. The addition of surfactant reduces the interfacial tension (Tadros 2013). This results in a reduction in droplet length but an increase in the frequency of droplet generation (Peng et al. 2011) for a constant mass flow rate. The concentration of surfactants such as SDS (sodium dodecyl sulphate) or Tween 20 added to silicon oil has been experimentally studied, wherein the interfacial tension was evaluated by recording the droplet generation using a high-speed camera (Wehking et al. 2014). Further, based on their study an analytical model was formulated to determine the interfacial tension due to increased surfactant concentration. The influence of Span 80 on water droplet generation in mineral oil was investigated (Bashir et al. 2014). This study focuses on changing surface wetting conditions due to the addition of surfactants and the reduction in droplet length with an increase in capillary number and surfactant concentration. Most of these experimental studies consider the uniform distribution of surfactant molecules at the droplet interface and focus on the influence of surfactant and its increasing concentration on both size and frequency of droplet generation in various regimes. Numerical simulations were carried out to study the effect of surfactant concentration at the droplet/bubble interface (Bastani et al. 2018). The effect of surfactant (Span 80 mixed with octane) on droplet generation was numerically investigated using the Lattice Boltzmann Method by Riaud et al. (2018). This study uses two computational models to present a uniform and non-uniform distribution of surfactant at the interface. The model adopted for the non-uniform distribution of surfactant explains the droplet generation mechanism which was experimentally demonstrated (Wang et al. 2016). Using numerical simulations it was observed that the frequency of droplet generation increases when interfacial tension is reduced (Han and Chen 2019a).

To capture individual microdroplets for further analysis, trapping the generated droplets in an array of micro-wells is convenient. It was shown that surface energy-based trapping is achieved by proper choice of the geometry of the device and the micro-wells (Abbyad et al. 2011; Dangla et al. 2011). In this device, a pinhole is made in the microchannel. When the hydrodynamic drag force is less than the force due to the surface energy gradient, the droplet gets anchored to the pinhole and partially enters the pinhole. The effect of surface energy change leading to trapping was numerically studied (Nagel et al. 2014). Further, the change in Laplace pressure of droplets entering the pinhole was also determined. The critical capillary number at which droplet anchoring happens was determined for different liquids (Amselem et al. 2015). The anchoring of a single droplet to a pinhole was studied using Lattice Boltzmann Method (Liu and Zhang 2017). This study demonstrates that the anchoring efficiency increases with an increase in the diameter of the micro-well.

3.2. Effect of Surfactant on Droplet Generation:

During the droplet formation process, when the dispersed phase liquid (water) enters the main channel, it progressively blocks the flow of the continuous phase liquid (Oil) leading to an increase in the pressure at point P_c (Fig 3.1). It reaches a peak value and decreases sharply to a very low value which indicates the release of one droplet (Fig 3.2d to 3.2f). This process repeats periodically leading to the generation of multiple droplets at a definite frequency. It has been shown that at low liquid flow rates, the droplet generation occurs due to the Squeezing mechanism, and at somewhat higher flow rates the generation occurs due to the dripping mechanism (Garstecki et al. 2006). There is a gradual transition from the Squeezing regime to the Dripping regime as the flow rates are increased. We have investigated droplet generation in the transition regime also by simulation. Each simulation is carried out for a total liquid flow duration of 0.5 Sec.

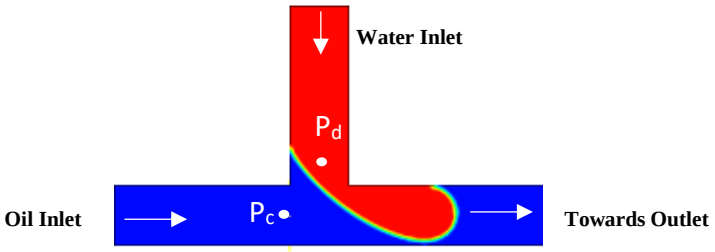

Fig 3.1: Location of pressure measuring points P_d and P_c in dispersed phase and continuous phase liquids respectively.

The interfacial tension between mineral oil and water is taken to be 24.5mN/m (Kagawa et al. 2014) in the absence of surfactant. Droplets of lengths 296µm, 228µm, and 192µm are generated in the squeezing regime as shown in fig 3.2a, 3.2b, and 3.2c, for the varying Q_c= 0.25µl/min, 0.5µl/min and 1µL/min, respectively and fixed Q_d= 0.2µL/min. At these flow rates, the time variation of pressure at point P_c is shown in Fig 3.2d to 3.2f and it is seen to reach a peak value of 526Pa, 573Pa, and 690Pa for the different Q_c values.

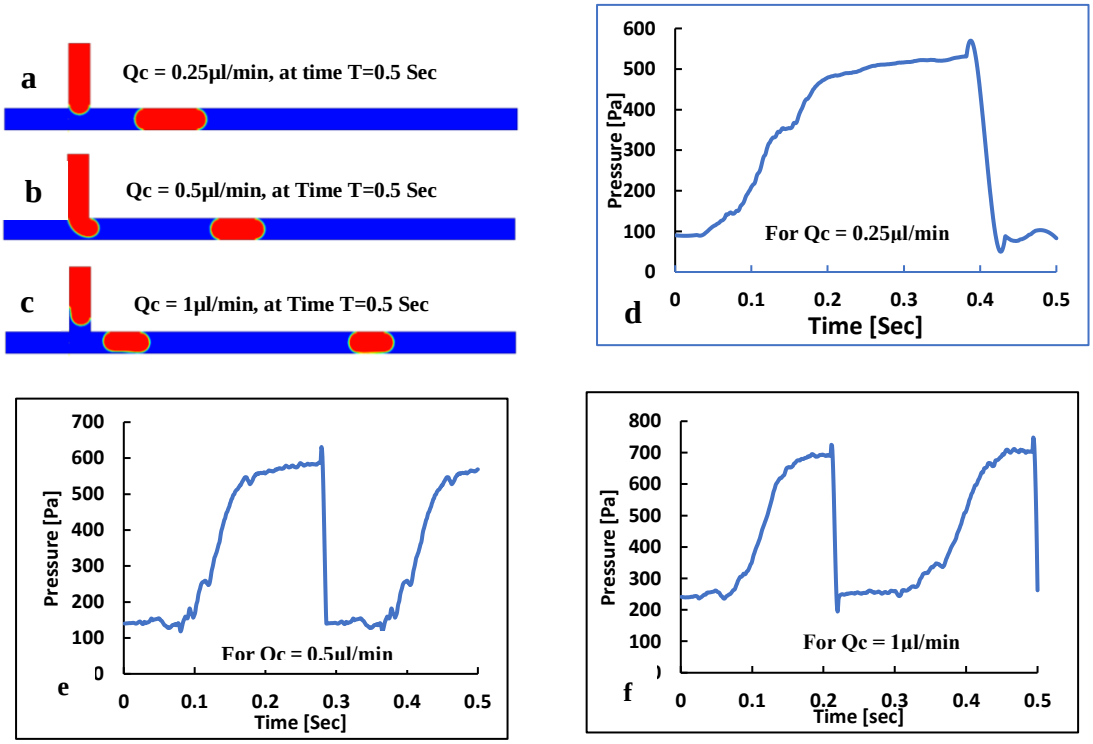

Fig 3.2: Droplet generation for different flow rate of continuous phase liquid without the surfactant at fixed value of Qd = 0.2µl/min. a) Qc= 0.25µL/min. b) Qc= 0.5µL/min c) Q_c = 1µL/min, (d-f) Pressure versus time at point P_c for Q_c values as in a-c respectively

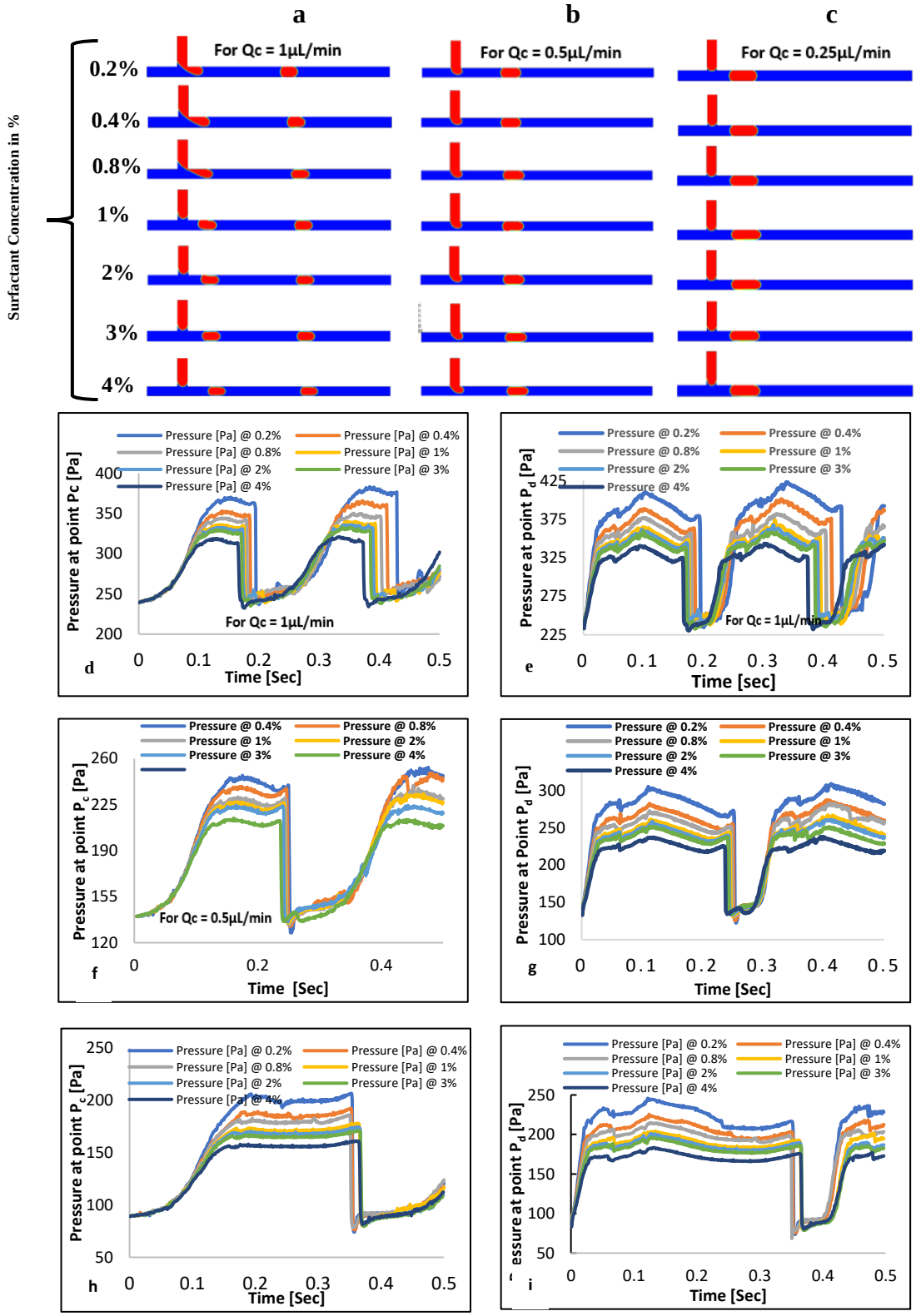

Fig 3.3: Droplet generation sequence and pressure versus time plots for various surfactant concentration (weight %) at a fixed value of Q_d at 0.2µl/min and changing Q_c a) Q_c = 1µL/min. b) Q_c = 0.5µL/min c) Q_c = 0.25µL/min, for a total flow time of 0.5Sec.; Pressure versus time at point P_c and P_d, respectively, for (d,e) Q_c = 1µL/min; (f,g) Q_c = 0.5µL/min and (h,i) Q_c = 0.25µL/min.

The rise time T_R of the pressure profile is estimated to be 0.115sec, 0.072Sec, and 0.067Sec for the flow rate values Q_c = 0.25µL/min, 0.5µL/min, and 1µL/min, respectively. The corresponding fall time T_F for all flow rates were found to be about 0.003Sec. The long rise time indicates a slow initial growth of the droplet and the much smaller fall time implies a very quick pinch-off leading to the release of the droplet. Fig.3.2c shows that at higher flow rates of Q_c, the droplet generation frequency increases. The pressure at point P_c attains a peak value just before the release of the droplet. In general, the pressure at point P_c increases with an increase in the flow rate Q_c(Abate et al. 2012; Menech et al. 2008).

The addition of a surfactant has been shown to alter the droplet size and the droplet frequency (Kovalchuk et al. 2018). Fig 3.3 shows the droplet generation using oil (continuous phase liquid) containing surfactant with concentrations varying from 0.2% to 4% by weight for different values of Q_c, keeping Q_d fixed at 0.2µl/min. Fig 3.3a shows droplet for flow rate Q_c = 1µl/min for different surfactant concentrations. At this flow rate, the addition of a surfactant results in a reduction of the maximum pressure at point P_c from 690 Pa to 352 Pa for a surfactant concentration of 0.2%, which further reduces to 329 Pa when the concentration is increased to 4% (Fig 3.3d). Similar trend is seen for Q_c = 0.5µl/min and 0.25µl/min as evident from 3.3f and 3.3h. The pressure at point P_d also shows a similar reduction as the concentration increases from 0.2% to 4% (Fig 3.3g and 3.3i). We may also conclude from Fig 3.3 that with increasing surfactant concentration the droplet length decreases monotonically and the droplet generation frequency increases. Fig 3.3 (d-i) also indicates that the droplet generation frequency increases as the flow rate of Q_c increases. Further, it is seen that the rise time of the pressure profile at point P_d is much shorter than that for the pressure profile at point P_c, whereas the fall time is practically the same for both cases. This indicates that the dispersed phase liquid relaxes to its initial state very fast after the droplet is released.

Table 3.1: Droplet release time based on the flow rate of oil (Q_c) at fixed Qd = 0.2µL/min.

Flow Rate Q_c	0.2µL/min	0.5µL/min	1µL/min
Droplet formation time	0.35 Sec	0.17 Sec	0.08 Sec

Table 3.2: Effect of surfactant concentration on droplet length & maximum pressure at points P_d and P_c

Flow rate Qc	No Surfactant			Surfactant Concentration 0.2%			Surfactant concentration 4%		
	Droplet Length in µm	Pressure at P_c in [Pa]	Pressure at P_d in [Pa]	Droplet Length in [µm]	Pressure at P_c in [Pa]	Pressure at P_d in [Pa]	Droplet Length in [µm]	Pressure at P_c in [Pa]	Pressure at P_d in [Pa]
1µl/min	192	690	820	160	352	393	148	329	322
0.5µl/min	228	573	690	200	237	282	196	218	220
0.25µl/min	296	526	610	268	199	208	268	155	166

The plateau in the pressure profiles is longer for the pressure plots at point P_d compared to that for the plots at point P_c. The duration corresponding to the plateau in the pressure plots at point P_d may be taken to be the duration required for the formation of the droplet as shown in Table 3.1. The results of the pressure change are summarised in Table-3.2.

The droplets were generated for a fixed value of Q_d = 0.2µL/min and varying Qc = 0.2µL/min to 2µL/min. This study was repeated for surfactant concentrations ranging from 0% to 4%. The droplet length reduces significantly for low Q_c values and acquires a minimum value as Q_c increases to higher values as shown in Fig 3.4a. The variation of L/w, the dimensionless droplet length, with the flow rate ratio Q_d/Q_c is shown in Fig 3.4b. The linear scaling of L/w with flow rate ratio is specific to the range $0.01 < Q_c/Q_d < 0.1$ (Garstecki et al. 2006).

We have computed the surfactant concentration profile at the droplet interface. The surface density of the surfactant is higher at the two poles of the droplet than at the flat parts adjacent to the channel walls. It is a little higher at the front pole of the droplet as compared to that at the rear which is in confirmation by the results of Riaud et al 2018. The variation of the surfactant concentration at the front pole of the droplet is shown in Fig.3.4c to 3.4f, for bulk surfactant concentrations of 0.2%, 1%, and 4%. The entire droplet surface is covered by a thin layer of surfactant molecules since the adsorption of these molecules is much faster than the droplet formation time. Once the droplet is released, it is seen to conserve its volume and shape till it reaches the micro-well where

it may be trapped. The presence of surfactant is seen to influence the trapping of the droplet.

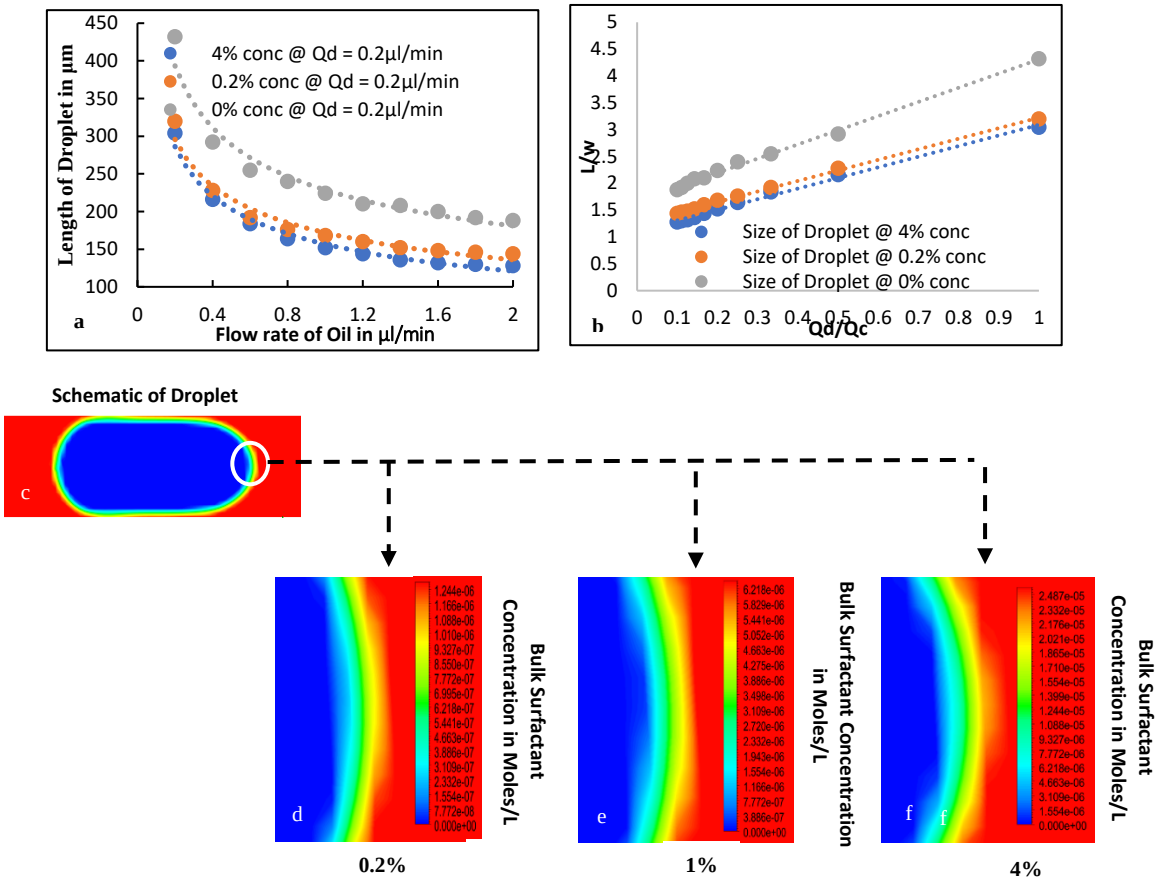

Fig 3.4: a) Droplet length versus flow rate of oil (for fixed Q_d = 0.2µl/min). b) Dimensionless droplet length (L/w) versus flow rate ratio. c) Surfactant concentration profile (in moles/litre) at the front pole of the droplet (oil is shown in red and water in blue colour). d-f) interface of the droplet for concentration 0.2%, 1% and 4% respectively.

The surfactant concentration also influences the velocity field vector in the dispersed phase liquid. It shows a recirculation pattern during the droplet generation process (Fig 3.5). In the case of Q_c = 0.25µl/min, there is no significant change in the velocity field vector with increased surfactant concentration with time t = 50msec to 200msec.

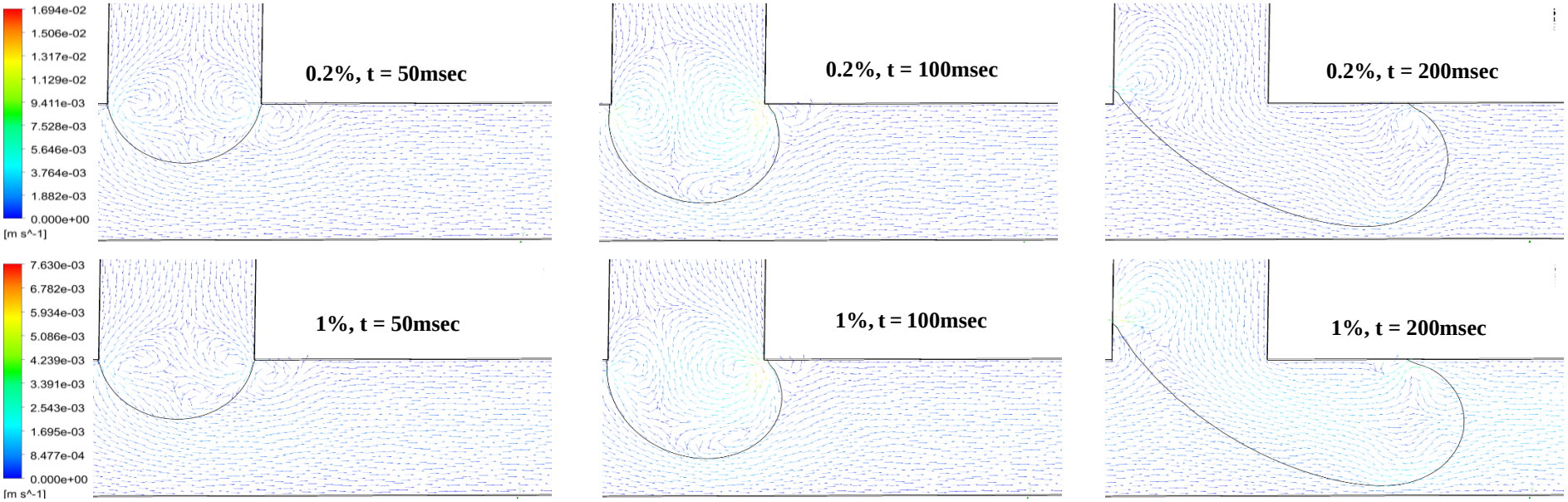

Fig 3.5: Influence of surfactant at various concentration on velocity vector profile in the dispersed phase liquid during the droplet formation process at a fixed value of Q_d at 0.2µl/min and Q_c = 0.25µL/min.

3.3 Droplet Trapping

In the simulations, we monitored the dynamic change in the droplet shape to get a better understanding of the trapping conditions (Dangla et al. 2011). The surface energy of the droplet reduces by modifying the geometry of the straight microchannel. The droplet reduces its size when it enters the shallow Pit in the microchannel.

The droplet length depends on the flow rate ratio of the two liquids. In our studies, the droplet length ranged from 70µm to 200µm. This compares well with previous experimental data (Bashir et al. 2014). Hence, for trapping studies, we consider droplets of lengths 200µm, 100µm, and 50µm (A A' in Fig 3.6f). It is seen that beyond a certain velocity the droplets do not get trapped. We define the maximum droplet velocity at which the trapping happens as the critical trapping velocity. In addition to droplet length, we have also investigated the dependence of trapping on the micro-well depth (200µm, 150µm, and 50µm) and the alignment of the two plates of the Slip-Chip device. In the 3D simulation, the velocity U_c of the continuous phase liquid was initially set to 1mm/s. The droplet is transported by the continuous phase liquid and, thus has the same velocity U_c. Simulations were repeated for increasing values of U_c until the critical trapping velocity is reached. Normal outflow boundary conditions were set at the outlet. The simulations were repeated for different micro-well alignments (100%, 75%, 50%, 25%, 0%) with the channel plate as shown in Fig.6a-e.

After its release at the T-junction, a droplet acquires an elongated pancake shape due to the rectangular cross-section of the main channel in our device; we shall call such a droplet to be a "Plug". The surface energy of the droplet is given by $E = \gamma A$, where γ is the interfacial tension and A is the surface area of the droplet. Since the Plug is not spherical, its surface energy is larger. As the droplet enters the micro-well, meant for trapping it, the droplet encounters the micro-well as well as the Pit in the two plates of the device. Here the droplet spreads into the circular micro-well and the Pit and acquires a shape such that its surface energy reduces. This change in surface energy over the spatial region of the micro-well leads to an attractive force on the droplet proportional to the gradient of the surface energy. This mechanism is shown to be responsible for

the trapping of the droplet (Dangla et al. 2011). We have studied the trapping of a single microdroplet into the micro-well for different flow rates Q_c in the presence of surfactants. The droplets experience lower shear stress in the region where the micro-well is located (Li et al. 2009). We have studied the trapping of droplets of different lengths (200µm and 100µm) in the micro-well under the influence of the pit. To understand the trapping mechanism better we have varied the diameter of the pit, its alignment with the micro-well, and the depth of the micro-well in the simulations. Fig.3.6 (a-e) shows the alignment of the micro-well and the Pit. Fig.3.6 (f and g) illustrates the top view and the side view of the device geometry adopted for the simulations.

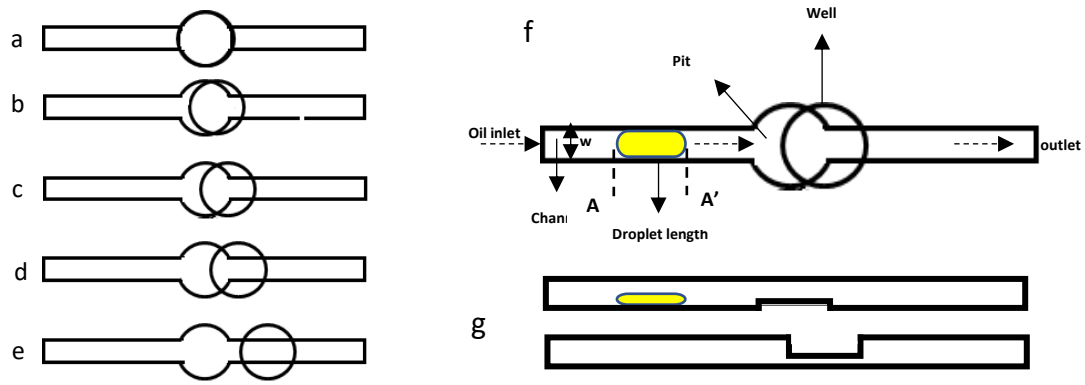

Fig 3.6: Top view of the microchannel geometry with the micro-well shown as a full circle and the Pit with the channel. The different extents of alignment of the micro-well and the Pit are, a) 100% alignment b) 75% Alignment c) 50% alignment d) 25% alignment and e) total misalignment; f) Top view of the droplet in the channel; g) Broadside view of the droplet in the channel.

Fig 3.7 shows the change in the shape of the droplet (plugs) of different lengths due to the Pit as they get close to the micro-well. For the different extent of alignment between the micro-well and the Pit, as shown in Fig 3.7(a-e), the change in the shape of the droplets is more for larger alignment. This change in shape is such that the surface energy of the droplet gets reduced and this contributes to the trapping of the droplet in the micro-well. In these simulations, the diameters of the micro-well and the Pit are both taken as 200µm.

In the case of droplet length of 200µm, we have investigated the trapping of droplets for different Pit diameters keeping the micro-well diameter as 200µm, micro-well depth as 200µm, and for perfect alignment of the Pit with the micro-well. We varied the

diameter of the Pit from 200µm to 20µm, the flow velocity U_c of oil from 3mm/s to 10mm/s, and the bulk surfactant concentration in oil was kept at 4%.

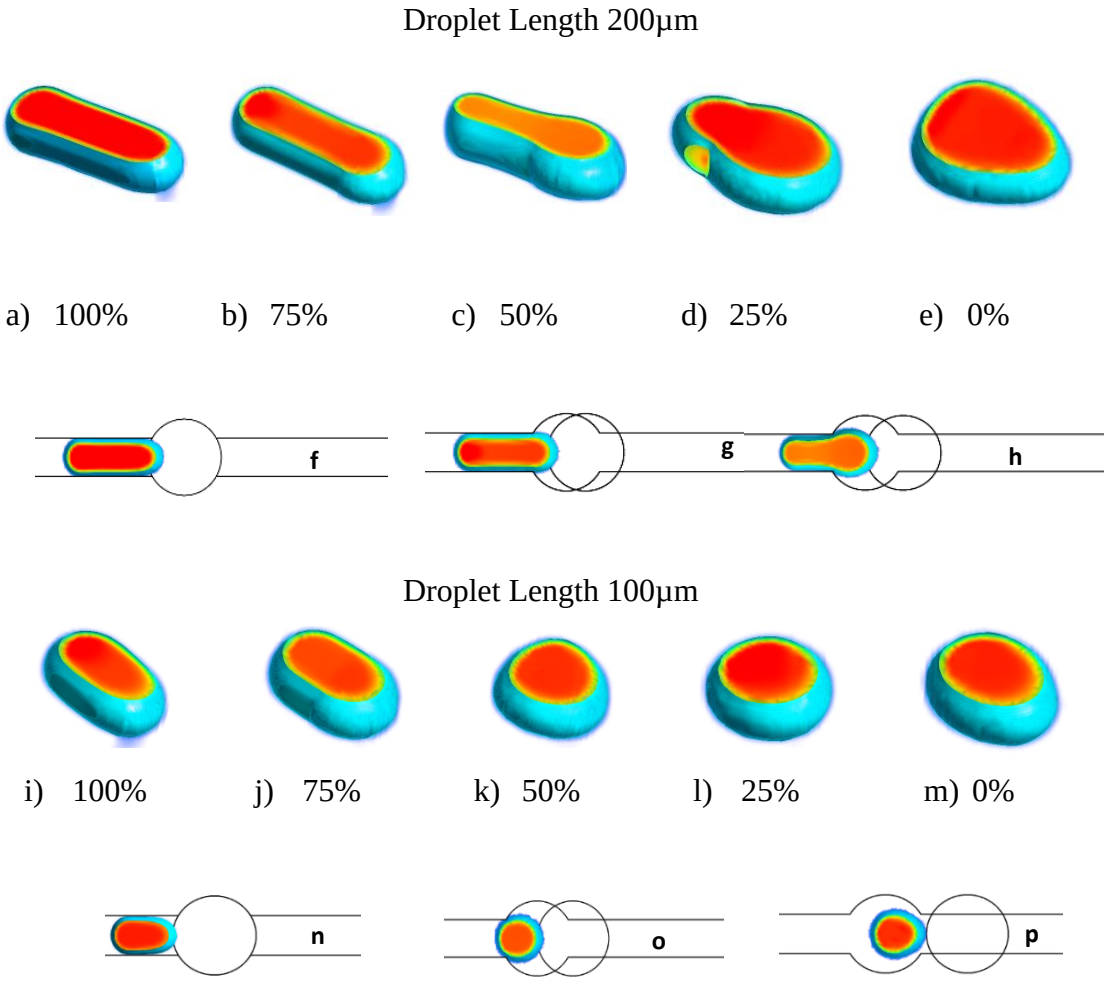

Fig 3.7: a-e) Shape of the droplet of different lengths just before entering the micro-well, for different Pit-Micro-well alignments. f-h) Top View of droplet motion (length 200µm) in microchannel before entering the Micro-well, f) 100% alignment, g) 75% Alignment h) 50% alignment. (i-m) The shape of the droplet (length = 100µm) just before entering the micro-well, for different Pit-Micro-well alignments. n-p) Top View of droplet motion (length 100µm) in microchannel before entering the micro-well, n) 100% alignment o) 50% alignment p) 0% alignment.

Our simulations reveal that the droplet is trapped in the micro-well only if the flow velocity U_c is less than a critical value U_{cr}. The droplet becomes spheroidal in shape as it gets into the micro-well and its surface energy is also lowered. Thus, we conclude that when the flow velocity exceeds U_{cr} the viscous drag force on the droplet overcomes the force due to the surface energy gradient, which anchors it to the micro-well. Consequently, the droplet gets out of the micro-well and moves downstream with the

oil. The value of U_{cr} is seen to depend on the bulk surfactant concentration. For a Pit diameter in the range of 20μm to 100μm and surfactant concentration of 4%, the droplet is seen to get trapped in the micro-well for oil flow velocity $U_c < U_{cr} \sim 4.5$ mm/s and at a higher flow velocity, it escapes from the micro-well. The simulations also reveal that, before the droplet moves out of the micro-well, a few tiny water droplets break away from it and move downstream. When the Pit diameter is increased beyond 100μm (the width of the channel) the critical velocity increases to ~ 7.3mm/s. This may be ascribed to the change in the geometry of the micro-well-pit combination in the device for Pit diameter > 100μm. Without surfactant, the critical velocity is seen to be > 15mm/s. Thus, surfactants cause a significant reduction in the critical velocity for trapping.

The trapping of droplets is seen to depend on the depth of the micro-well. To study this aspect we carried out simulations on droplet trapping for micro-well depth ranging from 200μm to 50μm keeping the flow velocity U_c constant at 4mm/s and micro-well and Pit diameter at 200μm. The alignment of the micro-well and the Pit was kept at 100% and 50%. Droplet trapping occurred only if the micro-well depth was above 100μm irrespective of the micro-well-Pit alignment. We also studied the role of the alignment of the micro-well with the Pit, keeping the micro-well and Pit diameter and the micro-well depth at 200μm. For flow velocities $U_c < U_{cr}$ the droplets are invariably trapped, but for higher flow velocities the droplets do not get trapped irrespective of the extent of alignment. For flow velocity of oil $U_c = 7$mm/s which is close to $U_{cr} \sim 7.3$mm/s, the simulations reveal that the droplet gets trapped if the micro-well-Pit alignment is < 50% and does not get trapped for alignment > 80%. For alignment between 50% and 80%, the droplet is just trapped and several small daughter droplets break off from the main droplet and travel downstream. This confirms the conclusion that close to the critical velocity for droplet trapping, the escape of the droplet from the micro-well is preceded by the generation of several tiny daughter droplets.

In the case of droplet length of 100μm, U_c is varied between 1mm/sec to 12mm/s. The droplet experience lesser drag force (as compared to droplet length of 200μm) due to the reduced surface area for different pit-micro-well alignments. The change in the surface area is shown in Fig 3.7i-m. The reduced surface energy shows that the droplet

is trapped if U_c is less than 1.3mm/s, 5mm/s, 6mm/s, and 10mm/s for Pit-micro-well alignment of 100%, 75%, 50%, and 25% respectively when the micro-well depth is 200µm. This reduces to 3mm/s, 5mm/s, and 6mm/s for alignment of 75%, 50%, and 25% respectively when the micro-well depth reduces to 150µm.

3.4. Conclusion

We have carried out numerical simulations to investigate the influence of surfactants on droplet generation and trapping in a T-Junction microfluidic device for capillary numbers ranging from 0.0028 to 0.02 using the VOF method in ANSYS Fluent software. This range of the capillary number corresponds to the squeezing regime and the Squeezing-to-Dripping transition regime for droplet generation.

Our simulations reveal that in the presence of surfactants the length of the droplet reduces from 192µm to 148µm, 228µm to 196µm, and 296µm to 268µm when the surfactant concentration is increased from 0% to 4% for Q_d / Q_c = 0.2, 0.4 and 0.8, respectively. The frequency of droplet generation is 4.54 Hz, 3.33 Hz and 2.38 Hz for (Q_d / Q_c) = 0.2, 0.4 and 0.8, respectively. Thus, as the flow rate, Q_c increases the droplet generation frequency increases significantly. Our simulations also indicate that a rise in the concentration of surfactant by 4%, increases the frequency of droplet generation by 16% at the higher capillary number (C_a = 0.02), whereas there is only a marginal, or no change, in the squeezing regime (C_a = 0.0028 – 0.008).

The 3D simulations on droplet trapping show that to successfully trap the droplet in a micro-well, various factors such as droplet length, its velocity, dimensions of the Micro-well and the Pit, and alignment of the micro-well and the Pit, are important. It is seen that a droplet of a length of 200µm gets trapped in the micro-well, of volume more than twice the volume of the droplet, if the droplet velocity in the channel exceeds a critical velocity for trapping. The critical velocity U_{cr} depends on the geometry of the micro-well-Pit combination. For a micro-well having fixed dimensions (200µm diameter and 200µm depth), the critical velocity for trapping remains almost constant (4.5mm/s) for a Pit diameter smaller than the channel width. For a Pit diameter larger than the channel

diameter, the critical velocity increases significantly (~7.3mm/s). More significant than this is the fact that the critical velocity in the absence of a surfactant is ~ 18mm/s. The surfactants cause a drastic change in the droplet trapping mechanism. Further, droplet trapping is seen to depend on the depth of the micro-well for fixed values of the other device parameters. The droplets get trapped only when the micro-well depth is more than the channel width, irrespective of the extent of Micro-well alignment with the Pit.

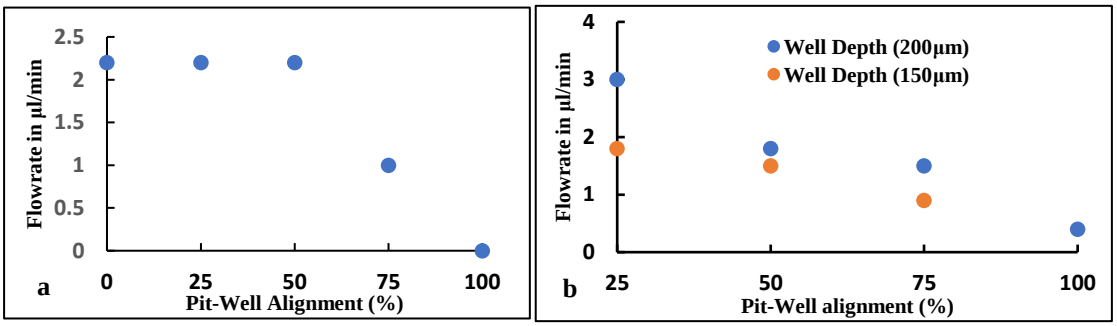

Fig 3.8: Flowrate versus trapping for various Pit-well alignment (%). a) for droplet length 200µm and b) for droplet length 100µm

If only the micro-well alignment with the Pit is changed from 0% to 100%, keeping all other parameters fixed, it is seen that, for droplet velocity U_c lower than the critical velocity U_{cr}, the droplet invariably gets trapped in the micro-well. For $U_c > U_{cr}$, the droplet does not get trapped irrespective of the alignment. Very interestingly, if Uc is close to U_{cr}, it is seen that the droplet gets trapped if the Micro-well-Pit alignment is less than 50% and does not get trapped for alignment above 75%. For alignment between 50% and 80%, the droplet gets trapped, but several tiny droplets emerge from the main droplet and flow downstream. The trapping of droplets are summarised via the graphical representation as shown in Fig 3.8. Thus, the escape of the droplet from the micro-well is often preceded by the release of tiny daughter droplets. Our simulation studies have revealed that micro-droplet generation and trapping is a complex phenomenon depending on the device dimensions, liquid properties, surfactant properties, and liquid flow parameters. For an efficient generation of micro-droplets for a specific application, a detailed simulation of the process is essential.

CHAPTER 4

MICRODROPLET GENERATION AND TRAPPING BY PULSED FLOW OF DISPERSED PHASE LIQUID IN T-JUNCTION MICROFLUIDIC DEVICES.

4.1. Introduction

In this chapter, we present the results of simulation studies on droplet formation by pulsing the flow of dispersed phase liquid while the flow rate of continuous phase liquid is held constant. The two liquids employed for the studies are (i) mineral oil as the continuous phase liquid and (ii) water as the dispersed phase liquid. Two different T-junction devices are considered in the study. In both devices, the width of the main channel is the same. The width of the side channel in the first device is half the width of the main channel and that in the second device is one-fourth the width of the main channel (Table 2.5). First, the scaling of dimensionless droplet length with the ratio of the flow rates of the two liquids is confirmed for a steady flow of the two liquids. The plot of normalised droplet length as a function of flow rate ratio (Q_d/Q_c) for both the devices is shown to be similar to results reported in the past. This study facilitated the investigation of droplet generation in the jetting regime. Typically, in the jetting regime, the droplets are generated away from the T-junction. A rectangular pulse waveform was selected to modulate the flow of the dispersed phase liquid. The pulse parameters such as ΔT_1 (when liquid flows: ON state) and ΔT_2 (when liquid does not flow: OFF state) are varied according to Table 2.6. To get an insight into the droplet generation mechanism at the T-junction device, the variation of pressure in the dispersed phase liquid with time close to the junction was studied. The droplet generation was investigated for varying concentrations of a surfactant (Span 80).

Another important study reported in this chapter is the trapping of pancake-shaped and spherical microdroplets in a micro-well. Trapping of droplets is investigated as a function of the flow speed of mineral oil, the continuous phase liquid, which is also the speed of the droplets in the main channel. The effect of a Pinhole, located in the main channel, on the trapping process was investigated. The effect of surfactant on the trapping process was also studied.

One of the major advantages of generating the droplet by pulsing the dispersed phase liquid is that it ensures optimum use of liquids, thereby reducing the costs. The flow of the dispersed phase liquid is controlled by using commercially available microvalves at the inlet of the side channel through which it flows into the device. It was first demonstrated by Lin et al in 2008, that the generation of droplets of different volumes can be achieved by controlling the inlet pressure of the dispersed phase liquid and the duration for which the valve was kept open (Lin and Su 2008). In such devices, both pneumatic and electromagnetic microvalves were used (Churski et al. 2010). Piezoelectric microvalves have been used to produce droplets of nanolitre to picolitre volumes at frequencies ranging from 20Hz to 400 Hz (Jakiela et al. 2014). The microvalves are usually operated in the pulsed mode by adopting standard pulse waveforms such as rectangular, triangular, and sinusoidal forms. In a recent study, it has been shown that the use of rectangular voltage waveforms for operating the microvalves leads to better control of the droplet volume (Qian et al. 2019). Very recently, the generation of water droplets in FC-40, using surfactants such as 1H,1H,2H,2H-perfluoro-1decanol, and PEG-Krytox was studied. It was observed that the flow velocity of the droplet increased by 25% due to the addition of surfactant, which was exploited to control the distance between the droplets and also for an on-demand merging of two droplets (Ferraro et al. 2018). The use of surfactants such as Picosurf-1 in such a device has been shown to stabilize the generated droplets and improve the wetting of the main channel walls of the device (Totlani et al. 2020).

The trapping of microdroplets in an array makes it convenient for chemical/biological investigations. Several mechanisms have been explored to trap the droplet in a micro-well based on the surface energy of the microdroplet (Dangla et al. 2011), Laplace pressure (Simon et al. 2012), and hydrodynamic based trapping (Wang et al. 2009b). In the case of a surface energy-based trapping mechanism, a pinhole is made in the microchannel which is much smaller than the droplet (Abbyad et al. 2011; Dangla et al. 2011). At flow rates below the threshold value, the droplet anchors to the pinhole. The droplet experiences a force proportional to the gradient of surface energy as it gets attached to the pinhole resulting in a change in its shape. When the surface energy gradient is dominant over the hydrodynamic drag force, the droplet anchors to the

pinhole. The threshold velocity at which larger droplet anchors to the pinhole was also determined (Nagel et al. 2014) with various viscous media (Amselem et al. 2015). This mechanism has also been studied using the Lattice Boltzmann Method (Liu and Zhang 2017). This study demonstrates that anchoring efficiency increases with an increase in the diameter of the pinhole.

4.2. Droplet generation – Steady flow rate of the two liquids

In the following discussions, we shall denote Device 1 and Device 2 mentioned in Table-2.5 as D1 and D2. The flow rate Q_d of water is varied such that the flow rate ratio $Q = Q_d/Q_c$ varies from 0.01 to 1; Q_c is the flow rate of mineral oil. In device D1, the length of the droplet decreased gradually from 232μm to 94μm as the flow rate Q_c was increased from 0.06μl/s to 2μl/s while Q_d is fixed at 0.05μl/s. In contrast, the droplet length increased from 118μm to 452μm when Q_d is increased from 0.003μl/s to 0.07μl/s keeping Q_c fixed at 0.05μl/s. Similarly, in the device D2, the length of the droplet decreased from 256μm to 80μm when Q_c was increased from 0.04μl/s to 2μl/s while Q_d was fixed at 0.05μl/s. The length of the droplet increased from 120μm to 250μm when Q_d was increased from 0.003μl/s to 0.06μl/s while Q_c was fixed at 0.05μl/s. In the squeezing regime, as the dispersed phase liquid enters the main channel, it starts blocking partially the flow of the continuous liquid. This leads to a gradual rise in the pressure upstream in the continuous liquid, which in turn results in squeezing the column of the dispersed phase liquid at the T-junction, thus creating a neck in the column at the junction. As more dispersed liquid enters the main channel, a plug shaped droplet of the dispersed phase liquid is generated, and, simultaneously, the diameter of the neck gets increasingly reduced. In other words, the neck is continuously squeezed till the plug breaks off from the T-junction, thereby forming one droplet. Following release of the droplet, it is observed that the dispersed phase liquid retracts back into the side channel and the pressure in the main channel drops back to the initial value. This process repeats itself resulting in generation of a continuous stream of droplets. In the model proposed by Garstecki et.al., 2006, the dimensionless length of the droplet (plug) is given by:

$$\left(\frac{L}{w}\right) = 1+\propto \left(\frac{Q_d}{Q_c}\right)$$

where L is the length of the droplet, w is the width of the main channel, Qd and Qc are the flow rates of the dispersed phase liquid and the continuous phase liquid. The parameter α is of the order of unity. We may consider droplet formation in the following two special cases:

- $Q_d << Q_c$: in this case L/w = 1 and the droplet length remains almost constant.
- $Q_d >> Q_c$: in this case L/w ≈ Qd / Qc and the droplet length depends on the flow rates of the two liquids.

Alternatively, we may understand the droplet length variation with the flow rates in terms of:

- Droplet filling time $T_{fill} \sim 1/Q_d$ which is the time for which the dispersed phase liquid enters the main channel.
- Neck squeezing time $T_{sqz} \sim 1/Q_c$ which is the time duration over which the neck is fully squeezed.
- Droplet formation time $T = T_{fill} + T_{sqz}$.
- Droplet length $L \approx TQ_d$.

Thus, when $Q_d << Q_c$, $T \approx T_{fill}$ and $L \approx T_{fill}\ Q_d \sim 1$, i.e. L is independent of flow rates. In the other limit $Q_d >> Q_c$, $T \approx T_{sqz}$ and $L \approx T_{sqz}\ Q_d \sim Q_d / Q_c$, which implies that droplet length depends on the flow rates.

The variation of dimensionless droplet length with the flowrate ratio Q (Fig 4.1) is in good agreement with reported experimental results (Garstecki et al. 2006). Our simulations indicate that the droplets are generated in the jetting regime when Q_c is kept constant at 0.05μL/s and Q_d is kept at a low value of 0.07μL/s in both the devices D1 and D2. When Q_d is increased to 0.09μL/s, the droplet is released farther away from the T-junction. Further increase in Q_d leads to a steady flow of the two liquids, in parallel streams, in the main channel, without the formation of any droplets (Wehking et al. 2014).

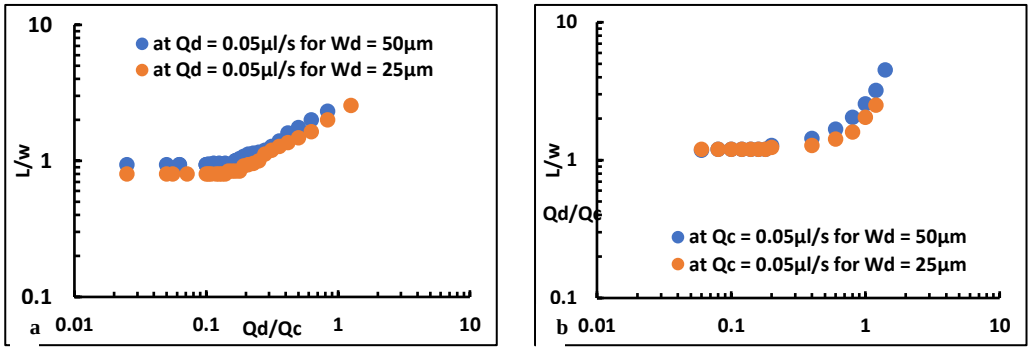

Fig 4.1: a) Dimensionless length of the droplets (L/w) plotted as a function of the ratio of flow rates (Q_d/Q_c) of fluids a) when Q_d is fixed and Q_c is varied, and b) when Qc is fixed and Q_d is varied.

4.3 Droplet generation – Pulsed flow of dispersed phase liquid

In this section, we present simulation results for droplet generation obtained by periodically varying the flow rate (Q_d) of water and keeping the flow rate of mineral oil (Q_c) constant.

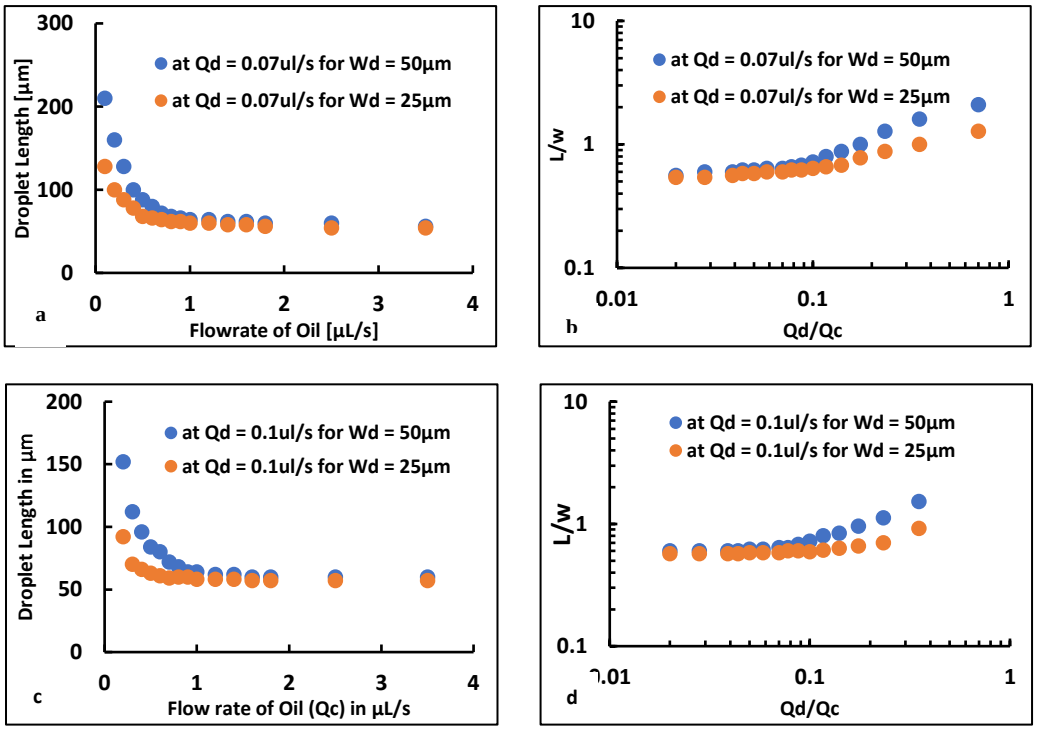

Fig 4.2: Generation of droplets for various flow rates of Q_c and Q_d for both D1 and D2. a) Droplet length versus flow rate of oil at a fixed flow rate of water, b) Dimensionless length of the droplets (L/w) plotted as a function of the ratio of flow rates of fluids, c) Droplet length versus flow rate of water at a fixed flow rate of oil, d) Dimensionless length of the droplets (L/w) plotted as a function of the ratio of flow rates of fluids,

The choice of the flow rate is made based on the results of Sec. 4.2. As seen in the previous section, droplet generation happens in the jetting regime at low values of Q_d (0.07μL/s) and for higher values of Q_d the dispersed phase liquid flows a separate stream parallel to the continuous phase liquid. Droplet length versus flow rate of oil is mapped. The value of Q_c ranges from 0.1μL/sec to 3.5μL/Sec and that of Q_d is fixed at 0.07μL/Sec and 0.1μL/Sec. The length of the droplet decreases approximately from 210μm to 54μm and from 152μm to 56μm in the case of Q_d = 0.7μl/Sec and 0.1μl/Sec, respectively. This is schematically shown in Fig 4.2.

In the simulations, the flow rate Q_c is kept constant at 0.2μl/s while Q_d is varied between 0.1μl/s and 0μl/s. The time interval between two successive droplets was found to be 6.5msec and 7msec, respectively, for devices D1 and D2. In the case of D2, the generation of the larger droplets is followed by a few small droplets (called daughter droplets) when the pulse repetition time is kept at 7msec. Therefore, we studied the droplet generation for pulse parameters shown in Table-2.6 and for a total simulation duration of 100msec.

Fig .4.3 shows the successive stages of droplet formation, in device D1, at five instants of time for five different surfactant concentrations. When no surfactant (0%) is added, a single plug-shaped droplet of about 150μm in length is formed close to the T-junction due to the squeezing mechanism. Addition of a small amount (0.2%) of surfactant results in the formation of the droplet (of length ~ 170μm) further away (~50μm) from the T-junction.

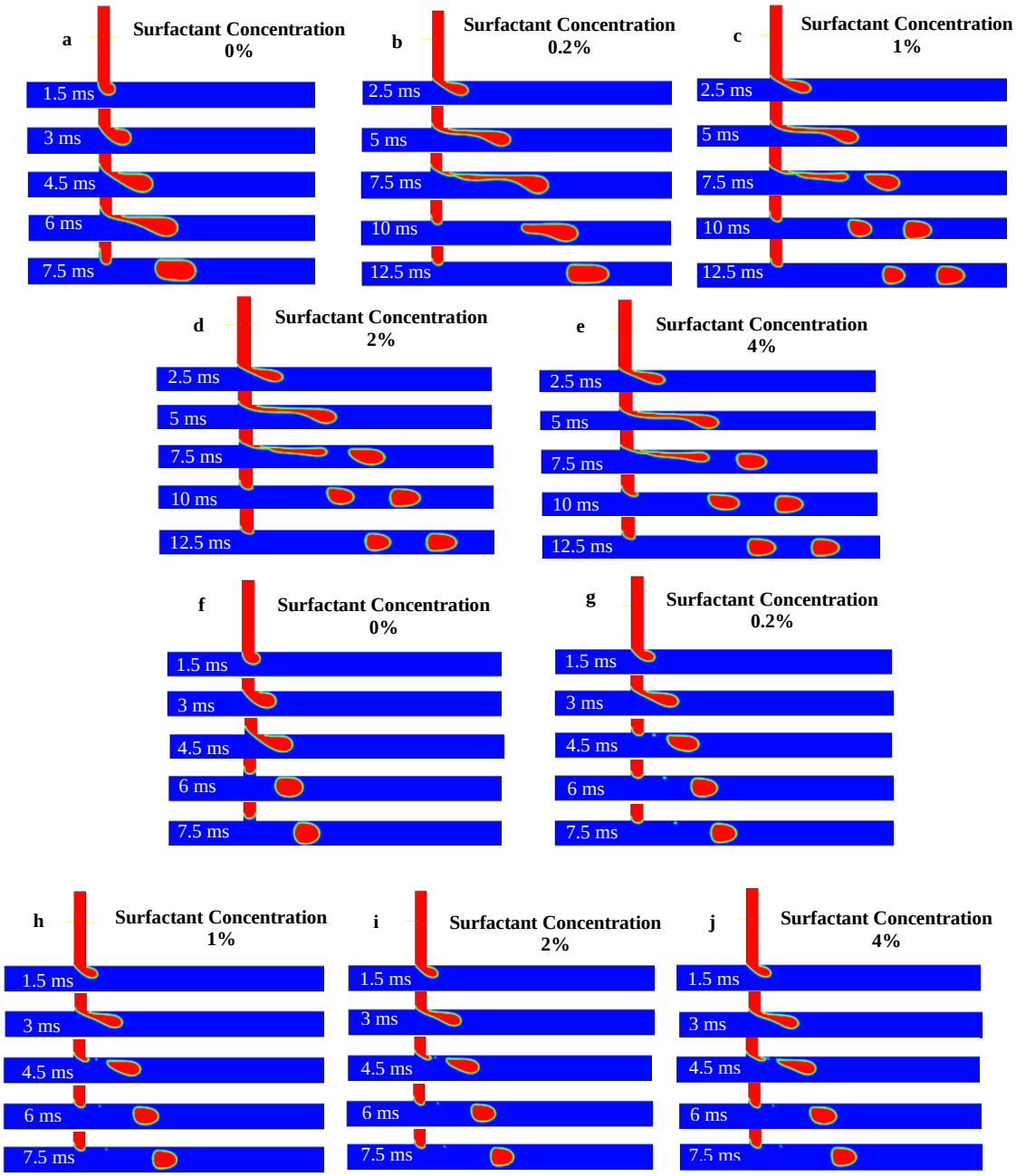

Fig 4.3: Sequence of droplet generation with and without surfactant for D1; Q_c = 0.2µL/Sec and Q_d = 0.1µL/Sec. a-e) ΔT_1 = 6.5msec and ΔT_2 = 6.5msec, a) 0%, b) 0.2%, c) 1% d) 2%, e) 4%, and (f-j) ΔT_1 = 3.25msec and ΔT_2 = 6.5msec, f) 0%, g) 0.2%, h) 1% i) 2%, j) 4%.

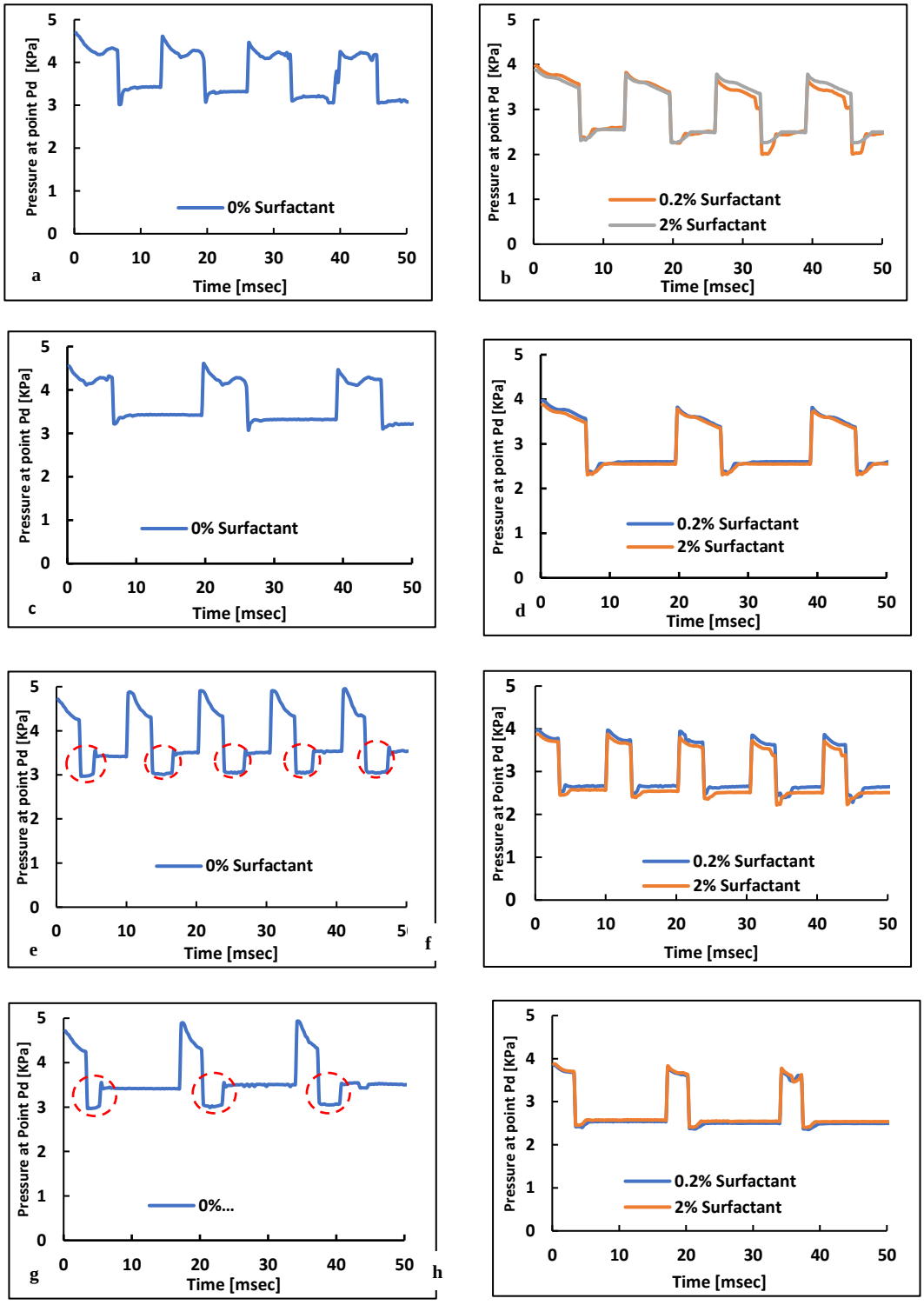

Fig 4.4: Pressure Vs time at point P_d for D1 with and without surfactant. a,b) $\Delta T_1 = \Delta T_2 = 6.5$msec, c,d) $\Delta T_1 = 6.5$msec and $\Delta T_2 = 13$ msec, e,f) $\Delta T_1 = 3.25$msec and $\Delta T_2 = 6.5$msec, g,h) $\Delta T_1 = 3.25$msec and $\Delta T_2 = 13$msec. Operating flow rates are $Q_d = 0.1\mu L/s$ (ON State), $0\mu L/s$(OFF State) and $Q_c = 0.2\mu L/s$

Increasing the surfactant concentration further leads to the formation of two droplets instead of one; the two droplets are also formed well away from the T-junction (Sontti and Atta 2019). This indicates that surfactants reduce the interfacial tension (Bashir et al. 2014) which, in turn, leads to the formation of two smaller droplets, each of length ~ 100μm, instead of one large droplet for each pulse cycle. When the on-time pulse duration ΔT_1 is reduced to 3.25msec, keeping ΔT_2 at 6.5msec, it is seen that, irrespective of the surfactant concentration, only one droplet, of length ~ 100μm, is generated (Fig 4.3f-4.3j). Further, the droplets are invariably generated close to the T-junction. This indicated that a shorter pulse duration gives better control over the droplet generation and that the use of surfactants is desirable for obtaining smaller droplets.

Pressure variations at points P_c and P_d in the device (Fig.3.1) occur with the same periodicity as the pulse waveform imposed on the flow rate Q_d of the dispersed phase liquid. The graphs in Fig 4.4 and Fig 4.6 clearly show that the pressure profiles, for the point P_d are considerably distorted compared to the rectangular waveform for Q_d. The pressure variations at point P_d in the side channel are shown in Fig.4.4. It is seen that the pressure in water (dispersed phase liquid) alternates between 4.2kPa and 3.4kPa, on average. At each fall-time in the graphs shown in Fig.(4.4a and 4.4c) for ΔT_1 = 6.5msec, an under-shoot is seen which is indicative of droplet release and immediate retraction of water thread into the side channel. If the on-time pulse duration is reduced to ΔT_1 = 3.25msec, a small step profile is seen just at the fall-time (shown by a circle in Fig.4.4e and 4.4g). This is seen to indicate the release of the droplet followed by the retraction of the water thread after about 3msec (~ ΔT_1).

In contrast, the addition of a surfactant suppresses these variations at the fall-time, thereby implying that the droplet release is immediately followed by retraction of the water thread. This is observed for both values of ΔT_1. Further, the addition of a surfactant leads to a reduction in the average pressure values to 3.5kPa during on-time and 2.5kPa during off-time for the pulse (Fig 4.4b, 4.4d, 4.4f, 4.4h).

The droplet generation process in device D2 is seen to be similar to that in device D1. The length of the droplet produced was found to be 120µm for ΔT_1 = 6.5msec and 90µm for ΔT_1 = 3.25msec as shown in Fig 4.5a and 4.5f, respectively.

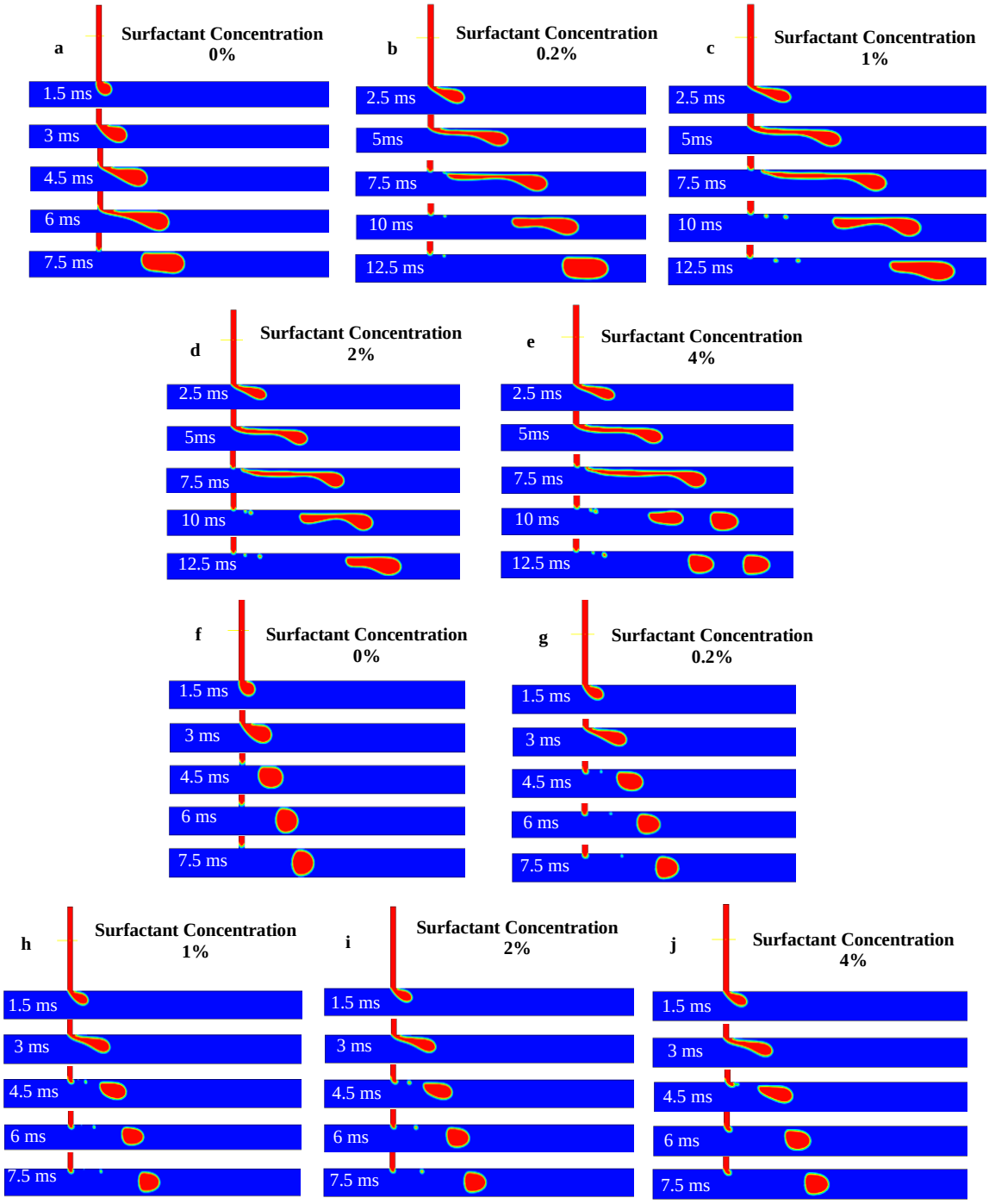

Fig 4.5: Sequence of droplet generation with and without surfactant for D2; Q_c = 0.2µL/Sec and Q_d = 0.1µL/Sec. a-e) ΔT_1 = 6.5msec and ΔT_2 = 6.5msec, a) 0%, b) 0.2%, c) 1% d) 2%, e) 4%, and (f-j) ΔT_1 = 3.25msec and ΔT_2 = 6.5msec, f) 0%, g) 0.2%, h) 1% i) 2%, j) 4%.

Maintaining the same flow rate for water as in device D1 implied that the flow velocity of water was higher in device D2 as compared to D1 since the width of the side channel in D2 was half that in D1. Due to this reduction in the width of the side channel of device D2, the length of the droplets generated in D2 is smaller than those in D1. Another significant difference is that the generation of a pair of droplets in device D2, for ΔT_1 = 6.5msec, occurs at a higher concentration (4%) of the surfactant than in D1. As in the case of device D1, for pulses of width ΔT_1 = 3.25msec, only single droplets are generated in device D2. This confirms the conclusion that smaller pulse width (ΔT_1) leads to better control of droplet generation (Fig 4.5f-4.5j).

Fig.4.6 shows the profiles of pressure in the water at point P_d in device D2. It is seen that the average pressure during the on-state of the pulse is much higher in device D2 than in D1, whereas the pressure during off-state is the same as in D1. This is due to the higher flow velocity caused by the smaller width of the side channel in D2. At the start of the on-state, a sharp spike in the pressure (~ 5.7kPa) is seen, which is followed by a minimum and then a steady value (~5kPa) is reached (Fig 4.6a, 4.6c, 4.6e, and 4.6g). The addition of the surfactant suppresses this variation in pressure, and it is seen to reduce gradually from a maximum value (~ 4.2kPa) at the start of the on-state to a lower value (~3.8kPa) at the end of the on-state of the pulse.

The pressure at P_d in the off-time of the pulse is seen to reduce from ~ 3kPa to ~2.5kPa as the surfactant concentration is increased from zero to 4% (Piccin et al. 2014). This is shown in Fig 4.6b, 4.6d, 4.6f, and 4.6h. The pressure variation in the off-state indicates that the droplet is released at the pulse fall-time instant and the retraction of the water thread back into the side channel follows immediately without any time gap. These results reveal that the effect of surfactants is stronger in device D2. Thus, the control on droplet generation is better with a side channel of width smaller than the main channel by a factor of about 0.25.

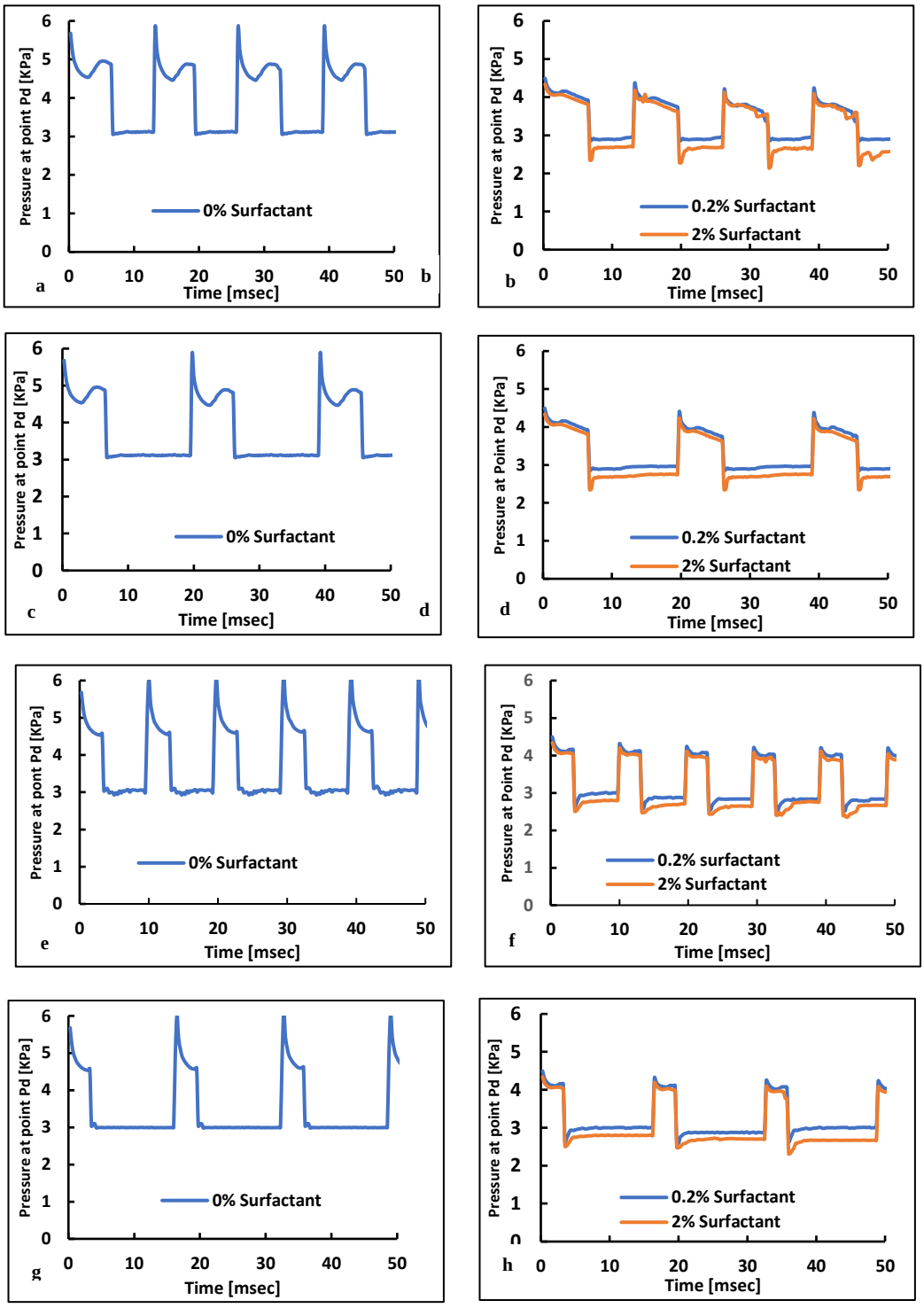

Fig 4.6: Pressure Vs time at point P_d for D2 with and without surfactant. a,b) $\Delta T_1 = \Delta T_2 = 6.5$msec, c,d) $\Delta T_1 = 6.5$msec and $\Delta T_2 = 13$ msec, e,f) $\Delta T_1 = 3.25$msec and $\Delta T_2 = 6.5$msec, g,h) $\Delta T_1 = 3.25$msec and $\Delta T_2 = 13$msec. Operating flow rates are $Q_d = 0.1\mu L/s$(ON State), $0\mu L/s$(OFF State) and $Q_c = 0.2\mu L/s$

4.4 Droplet Trapping

The generated droplets are generally collected in a vial (Crawford et al. 2017) or it is trapped in a micro-well assay (Shi et al. 2013). In our previous work, we have shown that the trapping of droplets in a micro-well occurs if the flow velocity of the continuous phase liquid is less than a critical velocity (Sripadaraja et al. 2020). Trapping is also assisted by the presence of a circular Pit, located just above the well. In the present work, we have adopted a simpler geometry as indicated in Fig.2.2(c and d), wherein a small pinhole is placed close to the well. Our simulations indicate that the depth of the pinhole does not affect the trapping of droplets. Hence, the depth of the pinhole is fixed at 40μm, whereas the diameter is varied.

We have simulated the trapping of water droplets of length 40μm in a well of diameter 200μm and depth of 200μm. The pinhole depth is kept at 40μm in all the simulations. In the case of droplet length 40μm, initially the diameter of the pinhole is fixed to 5μm, and the flowrate Q_c is gradually increased. The maximum flowrate to trap the droplet was found i.e.., Q_c = 0.01μl/s. When Q_c = 0.01μl/s, the diameter of the pinhole is increased, and droplet trapping were found for pinhole diameter of 15μm. With further increase in the diameter of the pinhole beyond 15μm, the droplet hooks to the pinhole. The droplet gets trapped in the absence of the pinhole. If Q_c is further increased to 0.02μL/s, no trapping of the droplet is seen for pinhole diameter in the entire range of 20μm to 60μm. If a surfactant is added to the mineral oil at 0.05% concentration, the droplets do not get trapped even for Q_c = 0.01μL/s.

In the case of droplet length 80μm, initially the diameter of the pinhole is fixed to 10μm, and the flowrate Q_c is gradually increased. The maximum flowrate to trap the droplet was found i.e.., Q_c = 0.01μl/s. When Q_c = 0.01μl/s, the diameter of the pinhole is increased, and droplet trapping were found for pinhole diameter < 50μm. With further increase diameter of the pinhole beyond 50μm, the droplet hooks to the pinhole and does not move further. For both droplets of length 40μm and 80μm, the maximum flowrate was found to be Q_c = 0.01μl/s. Droplets do not get trapped beyond this flowrate. In the absence of a pinhole, no trapping of the droplet is seen. If Q_c is further

increased to 0.02μL/s, no trapping is observed. No trapping of the droplets is seen if a surfactant is added at a concentration of 0.05%. Thus, the larger droplet shows a behaviour similar to that of the smaller droplet.

Table 4.1: Trapping status of the droplet (length 80μm) based on the flow rate of oil (Depth of pinhole is 40μm)

Diameter of Pinhole (μm)	The flow rate of Oil (Q_c)			
	0.01μL/s	0.0125μL/s	0.015μL/s	0.02μL/s
20	Trapped	Trapped	Not Trapped	Not Trapped
30	Trapped	Not Trapped	Not Trapped	
40	Trapped	Trapped	Not Trapped	
45	Trapped	Trapped	Not Trapped	
50	Attached to Pinhole	Trapped	Trapped	
55	Attached to Pinhole	Trapped	Trapped	
60	Attached to Pinhole	Attached to Pinhole	Attached to Pinhole	

Therefore, we conclude that droplet trapping is seen to occur only for optimum values of pinhole diameter and Q_c less than 0.02μL/s. Our simulations also show that if the pinhole is removed from the device, the droplets do not get trapped in the well for the entire range of parameters used in our simulations. Thus, the pinhole is seen to facilitate trapping the micro-droplets.

4.5 Conclusion

We have investigated the generation and trapping of droplets in a T-junction microfluidic device. The droplets generated in both devices D1 and D2 show that, the length of the droplet scales as reported by Garstecki et al 2006. Droplets were also generated by pulsing the dispersed phase liquid between 0.1μL/Sec and 0μL/Sec while Qc is at a steady flow rate of 0.2μL/Sec. With device D1, when the pulse duration ΔT_1 = 6.5msec, a single droplet is generated, but with the addition of a small amount of surfactant, a pair of droplets is generated for each pulse period. On the other hand, in the case of device D2, which has a smaller side-channel width, droplet generation in

pairs happens only when the surfactant concentration is increased to 4%. The generation of droplets is well controlled when ΔT_1 = 3.25msec in both devices D1 and D2. The average pressure at point P_d switches between 4.2kPa and 3.4kPa for ON and OFF states, respectively. If the on-time pulse duration is reduced to ΔT_1 = 3.25msec, a small step profile is seen just after the fall-time which indicates the release of the droplet followed by the retraction of the water thread into the side-channel over a small-time duration. This time duration for the retraction of water reduces drastically with the addition of surfactant. The pressure (P_d) increases in the case of device D2 due to the smaller width of the side channel. In the ON state, the pressure reduces from 5kPa to 4.2kPa and in OFF state 3kPa to 2.5kPa, and the droplet is also released at pulse fall time without delay when the surfactant concentration increases from 0% to 4%.

Droplets of length 80μm get trapped in the micro-well when Qc ≤ 0.01μL/Sec for pinhole diameter from 20μm to 50μm. At Q_c = 0.0125μL/Sec the trapping of the droplet is seen for pinhole diameter between 45μm to 55μm. When Qc is increased to 0.02μL/Sec no droplet trapping is seen. In the case of droplets of length 40μm, trapping of the droplet is seen when Q_c = 0.01μL/Sec for the diameter of pinhole < 20μm. When a surfactant is added, no trapping of droplets is seen. Thus, an optimum design of the microfluidic device together with a choice of optimum fluid flow parameters is essential for droplet microfluidics. Our simulations indicate microdroplets can be generated in a controlled manner, by pulsed flow technique, and trapped in micro-wells in microfluidic devices.

CHAPTER 5

MICRODROPLET GENERATION IN DOUBLE T-JUNCTION MICROFLUIDIC DEVICES.

5.1 Introduction

In this chapter, we present the results of simulation studies on droplet formation in a double T-junction device. The study on this device makes it interesting as the average pressure in the side and the main channel and capillary number variations due to the change in width of the microchannel are similar to a single T-junction device. Dispersed phase liquid from both the side channel merges at the junction and a droplet is released when the capillary number is below (approximately) 0.024 (Ngo et al. 2015; Surya et al. 2015). This mechanism of droplet generation is termed to be in the merging regime. When the capillary number increases beyond 0.024 droplets are generated from each side channel alternatively. This mechanism is termed to be an alternate regime (or ADF – Alternate Droplet Formation). In this mechanism, droplets are generated alternately from each of the two side channels by the squeezing mechanism discussed in Chapter 3. When a droplet is released from one of the side channels, the dispersed phase liquid retracts back. During this retraction, dispersed phase liquid from another side-channel enters the main channel at the junction to form the droplet. This mechanism continues and alternate droplet generations are produced (Yesiloz et al. 2015). This push and pull mechanism causes pressure fluctuations between the two side channels. We have validated our simulation results with an experimental result reported by Zheng et al 2004.

In the interest of producing comparative studies, we perform simulation on a single T-junction device. The droplet generation is studied by varying the width of both channels (side and main channel) but one at a time. (i) Initially, the width of the main channel is fixed, and the width of the side channel is varied. (ii) Secondly, the width of the side channel is fixed, and the width of the main channel is varied. This study facilitated the investigation of droplet generation in a double T-junction device. In the double T-junction device, droplet generation in an alternate regime is studied by varying the

width of one of the side channels, and the change in pressure and the capillary number is noted. Similarly, the width of the main channel is varied to find the minimum dimension at which an alternate regime is seen for the given velocity of the two liquids. The change in pressure and the capillary number is noted. The results of similar variations in a single T-junction device are compared with a double T-junction. The influence (reduced interfacial tension and increased contact angle) of varying surfactant concentration (Span 80) is studied on both merging and alternate regimes. Temporal variations of pressure in the side channel provide information about the droplet generation mechanism in a double T-junction device in both merging and alternate regimes.

Double T-junction devices are useful for merging two droplets during droplet generation. Such devices were used for investigating protein-protein interaction and cell-based assay (Um et al. 2008). Droplet merging efficiency of two different reagents with hydrogel droplets showed 90% efficiency while Q (ratio of the flow rate of dispersed phase liquid - Q_d, to flow rate of continuous phase liquid - Q_c) was maintained between 0.1 to 0.6. The velocity vector fields during the droplet merging process in straight and diverging microchannels were studied. In this device, the merging happens farther away from the junction. Droplets were generated in double T-junction and Y-junction (side-channel is at 45^o to the main channel) (Jin and Yoo 2012). The study emphasizes the velocity field vector inside the droplet in both straight and diverging microchannel. In a similar device, water droplets were generated in mineral oil with different concentrations (0% to 5%) of Span 80 (Surfactant) (Liu and Qin 2013). Merging efficiency was reduced with an increase in surfactant concentration up to 3% and no merging was seen at 5% of surfactant concentration. It was demonstrated that droplets can also be merged with two T-junctions (two side channels are parallel) for synthesizing inorganic-organic block copolymer (Hoang and Dien 2014). Using simulation, it was shown that the droplet generation in the merging regime in a double T-junction device can be understood by plotting pressure versus time (Han and Chen 2019a). In this study, pressure change with time shows that blocking time (time until dispersed phase liquid blocks the flow of continuous phase liquid at the junction) and breaking time (time until pinching of the dispersed phase liquid happens) of dispersed

phase liquid increases with interfacial tension from 3mN/m to 12mN/m. Further, it was shown that the average pressure in the main channel increases with an increase in the viscosity of continuous phase liquid from 0.2mPa.s to 4mPa.s. The frequency of droplet generation and average pressure (point at front edge of the junction) increases with an increase in the flow rate of continuous phase liquid from 0.2μL/hr to 0.8μL/hr. They also studied droplet merging by varying the angle between the side channel and the main channel between 30^o to 150^o (Han and Chen 2019b). The study showed that increased droplet generation frequency and smaller diameters of droplets were found when the angle between the side and main channel is at 60^o.

The droplet generation in double T-junction transits from merging to an alternate regime with an increase in capillary number. The first study on the double T-junction device model to produce alternate droplets in different regimes namely merging, alternating, alternate-jetting, and jetting for capillary numbers ranging from 0.001 to 0.05 was reported by Zheng et al. 2004 (Zheng et al. 2004a). A novel design was made and droplet generation was produced in various regimes to synthesise CdS nanoparticles (Hung et al. 2006). In this device, droplets of different volumes were produced from each of the two side channels by controlling the flow rate of dispersed phase liquid. The inclination of the side-channel at 45^o (Jin and Yoo 2012) and 90^o (Surya et al. 2015) to the main channel can also produce droplets in the alternate regimes. A numerical study focuses on droplet generation of a double T-junction device for various widths of the side-channel to the main channel (Λ) (in the range of 0.5, to 1.5). In this study, the minimum capillary number to generate droplets in an alternate regime was found to vary between 0.02 to 0.05 (Ngo et al. 2015). Finally, pressure variations with time show that the droplet generation shift from merging to the alternate regime, and the duration of the merging regime shortens with an increase in capillary number from 0.02 to 0.06. It was found that in the merging regime, the pressure at points P_1 and P_2 are equal. In an alternate regime, it fluctuates as explained earlier. This was demonstrated by an experiment with matching simulation results using a double T-junction device that has symmetric tapered side channels (Saqib et al. 2018).

5.2 Validation of simulation results

The VOF model (single T-junction device) used in the present study is validated with an experimental study (Bashir et al. 2014). The droplet length reduces with an increase in the flow rate of mineral oil. The associated power law to the fitting lines agrees well with each other. Although 3D simulations are important to understand the breakup dynamics of droplets in T-junction devices, the comparative study presented in Fig 5.1a with 2D simulation demonstrates a qualitative prediction of droplet length at 4% surfactant concentration.

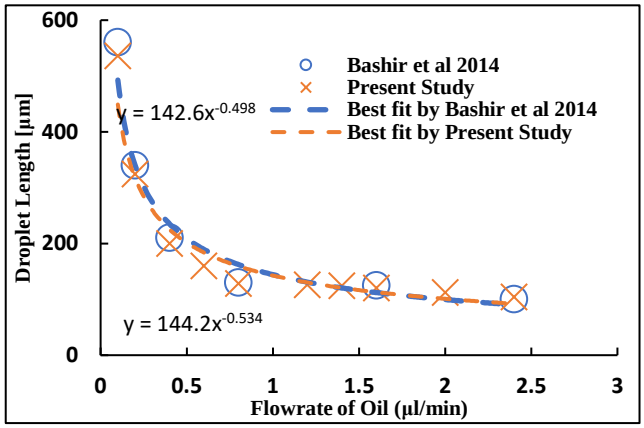

a

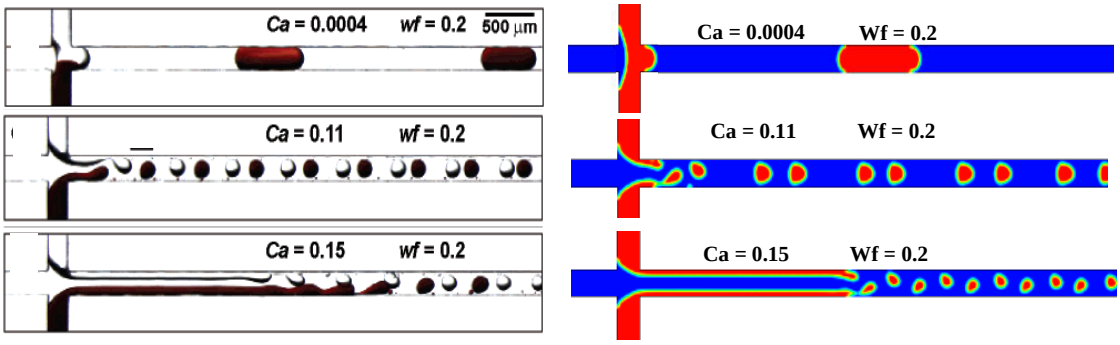

b c

Fig 5.1: Droplet generation in single and double T-junction device. (a) Droplet length versus flowrate of oil at a fixed flowrate of water (0.2 µl/min) in single T-junction device: Comparative study with the experimental results reported by Bashir et al 2014 at 4% surfactant concentration, (b) Double T-junction device, experimental results from the work of Zheng et al. 2004a, (c) Computational results of the present study. (Q = W_f = water fraction). $\Lambda = 1$ and $\lambda_d = \lambda_c = 16$ mPa.s.

Further, our simulations on alternate droplet generation on a double T-junction device are validated by the experiments done in the past. Fig 5.1b shows the alternate droplet generation in a double T-junction device by experiment for three different capillary numbers (Zheng et al. 2004a). The simulation results are in close comparison with the experimental data (Fig 5.1c). When simulations are validated with experimental data as shown, there can be minor discrepancies associated between the experimental procedures reported and 2D simulations. However, our simulations on alternate droplet generation are reproduced with some consistent geometric scale. This shows that our numerical model is acceptable to study droplet generation in single and double T-junction devices.

5.3 Effect of increase in width of side-channel on droplet generation.

In the case of a single T-junction device, the width of the side channel plays a significant role in droplet generation as it determines the interface area between the two liquid phases (Fig 2.3a). The dispersed phase liquid experiences viscous shear force induced by continuous phase liquid at the junction. In our single T-junction device droplet generation shifts from dripping to the jetting regime for an increase in the width of the side channel from 50μm to 100μm while the width of the main channel is fixed to 100μm (Fig 5.2a-f). The length of the droplet produced is proportional to the width of the side channel. The length of the droplet produced is proportional to the width of the side channel. The droplet length scales as $l = ae^{0.01W_d}$ (Fig 5.2g) while the droplet generation frequency does not show any significant change. The frequency of droplet generation scales as $f = be^{-0.02W_d}$(Fig 5.2g). The terms “a” and “b” are the parameter specific to device geometry. The change in droplet length and frequency, for the increase in width of the side-channel, are in good agreement with an earlier study using the Lattice Boltzmann method (Shi et al. 2014). The average pressure at point P_c and P_d increases from 1670Pa to 1775 Pa and 1750 Pa to 1900 Pa, respectively which is approximately 6% to 8% as the width of the side channel increases from 50 μm to 100 μm (Fig 5.2h). Similarly, the capillary number increases from 0.225 to 0.267 (Fig 5.3a) which is approximately 16%.

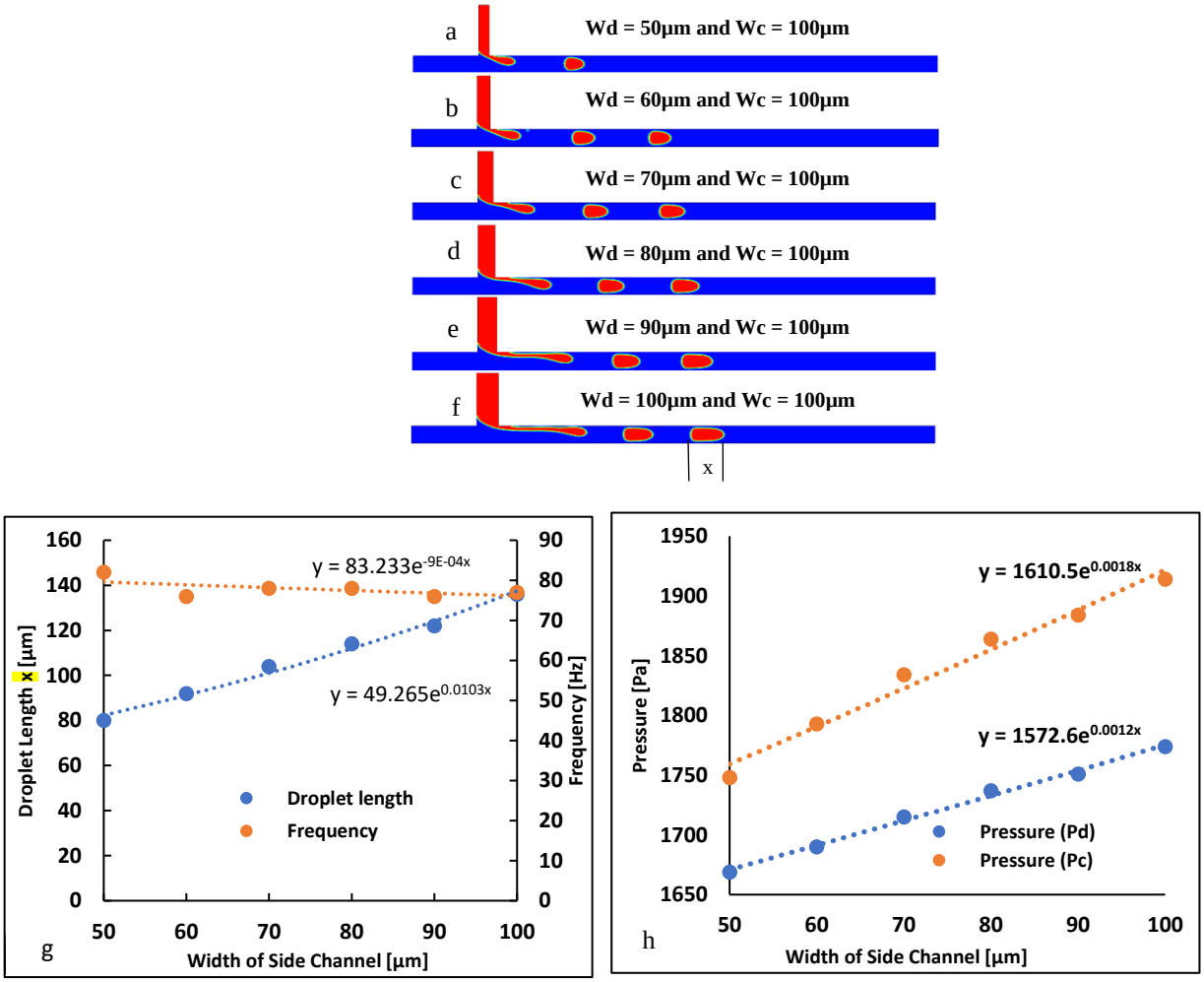

Fig 5.2: Effects of increase in the width of side-channel in single T-junction device a-f) Droplet generation showing the transition from dripping to the jetting regime ("x" represents the droplet length), g) Droplet length and frequency in single T-junction device, h) Pressure at point P_c and P_d in a single T-junction device.

In the case of a double T-junction device, the width of one of the side channels (SC1) is fixed to 100µm, and the width of another side channel (SC2) is increased from 50µm to 100µm (Fig 2.4c). In comparison to a single T-junction device, the double T-junction device contains an additional side channel. The dispersed phase liquid which flows from this additional side-channel adds to the capillary number and average pressure. The capillary number increases from 0.3 to 0.353 which is approximately 16% and the average pressure from 2130 Pa to 2270 Pa which is approximately 7% as the width of the side channel (SC2) increases from 50 µm to 100 µm (Fig 5.3a). When $\Lambda = 1$ (SC1 = SC2 =100 µm), the droplet generation is seen to be in the merging regime (Fig 5.3a)

until the flow time is 0.05 Sec. The average pressure in both the side channels is the same. With flowtime (> 0.05Sec) the pressure starts to vary in both the side channel. This results in the generation of droplets in the alternate regime. In addition, Fig 5.3b also shows that during the merging regime, the average pressure in both side channels is the same.

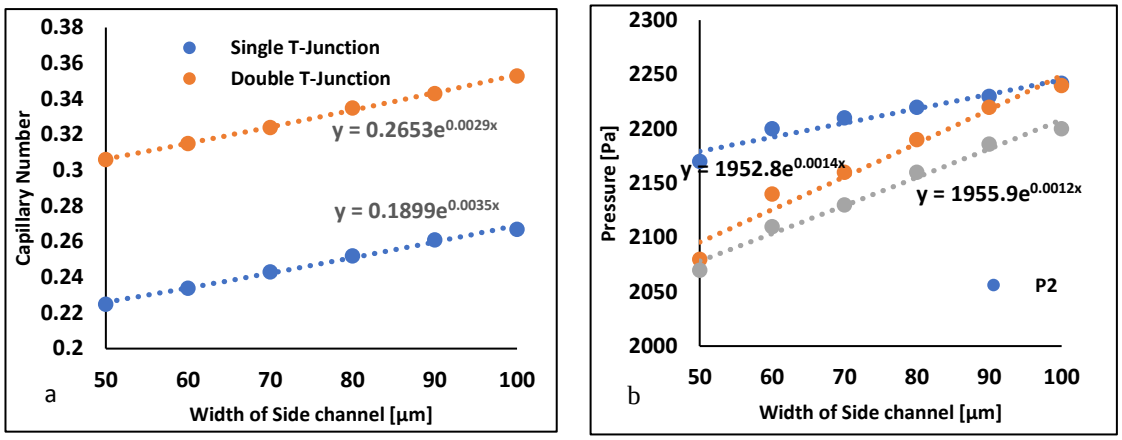

Fig 5.3: a) Capillary number in both single and double T-junction devices, b) Pressure at point P_1, P_2, and P_c in double T-junction device.

Fig 5.4a shows the droplet generation in the merging regime (flowtime between 0 sec to 0.05 sec). When the width of SC2 ≤ 90 µm droplets are generated in the alternate regime (5.4b-f). In this case, droplets of different sizes are generated alternatively and the pressure $P_2 > P_1$ (Fig 1d). The transition from merging to the alternate regime happens due to the periodic change of pressure between the points P_1 and P_2. It may be noticed that the average pressure in both the main and side channels in both devices (single and double T-junction) changes and is comparable with the change in the width of the side channel (Fig 5.2h and 5.3b). Similarly, the increase in capillary number is also comparable in both single and double T-junction devices as shown in Fig 5.3a. The distance between the two alternate generating droplets increases with a reduction in the width of one of the side channels (Fig 5.4h and 5.4i).

To describe alternate droplet generation, we mark out two regions in the double T-junction device as SC1 and SC2 as shown in Fig 5.4g. We know that the pressure surrounding the dispersed phase liquid and interfacial tension are the two major parameters contributing to droplet generation (Garstecki et al. 2006).

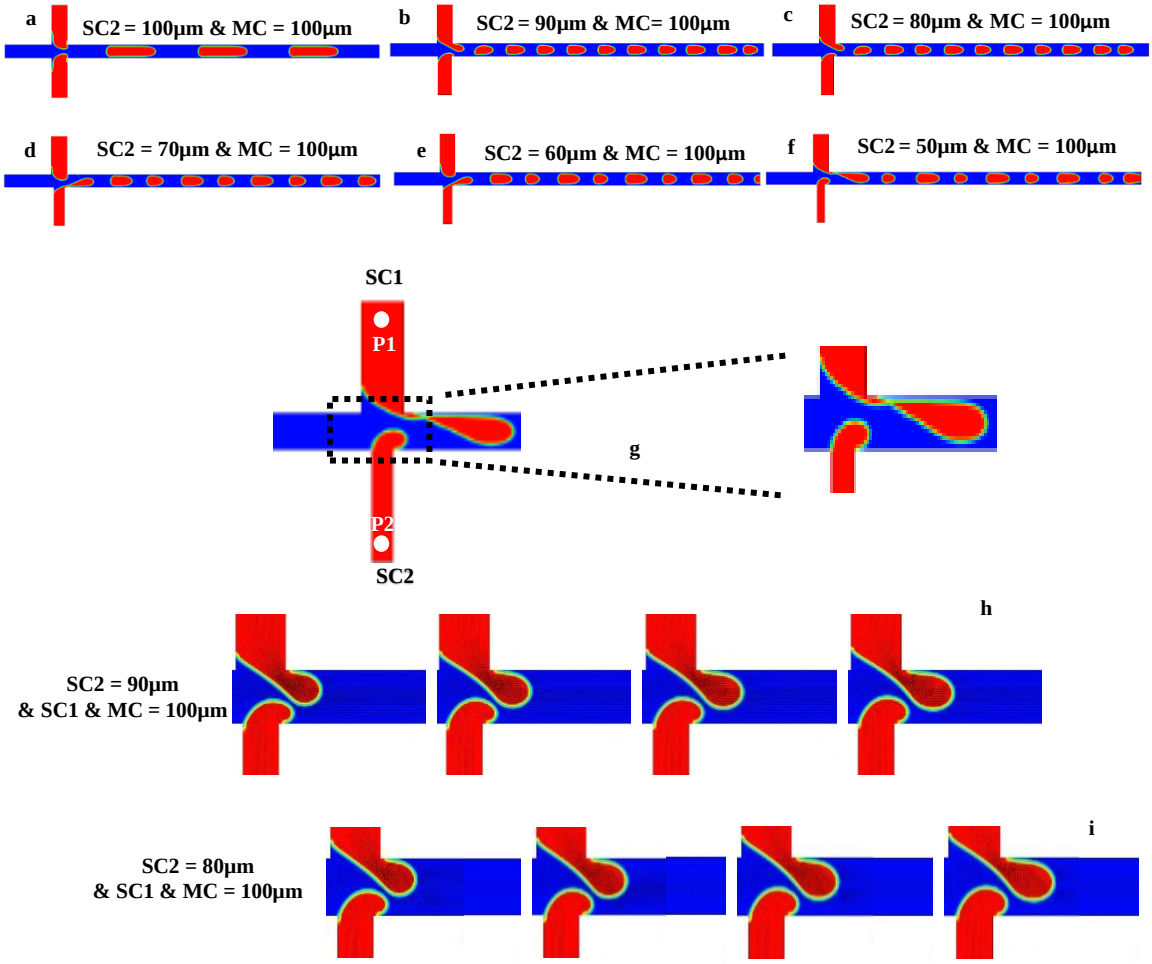

Fig 5.4: a-f) Droplet generation in double T-junction device for change in width of SC2 from 100µm to 50µm while SC1 is at 100µm. g) Representation of double T-junction device into two sections and deformation of dispersed phase liquid during alternate droplet generation. h-i) Sequence of droplet formation – Transition from merging to the alternate regime,

In the device shown in Fig 5.4g, the side channel SC2 has a smaller width than the side channel SC1. When dispersed phase liquid from the side channel SC1 enters the main channel, the pressure at point P_2 in section B increases. Once the droplet is formed from SC1, the dispersed phase liquid retracts back into the side channel of SC1 and the pressure at point P_1 drops. This enables the dispersed phase liquid from section B to enter the main channel and a droplet is generated from the side channel SC2. This cycle repeats and droplets are generated in alternate regime, which is primarily due to the difference in the widths of the two side channels. But in our case, when the width of side-channel SC2 < SC1, the average pressure is always high in the reducing side channel (SC2) (irrespective of droplet generating side channel), during alternate droplet

generation. Thus, it is seen that in the case of asymmetric double T-junction devices, the shear force dominates at the junction with the side-channel having larger width during the droplet generation (Section A in our device) due to the larger fluid interface.

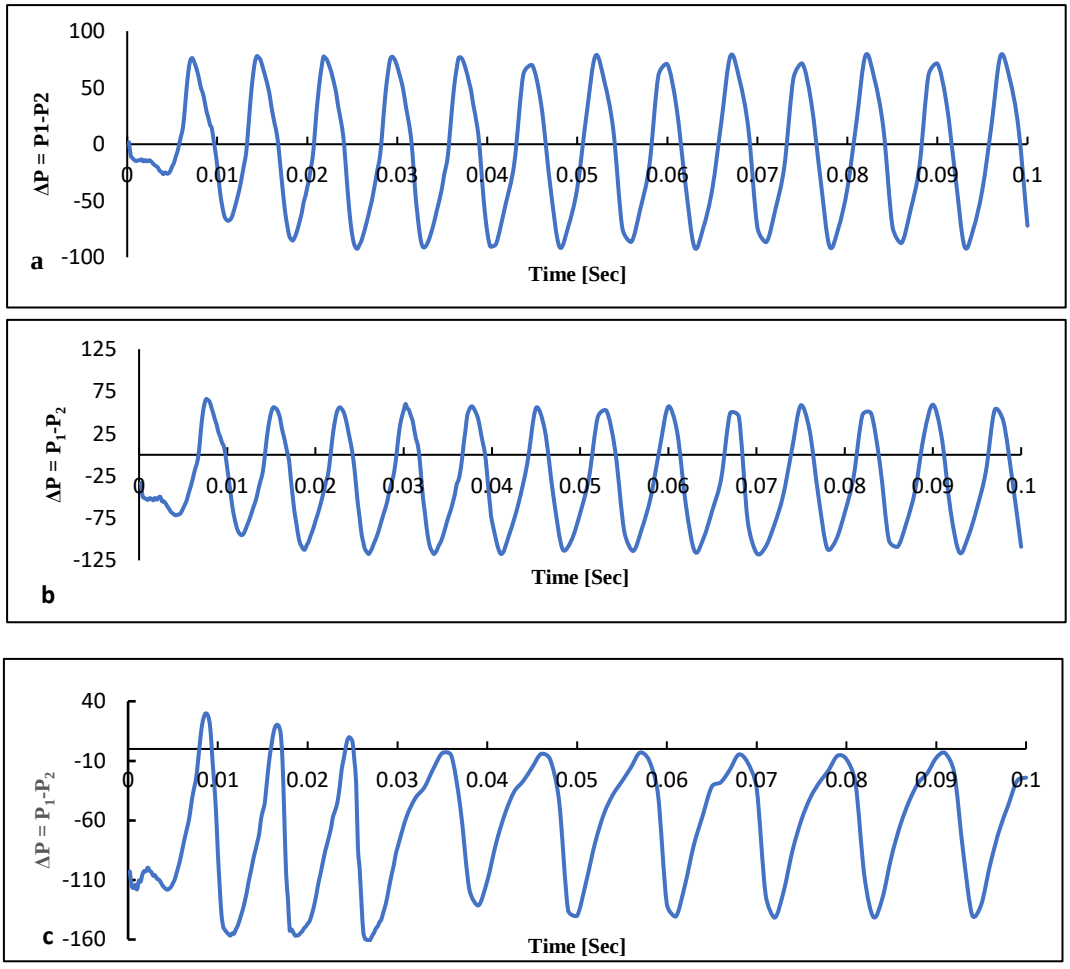

Fig 5.5: a-c) Pressure difference (ΔP) Vs time at point P_1 and P_2 for SC2 = 90µm, 70µm, 50µm, respectively.

This is witnessed by plotting $\Delta P = P_1-P_2$ with time. When SC2 is 90µm, 70µm, and 50µm the peak to peak of ΔP varies between 70Pa and -90Pa (Fig 5.5a), 60Pa and -110Pa (Fig 5.5b), and -10Pa and -140Pa (Fig 5.5c), respectively from its centre reference line with an initial stabilisation time. The time taken by the device to produce sustained droplets in an alternate regime is the stabilisation time. This indicates the dominance of pressure of P_2 during the alternate regime when SC2 < SC1. In addition,

concerning Fig 5.4g, the rate of deformation in SC1 is higher than in SC2, due to the shearing force.

5.4 Effect of increase in width of the main channel on droplet generation.

In contrast to the previous case on a single T-junction device, we study droplet generation by varying the width of the main channel from 50μm to 100μm while the width of the side channel is held constant at 50μm. The droplet generation remains in the dripping regime as shown in Fig 5.6 (a-f). With the gradual increase in W_c, the droplet length increases and frequency decreases, and scales as $l = be^{0.006Wc}$ and $f = ae^{-0.02Wc}$, respectively as shown in Fig 5.6g, where "a" and "b" are the parameter specific to devise geometry. These results are in good agreement with an earlier study using the Lattice Boltzmann method (Gupta and Kumar 2010c). The average pressure at points P_c and P_d approximately decrease from 7870 Pa to 1750 Pa and 7250 Pa to 1750 Pa, respectively as the width of the main channel increases from 50μm to 100μm (Fig 5.6h) which is approximately 75%. Similarly, the capillary number decreases from 0.267 to 0.225 (Fig 5.6i) which is approximately 15%.

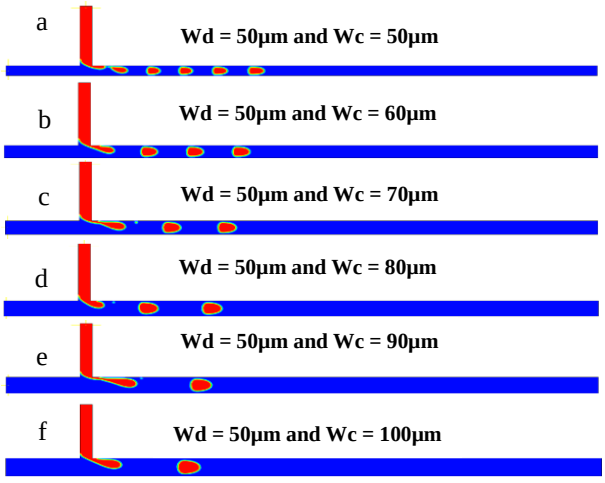

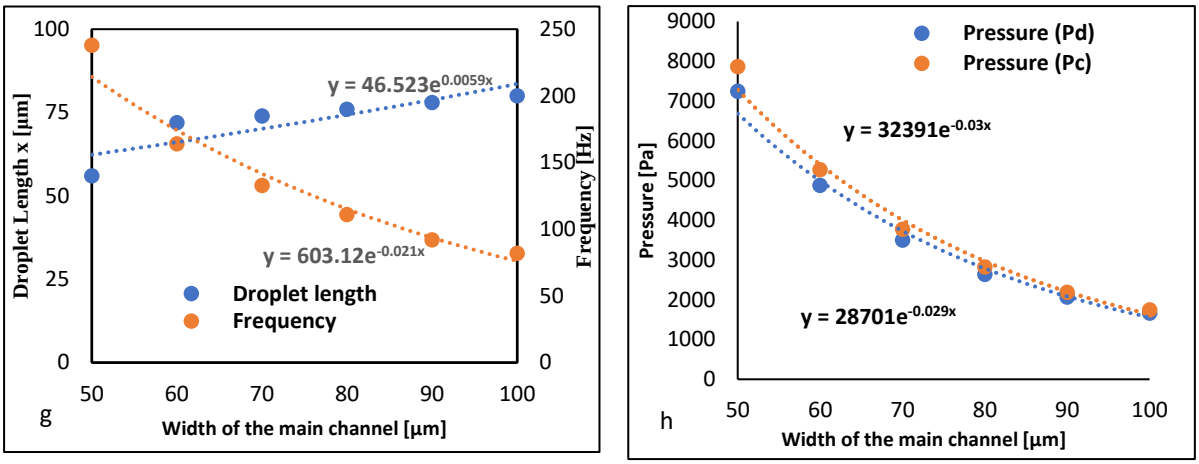

Fig 5.6: Effects of increase in the width of the main channel in single T-junction device a-f) The sequence of droplet generation, ("x" represents the droplet length) g) Droplet length and frequency, h) Pressure at point P_c and P_d.

.

In the case of a double T-junction device, the width of the main channel (MC) is increased from 50µm to 100µm while both the side channels are fixed at 50µm. In comparison to a single T-junction device, the pressure and the capillary number increase due to the addition of another side-channel similar to the previous case. In this case, the capillary number decreases from 0.354 to 0.306 which is approximately 16% (Fig 5.7a), and the average pressure from 8830 Pa to 1930 Pa which is approximately 78% for the increase in width of the main channel from 50 µm to 100 µm (Fig 5.7b). The decrease in average pressure and capillary number in the double T-junction device is in line with the single T-junction device as shown in Fig 5.7b.

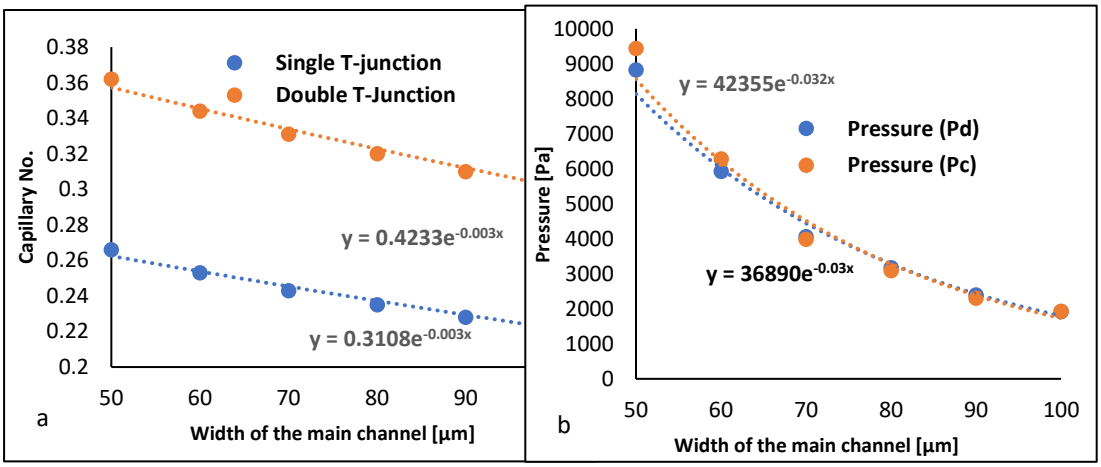

Fig 5.7: a) Capillary No. in both single and double T-junction device, b) Pressure at point P_d and P_c in double T-junction device.

With the gradual increase in the width of the main channel, droplet generation shifts from a merging regime to an alternate regime as shown in Fig 5.8 (a-f). This transition is seen when the width of the main channel is approximately 1.4 times the width of the side channel (Fig 5.8g). There will also be an increase in the distance between the generating droplets at the junction with an increase in the width of the main channel.

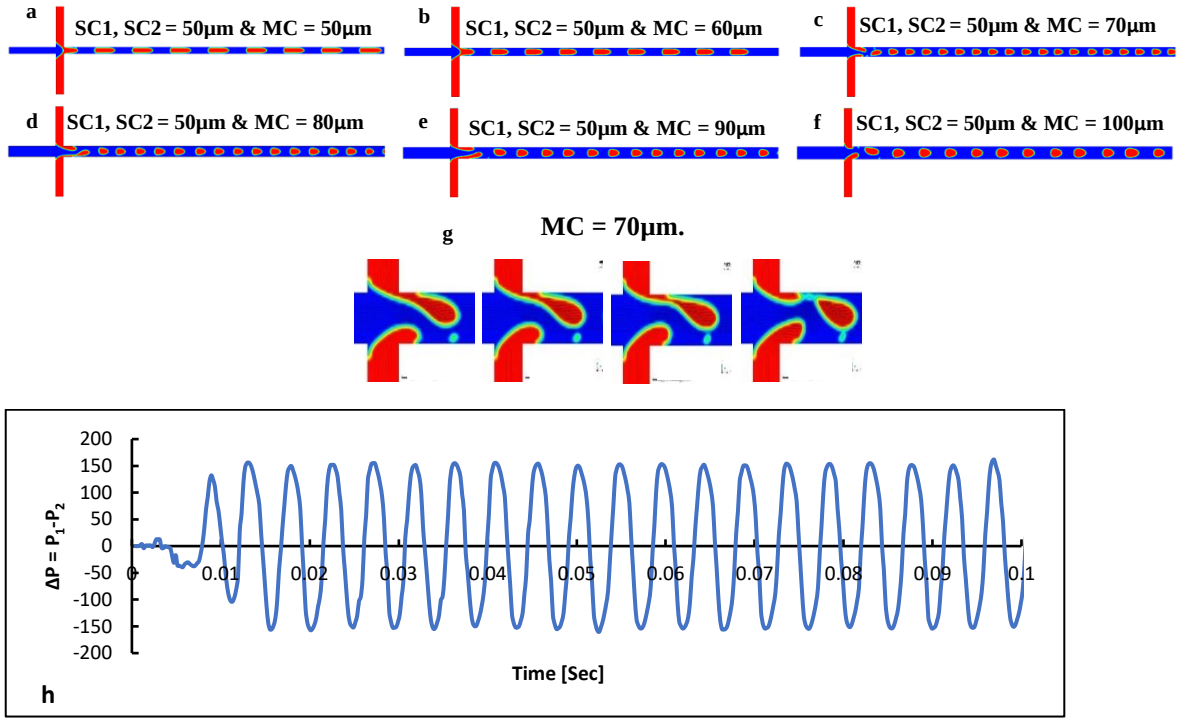

Fig 5.8: a-f) Droplet generation in double T-junction device for change in the width of the main channel between 50 µm to 100 µm. g) The sequence of droplet formation in the alternate regime, for the width of the main channel at 70 µm, h) ΔP Vs time at points P_1 and P_2 showing the transition from merging regime to the alternate regime (width of MC = 70 µm).

The dispersed phase liquid entering the main channel in both sections A and B experience equal viscous shear stress as the width of both the side channel are equal. The physical behavior of droplet generation in alternate regimes is analysed by studying the pressure at points P_1 and P_2 with time. When ΔP (P_1-P_2) is plotted against time, we see the peak-to-peak pressure switches between -150 Pa to 150 Pa indicating equal dominance of pressure alternatively from each side channel at points P_1 and P_2 over each other (Fig 5.6h). These periodic pressure variations prevail for MC ≥ 70 µm. The periodic pressure variations for MC = 70 µm are shown in Fig 5.6h.

5.5 Effect of Surfactant on Alternate droplet formation.

In practical applications, the addition of surfactant leads to change in both interfacial tension and wetting (contact angle of the droplet with the channel wall) conditions as mentioned earlier. It was shown that the contact angle of water increased with surfactant concentration, in addition to the reduction in interfacial tension. A similar study has also been the case with other surfactants like SDS (Sodium Dodecyl Sulfate)(Xu et al. 2006), and Picosurf (Totlani et al. 2020).

The addition of Span 80 in mineral oil increases the contact angle and reduces the interfacial tension with the gradual increase in its concentration. *Bashir et al 2014* showed that the contact angle increases from 152^o to 172^o and interfacial tension reduces from 7 mN to 4 mN when the concentration increases from 0.2% to 4% respectively. We study the droplet generation in a double T-junction device by implementing these changes caused due to the addition of surfactant for the device whose Λ= 0.5 (Fig 5.6f). We study the droplet generation in both merging and alternate regimes for the increasing contact angle and reducing interfacial tension due to the addition of surfactant and an increase in its concentration.

Merging of droplets

To study the effect of surfactant on droplet generation in the merging regime, we set the velocity of V_c and V_d to be 0.004 m/s and 0.002 m/s, respectively (Fig 5.7a). In the interest of reporting the results in the merging regime, the velocity of the two liquids has been reduced only in this section to maintain $C_a < 0.02$. The dispersed phase liquid from both the side channel enters the main channel and merges at the junction and pinches off due to the viscous shear force of the continuous phase liquid. The sequence of the merging of two droplets and their release is shown in Fig 5.7b. In our case, there is no significant change seen in the droplet generation mechanism with the addition of surfactant (interfacial tension reduces from 7 mN/m to 4 mN/m and increases the contact angle from 152^o to 172^o). This could be because the change in the interfacial tension is marginal and though the range of change in contact angle seems fairly good,

a numerical study on droplet generation on a single T-junction device shows that the frequency of droplet generation sees a marginal change in generating frequency with increasing contact angle from 100^o to 180^o for $\lambda < 1$ (Bashir et al. 2011). In our study, we show that it holds even in a double T-junction device.

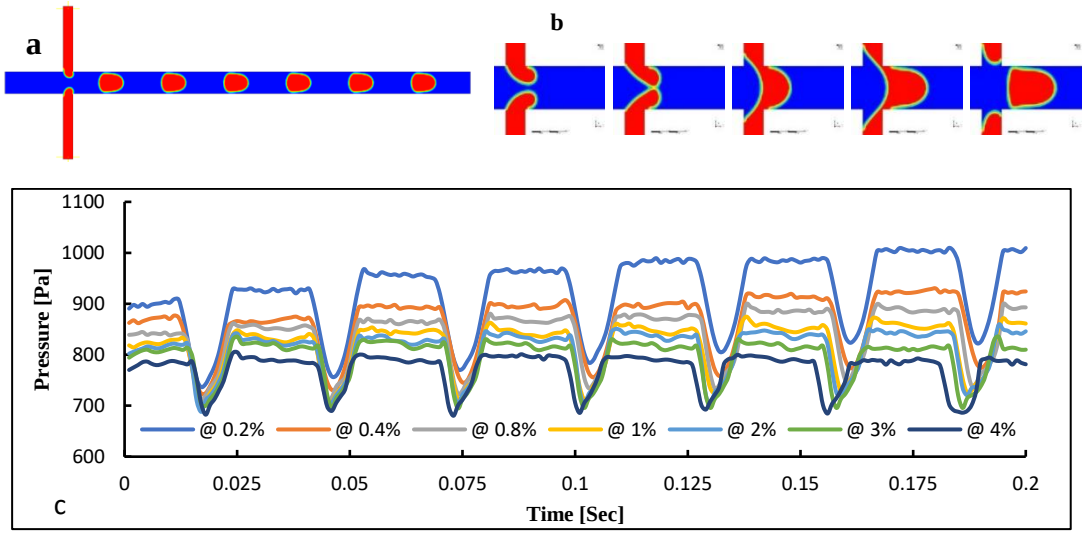

Fig 5.9: a) Droplet generation in merging regime. b) Sequence of Droplet generation in merging regime c) Pressure at the dispersed phase liquid inlet Vs Time for surfactant concentration.

The temporal variation in pressure also provides us with more information on droplet generation in the merging regime (Fig 5.7c). The number of pressure minima is equal to the number of droplets released (in Fig 5.7c each curve represents the release of 7 droplets). The pressure at point P_c increases as the dispersed phase liquid enters and blocks the main channel and it drops as the droplet is released. The maximum pressure during the first droplet release was found to be 830Pa and it increases to 1000Pa with time a stable droplet generation is seen when the surfactant concentration is at 0.2%. The maximum pressure during droplet generation gradually reduces with an increase in surfactant concentration. The maximum pressure during the first droplet release was found to be 780Pa and it continues to remain the same with time at a surfactant concentration of 4%. The average pressure (plateau region) during the droplet generation decreases with increased surfactant concentration (Fig 5.7c). In addition, the average pressure during the droplet generation increases gradually with time as the number of droplets is released and stabilises to a point. When the first droplet exits

through the outlet (in our case, in a given length of the main channel, 6 droplets are seen at any given time, so with the generation of the 7^{th} droplet, the 1^{st} droplet exists through the outlet). This increase in pressure is not seen with the increase in surfactant concentration. The frequency of droplet generation can be calculated depending on the droplet release time and it was found to increase marginally from 36Hz to 42Hz. The increase in frequency develops with time.

Alternate Droplet generation

To study droplet generation in an alternate regime, the velocity of the two liquids viz., V_c and V_d are set to 0.02 m/s and 0.01 m/s, respectively. The alternate droplet generation is investigated for an increase in surfactant concentration from 0.2% to 4%. The droplets are generated in the merging regime for surfactant concentrations ranging from 0.2% to 0.8%. The pressure at points P_1 and P_2 are the same in the merging regime. Hence the temporal variation of pressure with time overlaps (Fig 5.8a). Further increasing the surfactant concentration from 1% to 2%, 3% and 4%, the droplets are generated in alternate regime after 0.04 sec, 0.03 sec, 0.03 sec and 0.0075 sec of flow, respectively. This can be seen by plotting ($\Delta P = P_1 - P_2$). During the merging regime, the ΔP curve ($\Delta P = P_1 - P_2$) is flat. Periodic changes in the pressure between P_1 and P_2 develop with time, and it leads to alternate droplet generation. The flat region in Fig (5.8b-e) indicates that the initial droplets are produced in the merging regime.

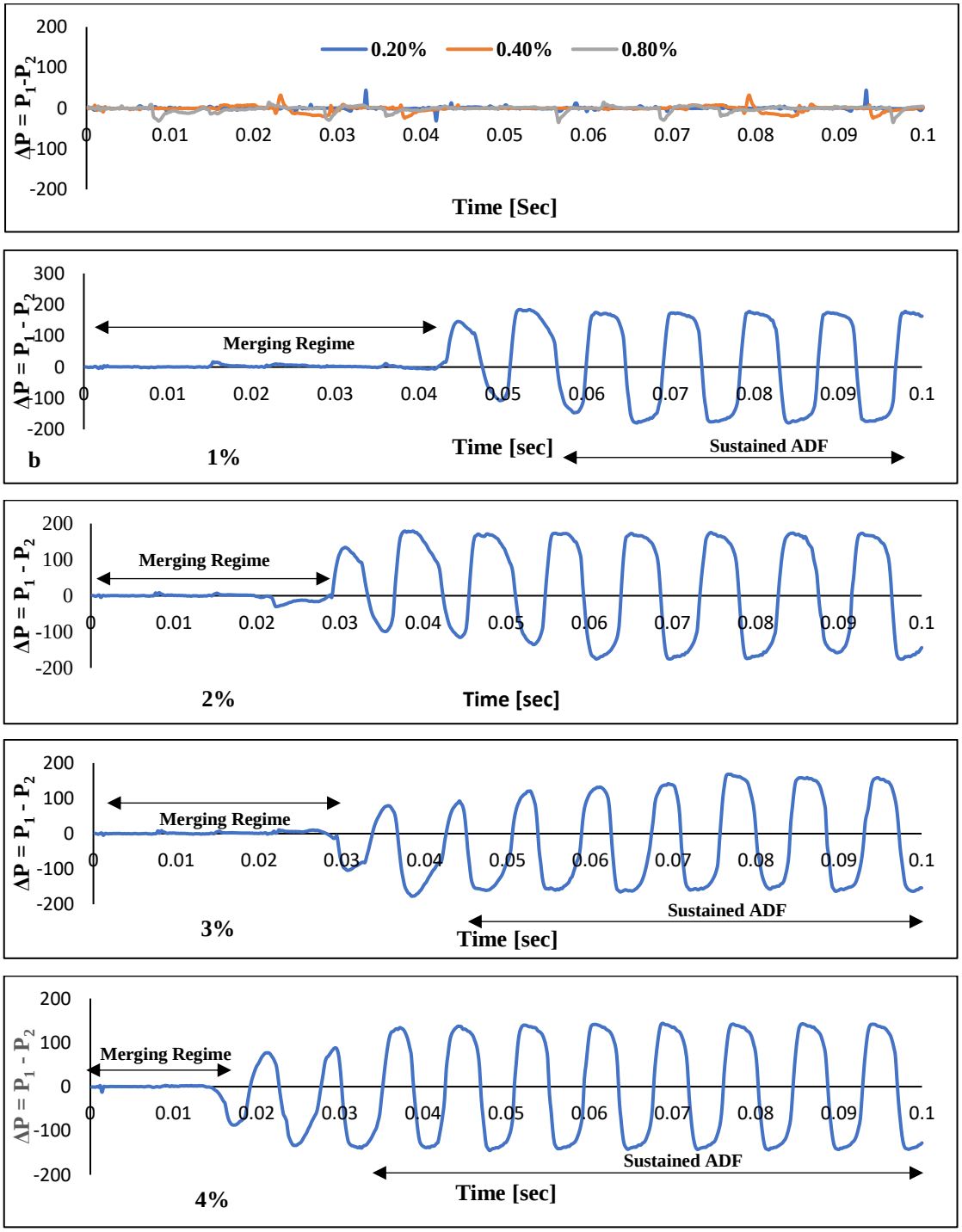

Fig 5.10: Pressure Vs time for various surfactant concentration, a) Difference of pressure ($\Delta P=P_1–P_2$) Vs time for surfactant concentration of 0.2%, 0.4% and 0.8%, b-e) for 1%, 2%, 3%, 4% of surfactant concentration respectively.

5.6 Conclusion

Numerical investigations were carried out on single and double T-junction microfluidic devices using the Volume of Fluid (VOF) method in 2D. The velocity of continuous phase liquid (mineral oil) and dispersed phase liquid (water) was set to 0.02 m/s and 0.01 m/s, respectively. We initially validate our simulation results with experimental data reported earlier for a single T-junction device (Bashir et al. 2014) and a double T-junction device (Zheng et al. 2004a). The droplet generation shifts from dripping to a jetting regime with the increase in the width of the side channel from 50 μm to 100 μm while the width of the main channel was fixed to 100 μm. The frequency of droplet generation reduces marginally from 82 Hz to 77 Hz, and droplet length increases from 80 μm to 135 μm. This change in channel dimensions increases the average pressure in the channel increases from 1670 Pa to 1770 Pa which is approximately 6% to 8% and the capillary number from 0.225 to 0.267 which is approximately 16% in the case of a single T-junction device. The addition of a side-channel to the single T-junction device and converting it to double T-junction devices increase the overall flow in the device. This is seen when the width of one of the side channels in double T-junction increases from 50 μm to 100 μm, the average pressure increases from 2130 Pa to 2270 Pa, which is approximately 7% and capillary number from 0.306 to 0.353 which is approximately 16%. The pressure variation in both the side channel plotted with time shows that the pressure is higher in the smaller side channel.

The frequency of droplet generation is seen to decrease from 238 Hz to 82 Hz and increase in droplet length from 56 μm to 80 μm for the increase in the width of the main channel from 50 μm to 100 μm while the width of the side-channel is fixed to 50 μm. This increase in the width of the main channel decreases the average pressure from 7870 Pa to 1750 Pa which is approximately 75% and the capillary number from 0.267 to 0.225 which is approximately 15%. Similarly, with a change in the width of the main channel in a double T-junction device, the average pressure decreases from 8830 Pa to 1930 Pa which is approximately 78%, and the capillary number from 0.354 to 0.306 which is approximately 16%. The gradual increase in width of the main channel also shows that droplet generation shifts from merging regime to alternate droplets regime

when the width of the main channel is 1.4 times the width of the side channel. The frequency of droplet generation and droplet length does not significantly change for the increase in the concentration of surfactant (Span 80) from 0.2% to 4% in the merging regime. However, in the case of an alternate regime, it is seen for concentration above 1%.

CHAPTER 6

SUMMARY AND CONCLUSIONS

6.1 Summary

This thesis reports simulation studies on droplet generation due to two immiscible liquids flowing in single and double T-junction devices and surface energy-based trapping of microdroplets in a micro-well in the devices. A Slip-Chip type microfluidic device is considered for the investigations. The Slip-Chip type device comprises two plates, viz., the Channel Plate and the micro-well Plate which are bonded temporarily using a sealant. The simulation studies on droplet generation in these devices have been carried out under the following flow conditions for the two liquids:

(i) a steady flow of two immiscible liquids in single T-junction devices.
(ii) the pulsed flow of the dispersed phase liquid in single T-junction devices while the continuous phase liquid flows at a steady flow rate.
(iii) a steady flow of two immiscible liquids in double T-junction devices.

The motivation for these investigations was to get a better understanding of the droplet generation mechanism under various flow conditions.

In the case of a steady flow of two immiscible liquids in single T-junction devices, the plots of pressure versus time in the side and main channels show that the use of surfactant (Span 80) results in increased frequency of droplet generation and reduced droplet length in squeezing to dripping transition regime. This is not seen in the squeezing regime. The surfactant concentration profile over the droplet surface is seen to be higher at the front and rear end of the droplet than over the rest of the surface.

In the case of pulsed flow of dispersed phase liquid in single T-junction devices, a single droplet is generated for each pulse duration. With the addition of a small amount of surfactant, a pair of droplets is generated for each pulse duration. When the pulse

duration is reduced to half, only single droplets are generated even with the addition of surfactant. The temporal variation of pressure in the side channel, in the case of shorter pulse duration, shows a small step profile which indicates the release of the droplet followed by the retraction of the water thread into the side channel. The small step profile disappears at a higher surfactant concentration. In addition, the average pressure in the side channel gets reduced with the addition of the surfactant.

In the case of droplet generation in double T-junction devices, droplets may be generated in the merging or the alternate regime by controlling the capillary number. The average pressure in the main channel and the capillary number increase with the increase in the width of one of the side channels in a double T-junction device. In addition, since the velocity of the liquids in both the side channels is fixed, pressure increases in the side channel whose width is reduced. The average pressure in both side and main channel and the capillary number decrease with the increase in the width of the main channel in the double T-junction device. The temporal variation in pressure in the side channel is periodic during alternate droplet generation. The decrease in the interfacial tension and increase in contact angle due to the addition of surfactant is negligible when the droplets are generated in double T-junction in the merging regime, whereas, the changes are significant in the alternate regime.

The simulation studies on the trapping of microdroplets were carried out to:

(i) study the effect of a Pit in the main channel on the trapping of droplets in the micro-well.
(ii) study the effect of a Pinhole in the main channel on the trapping of droplets in the micro-well.

The Pit in the microchannel facilitates the trapping of the droplet in the micro-well. In this study, the trapping of the droplet is seen to depend on various factors such as flow velocity in the main channel, droplet length, the droplet size, depth of the micro-well, and alignment of the Pit-micro-well constituting the device. To trap the droplet, its velocity must be less than the critical trapping velocity. The addition of a surfactant to

the mineral oil is seen to lead to a significant reduction in the critical velocity for the droplet trapping. The trapping of droplets traveling at velocities close to the critical velocity for trapping depends strongly on pit-microwell alignment.

A small pinhole located just before the micro-well facilitates the trapping of pancake-shaped droplets. In this study, the critical trapping velocity of the droplet was seen to increase with an increase in the pinhole diameter. The droplets do not get trapped in micro-wells if the surfactant concentration exceeds 0.05%.

Chapter 1 presents a brief account of the field of droplet microfluidics and its applications over the past two decades. The droplet generation mechanisms due to the flow of two immiscible liquids are discussed for various device configurations. The droplet generation mechanism in T-junction devices and the influence of surfactants are discussed. A literature review on microdroplet generation, trapping, and its applications are presented. The problems in this field that have not been adequately investigated have been mentioned.

In Chapter 2 the numerical methods adopted in the present research work are described. Fluid flow solver schemes and optimisation techniques used in the Volume of Fluid (VOF) method are presented. Simulation settings, fluid properties of the two immiscible liquids, flow boundary conditions, and flow rates of the two liquids for droplet generation and trapping of microdroplets at a varying concentration of surfactants are mentioned. The device geometries of the various device types investigated in the thesis are presented.

Chapter 3, presents the simulation results on the generation and trapping of microdroplets with a steady flow of two liquids in single T-junction devices. The effect of fluid flow rates and surfactant concentration (Span 80) on droplet generation has been investigated. From these studies it was concluded that a rise in the surfactant concentration by 4%, increases the frequency of droplet generation by 16% at the higher capillary number (C_a = 0.02), whereas there is only a marginal or no change in the case of squeezing regime (C_a = 0.0028 – 0.008). Further, the investigations on the trapping

of microdroplets reveal that the droplet is highly influenced by the viscous drag force, droplet's length, surface energy, speed, and depth of the micro-well for trapping and alignment of the two plates constituting the device (SlipChip device). It is shown that the droplets traveling faster than a critical trapping velocity, do not get trapped in the micro-well. The trapping of droplets traveling at velocities close to the critical velocity for trapping depends strongly on the alignment (Pit-micro-well alignment) of the two plates. The influence of Pit diameter, its alignment with the micro-well, and depth of micro-well on droplet trapping has also been studied.

Chapter 4 discusses the simulation results on the generation and trapping of microdroplet by pulsing the flow of dispersed phase liquid while the continuous phase liquid is at a steady flow rate. The flow rate of the continuous phase liquid is kept constant, whereas that of the dispersed phase liquid is pulsed between zero and 0.1μL/s. When the pulse On-time (ΔT_1) is 6.5msec, the device generates one droplet per pulse. When a surfactant, with a concentration of 1% or more, is added, the same device generates a pair of droplets per pulse. When ΔT_1 is reduced to 3.25msec, only a single droplet is generated per pulse irrespective of the concentration of the surfactant. Reduction in the width of the side channel of the device leads to the generation of smaller droplets. The trapping of droplets of length 80μm is seen to occur when the continuous liquid flow rate Q_c is $\leq$ 0.01μL/s and the pinhole diameter is in the range of 20μm to 50μm. Smaller droplets, of length 40μm, get trapped for pinhole diameters in the range of 5μm to 20μm. In the case of droplets of length 80μm, when Q_c = 0.0125μL/s, the trapping is seen for pinhole diameter between 45μm to 60μm. When Q_c = 0.02μL/Sec no droplet trapping is seen. Our investigations also show that, at such flow rate regimes, droplet trapping does not happen if the surfactant concentration exceeds 0.05%.

Chapter 5 discusses the droplet generation in double T-junction devices. We have compared the results with that presented in Chapter 3 in terms of the change in average pressure and capillary number. The pressure in the side channel increases by 6% and capillary number by 16% for an increase in width of the side channel from 50μm to 100μm in a single T-junction device. Similarly, when the width of one of the side

channels in a double T-junction increases from 50μm to 100μm, the pressure increases by 8% and the capillary number by 15%. The temporal variation of pressure in both the side channels shows that the pressure is higher in the smaller side channel. When the width of the main channel is increased from 50μm to 100μm, the pressure decreases by 77% and capillary number by 5% in the case of a single T-junction device. Similarly, when the width of the main channel in the double T-junction increases from 50μm to 100μm, the average pressure decreases by 80% and the capillary number by 6%. The gradual increase in width of the main channel shows that droplet generation shifts from merging to an alternate regime when the width of the main channel is 1.4 times the width of the side channel. In this case, the temporal variation in pressure in the side channel during the alternate regime is sinusoidal. The influence of surfactant on droplet generating in double T-junction is marginal in the merging regime but significant in the alternate regime. The droplet generation switches from merging to an alternate regime with surfactant concentration from 1%.

6.2 Conclusions

The important conclusions drawn from the thesis are listed below.

a) The decrease in the interfacial tension and increase in the contact angle due to the addition of surfactant on droplet generation is significant during squeezing to dripping transition regime and dripping regime (approx. C_a = 0.02) but not in the squeezing regime (C_a = 0.0028). The surfactant concentration profile on the droplet surface shows that the surfactant concentration is higher at the two poles of the droplet than at the other parts of the droplet. It is a little higher at the front pole of the droplet as compared to that at the rear pole. Once the droplet is generated, it moves along with the continuous phase liquid. In order to trap an elongated droplet in the micro-well, its velocity must be below the critical trapping velocity. The droplet generation mechanism with and without the presence of surfactant can be analysed using the pressure versus time plots for droplets of different sizes.

b) The droplet generation, in the case of pulsed flow, can be controlled by varying the pulse duration of dispersed phase liquid. The droplet generating in jetting regime with a steady flow of the two liquids can be switched to the dripping regime by pulsing the flow of dispersed phase liquid. This helps in controlling droplet length and droplet generation frequency. The reduction in interfacial tension and increase in contact angle caused due to the increase in surfactant concentration change the droplet generation mechanism for a given pulse duration. Droplet pairs are generated at relatively higher surfactant concentrations. The trapping of the generated droplets (pancake shape) in the micro-well can be facilitated by having a small pinhole just before it. Increased surfactant concentration reduces the critical trapping velocity of the droplet. The droplet generation mechanism for the case of pulsed flow of the dispersed phase liquid may be analysed using the pressure versus time plots. It is seen that the trapping of droplets is facilitated by a small pinhole close to the micro-well.

c) The droplet generation in a double T-junction device is seen to occur in two ways. Dispersed phase liquid stream from each side channel merges and a droplet is generated at capillary number Ca < 0.024. Above this value of Ca, droplet generation happens from each side channel alternatively and the droplets do not merge. For a given flow rate, the average pressure and capillary number in the side channel depend on the width of the side channel in both single and double T-junction devices. The temporal variations of pressure in the side channel show that the pressure variation pattern with time is different in the case of asymmetric and symmetric double T-junction devices. There is no change in the frequency of droplet generation or droplet length with an increase in the surfactant concentration from 0.2% to 4% in the merging regime (Ca < 0.02). However, in the case of the alternate regime (Ca > 0.024), droplets are produced by merging dispersed phase liquid from both the side channel till the surfactant concentration reaches 0.8%. Droplets from each side channel are produced alternatively for surfactant concentrations from 1% to 4% of surfactant concentration.

6.3 Scope and Future work

The investigations of the present research work can be extended future in the following directions.

- The role of temporary sealing (in the SlipChip type of device) on fluid flow can be studied. This will be useful because, at higher flow rates, liquids may seep between the two plates. Hence, it is good to identify the threshold flow rate.

- There are a lot of scopes in understanding the droplet trapping mechanism due to surface energy change. The role of surface wetting, interfacial tension, and viscosity ratio on trapping of microdroplet. This will be useful when trapping microdroplets in 96 micro-well plates.

- Droplets do not coalesce when surfactants are used. When a train of microdroplets is generated, the velocity of the droplet may be within the critical trapping velocity and still may not be trapped. This is because the droplet experiences body force by the subsequent droplet. Hence, in order to trap a single droplet in a micro-well it is important to identify the minimum distance between two successive droplets. This cannot be solved in the Volume of Fluid Method (VOF) and it requires Immersed Boundary Method (IBM).

- Glass-based droplet generating microfluidic devices are recommended for SlipChip configuration. The device can be fabricated by the microfabrication process. The channel profile can be circular (can be achieved by isotropic etching), rectangular (can be achieved by reactive ion etching), or with tapered sidewalls (wet etching). However, these methods can be expensive to current practices. This may open a lot of scopes in developing a method that can be affordable. This configuration of the device (SlipChip) is important because it provides access to trapped droplets in a micro-well array.

REFERENCES

Abate, A. R., Mary, P., Steijn, V. van, and Weitz, D. A. (2012). "Experimental validation of plugging during drop formation in a T-junction." *Lab Chip*, 12(8), 1516–1521.

Abbyad, P., Dangla, R., Alexandrou, A., and Baroud, C. N. (2011). "Rails and anchors: guiding and trapping droplet microreactors in two dimensions." *Lab Chip*, 11(5), 813–821.

Acrivos, A. (1983). "The Breakup of Small Drops and Bubbles in Shear Flows*." *Annals of the New York Academy of Sciences*, 404(1), 1–11.

Adzima, B. J., and Velankar, S. S. (2006). "Pressure drops for droplet flows in microfluidic channels." *J. Micromech. Microeng.*, 16(8), 1504–1510.

Amselem, G., Brun, P. T., Gallaire, F., and Baroud, C. N. (2015). "Breaking Anchored Droplets in a Microfluidic Hele-Shaw Cell." *Phys. Rev. Applied*, 3(5), 054006.

Anderson, D. M., McFadden, G. B., and Wheeler, A. A. (1998). "Diffuse-Interface Methods in Fluid Mechanics." *Annual Review of Fluid Mechanics*, 30(1), 139–165.

Anderson, J. R., Chiu, D. T., Jackman, R. J., Cherniavskaya, O., McDonald, J. C., Wu, H., Whitesides, S. H., and Whitesides, G. M. (2000). "Fabrication of Topologically Complex Three-Dimensional Microfluidic Systems in PDMS by Rapid Prototyping." *Anal. Chem.*, 72(14), 3158–3164.

Anna, S. L., and Mayer, H. C. (2006). "Microscale tipstreaming in a microfluidic flow focusing device." *Physics of Fluids*, 18(12), 121512.

Babahosseini, H., Misteli, T., and DeVoe, D. L. (2019). "Microfluidic on-demand droplet generation, storage, retrieval, and merging for single-cell pairing." *Lab Chip*, 19(3), 493–502.

Bashir, S., Rees, J. M., and Zimmerman, W. B. (2011). "Simulations of microfluidic droplet formation using the two-phase level set method." *Chemical Engineering Science*, 66(20), 4733–4741.

Bashir, S., Solvas, X. C. i., Bashir, M., Rees, J. M., and Zimmerman, W. B. J. (2014). "Dynamic wetting in microfluidic droplet formation." *BioChip J*, 8(2), 122–128.

Bastani, D., Fayzi, P., Lotfi, M., and Arzideh, S. M. (2018). "CFD simulation of bubble in flow field: Investigation of dynamic interfacial behaviour in presence of surfactant molecules." *Colloid and Interface Science Communications*, 27, 1–10.

Batchelor, G. K. (2000). *An Introduction to Fluid Dynamics*. Cambridge Mathematical Library, Cambridge: Cambridge University Press.

Borhan, A., and Mao, C. (1992). "Effect of surfactants on the motion of drops through circular tubes." *Physics of Fluids A: Fluid Dynamics*, 4(12), 2628–2640.

Brackbill, J. U., Kothe, D. B., and Zemach, C. (1992). "A continuum method for modeling surface tension." *Journal of Computational Physics*, 100(2), 335–354.

Brody, J. P., Yager, P., Goldstein, R. E., and Austin, R. H. (1996). "Biotechnology at low Reynolds numbers." *Biophysical Journal*, 71(6), 3430–3441.

Campanelli, J. R., and Wang, X. (1999). "Dynamic Interfacial Tension of Surfactant Mixtures at Liquid–Liquid Interfaces." *Journal of Colloid and Interface Science*, 213(2), 340–351.

Carrier, O., Funfschilling, D., and Li, H. Z. (2014). "Effect of the fluid injection configuration on droplet size in a microfluidic T junction." *Phys. Rev. E*, 89(1), 013003.

Cerdeira, A. T. S., Campos, J. B. L. M., Miranda, J. M., and Araújo, J. D. P. (2020). "Review on Microbubbles and Microdroplets Flowing through Microfluidic Geometrical Elements." *Micromachines*, 11(2), 201.
Churski, K., Michalski, J., and Garstecki, P. (2010). "Droplet on demand system utilizing a computer controlled microvalve integrated into a stiff polymeric microfluidic device." *Lab Chip*, 10(4), 512–518.
Clausell-Tormos, J., Lieber, D., Baret, J.-C., El-Harrak, A., Miller, O. J., Frenz, L., Blouwolff, J., Humphry, K. J., Köster, S., Duan, H., Holtze, C., Weitz, D. A., Griffiths, A. D., and Merten, C. A. (2008). "Droplet-Based Microfluidic Platforms for the Encapsulation and Screening of Mammalian Cells and Multicellular Organisms." *Chemistry & Biology*, 15(5), 427–437.
Cramer, C., Fischer, P., and Windhab, E. J. (2004). "Drop formation in a co-flowing ambient fluid." *Chemical Engineering Science*, 59(15), 3045–3058.
Crawford, D. F., Smith, C. A., and Whyte, G. (2017). "Image-based closed-loop feedback for highly mono-dispersed microdroplet production." *Scientific Reports*, 7(1), 10545.
Dalgleish, D. G., West, S. J., and Hallett, F. R. (1997). "The characterization of small emulsion droplets made from milk proteins and triglyceride oil." *Colloids and Surfaces A: Physicochemical and Engineering Aspects*, Frontiers in Colloid Chemistry an International Festschrift to Professor Stig E. Friberg, 123–124, 145–153.
Dangla, R., Lee, S., and Baroud, C. N. (2011). "Trapping Microfluidic Drops in Wells of Surface Energy." *Phys. Rev. Lett.*, 107(12), 124501.
DeBar, R. B. (1974). *Fundamentals of the KRAKEN code. [Eulerian hydrodynamics code for compressible nonviscous flow of several fluids in two-dimensional (axially symmetric) region]*. California Univ., Livermore (USA). Lawrence Livermore Lab.
Dreyfus, R., Tabeling, P., and Willaime, H. (2003). "Ordered and Disordered Patterns in Two-Phase Flows in Microchannels." *Phys. Rev. Lett.*, 90(14), 144505.
Elani, Y., I. Solvas, X. C., B. Edel, J., V. Law, R., and Ces, O. (2016). "Microfluidic generation of encapsulated droplet interface bilayer networks (multisomes) and their use as cell-like reactors." *Chemical Communications*, 52(35), 5961–5964.
Ferraro, D., Serra, M., Filippi, D., Zago, L., Guglielmin, E., Pierno, M., Descroix, S., Viovy, J.-L., and Mistura, G. (2018). "Controlling the distance of highly confined droplets in a capillary by interfacial tension for merging on-demand." *Lab Chip*, 19(1), 136–146.
Fidalgo, L. M., Abell, C., and Huck, W. T. S. (2007). "Surface-induced droplet fusion in microfluidic devices." *Lab Chip*, 7(8), 984–986.
"Fundamentals of Capillarity." (2012). *The Physics of Microdroplets*, John Wiley & Sons, Ltd, 5–64.
Garstecki, P., Fuerstman, M. J., Stone, H. A., and Whitesides, G. M. (2006). "Formation of droplets and bubbles in a microfluidic T-junction—scaling and mechanism of break-up." *Lab Chip*, 6(3), 437–446.
Glawdel, T., and Ren, C. L. (2012). "Droplet formation in microfluidic T-junction generators operating in the transitional regime. III. Dynamic surfactant effects." *Phys. Rev. E*, 86(2), 026308.
Griffin, W. C. (1949). "CLASSIFICATION OF SURFACE-ACTIVE AGENTS BY 'HLB.'" 1(5), 311–326.

Griffin, W. C. (1954). “CALCULATION OF HLB VALUES OF NON-IONIC SURFACTANTS.” 5(4).
Guo, F., Liu, K., Ji, X.-H., Ding, H.-J., Zhang, M., Zeng, Q., Liu, W., Guo, S.-S., and Zhao, X.-Z. (2010). “Valve-based microfluidic device for droplet on-demand operation and static assay.” *Appl. Phys. Lett.*, 97(23), 233701.
Gupta, A., and Kumar, R. (2010a). “Effect of geometry on droplet formation in the squeezing regime in a microfluidic T-junction.” *Microfluid Nanofluid*, 8(6), 799–812.
Gupta, A., and Kumar, R. (2010b). “Flow regime transition at high capillary numbers in a microfluidic T-junction: Viscosity contrast and geometry effect.” *Physics of Fluids*, 22(12), 122001.
Gupta, A., and Kumar, R. (2010c). “Flow regime transition at high capillary numbers in a microfluidic T-junction: Viscosity contrast and geometry effect.” *Physics of Fluids*, 22(12), 122001.
Gupta, A., Murshed, S. M. S., and Kumar, R. (2009). “Droplet formation and stability of flows in a microfluidic T-junction.” *Appl. Phys. Lett.*, 94(16), 164107.
Han, W., and Chen, X. (2019a). “New insights into the pressure during the merged droplet formation in the squeezing time.” *Chemical Engineering Research and Design*, 145, 213–225.
Han, W., and Chen, X. (2019b). “Effect of Geometry Configuration on the Merged Droplet Formation in a Double T-Junction.” *Microgravity Sci. Technol.*, 31(6), 855–864.
Haynes, D. H. (1988). “Microdroplets of water-insoluble drugs and injectable formulations containing same.”
He, M., Sun, C., and Chiu, D. T. (2004). “Concentrating Solutes and Nanoparticles within Individual Aqueous Microdroplets.” *Anal. Chem.*, 76(5), 1222–1227.
He, Z., Dagan, Z., and Maldarelli, C. (1991). “The influence of surfactant adsorption on the motion of a fluid sphere in a tube. Part 1. Uniform retardation controlled by sorption kinetics.” *Journal of Fluid Mechanics*, 222, 1–32.
Hirama, H., and Torii, T. (2015). “One-to-one encapsulation based on alternating droplet generation.” *Sci Rep*, 5(1), 15196.
Hirt, C. W., and Nichols, B. D. (1981a). “Volume of fluid (VOF) method for the dynamics of free boundaries.” *Journal of Computational Physics*, 39(1), 201–225.
Hirt, C. W., and Nichols, B. D. (1981b). “Volume of fluid (VOF) method for the dynamics of free boundaries.” *Journal of Computational Physics*, 39(1), 201–225.
Hoang, P. H., and Dien, L. Q. (2014). “Fast synthesis of an inorganic–organic block copolymer in a droplet-based microreactor.” *RSC Adv.*, 4(16), 8283–8288.
Hosokawa, K., Fujii, T., and Endo, I. (1999a). “Droplet-based nano/picoliter mixer using hydrophobic microcapillary vent.” *Technical Digest. IEEE International MEMS 99 Conference. Twelfth IEEE International Conference on Micro Electro Mechanical Systems (Cat. No.99CH36291)*, 388–393.
Hosokawa, K., Fujii, T., and Endo, I. (1999b). “Handling of Picoliter Liquid Samples in a Poly(dimethylsiloxane)-Based Microfluidic Device.” *Anal. Chem.*, 71(20), 4781–4785.
Hosokawa, K., Fujii, T., and Endo, I. (2000). “Formation and Active Mixing of Metered Nano/Picoliter Liquid Droplets in a Microfluidic Device.” *Micro Total Analysis Systems 2000*, A. van den Berg, W. Olthuis, and P. Bergveld, eds., Dordrecht: Springer Netherlands, 481–484.

Huckaby, J. L., and Ray, A. K. (1995). “Layer Formation on Microdroplets: A Study Based on Resonant Light Scattering.” *Langmuir*, 11(1), 80–86.
Hung, L.-H., M. Choi, K., Tseng, W.-Y., Tan, Y.-C., J. Shea, K., and Phillip Lee, A. (2006). “Alternating droplet generation and controlled dynamic droplet fusion in microfluidic device for CdS nanoparticle synthesis.” *Lab on a Chip*, 6(2), 174–178.
Hung, L.-H., Teh, S.-Y., Jester, J., and Lee, A. P. (2010). “PLGA micro/nanosphere synthesis by droplet microfluidic solvent evaporation and extraction approaches.” *Lab Chip*, 10(14), 1820–1825.
H. Xu, J., S. Luo, G., W. Li, S., and G. Chen, G. (2006). “Shear force induced monodisperse droplet formation in a microfluidic device by controlling wetting properties.” *Lab on a Chip*, 6(1), 131–136.
Jakiela, S., Debski, P. R., Dabrowski, B., and Garstecki, P. (2014). “Generation of Nanoliter Droplets on Demand at Hundred-Hz Frequencies.” *Micromachines*, 5(4), 1002–1011.
Jin, B.-J., and Yoo, J. Y. (2012). “Visualization of droplet merging in microchannels using micro-PIV.” *Exp Fluids*, 52(1), 235–245.
Kagawa, Y., Ishigami, T., Hayashi, K., Fuse, H., Mino, Y., and Matsuyama, H. (2014). “Permeation of concentrated oil-in-water emulsions through a membrane pore: numerical simulation using a coupled level set and the volume-of-fluid method.” *Soft Matter*, 10(40), 7985–7992.
Kopolow, S. L., Burlant, W. J., Helioff, M. W., Bires, C. D., Login, R. B., and Tazi, M. (1992). “Skin care compositions containing discrete microdroplets of an oil in water stabilized by in situ polymerization of water-soluble vinyl monomer.”
Kovalchuk, N. M., Roumpea, E., Nowak, E., Chinaud, M., Angeli, P., and Simmons, M. J. H. (2018). “Effect of surfactant on emulsification in microchannels.” *Chemical Engineering Science*, 176, 139–152.
Lankers, M., Popp, J., and Kiefer, W. (1994). “Raman and Fluorescence Spectra of Single Optically Trapped Microdroplets in Emulsions.” *Appl. Spectrosc., AS*, 48(9), 1166–1168.
Lee, M., Park, W., Chung, C., Lim, J., Kwon, S., Ahn, K. H., Lee, S. J., and Char, K. (2010). “Multilayer deposition on patterned posts using alternating polyelectrolyte droplets in a microfluidic device.” *Lab Chip*, 10(9), 1160–1166.
Lee, T. Y., Choi, T. M., Shim, T. S., Frijns, R. A. M., and Kim, S.-H. (2016). “Microfluidic production of multiple emulsions and functional microcapsules.” *Lab Chip*, 16(18), 3415–3440.
Li, G., Chen, Q., Li, J., and Jianlong, Z. (2009). “Optimization of surface-tension-induced droplet trapping for static microarray applications.” *Thirteenth international conference on miniaturised systems for chemistry and life science*, 761–763.
Li, L., Karymov, M. A., Nichols, K. P., and Ismagilov, R. F. (2010). “Dead-End Filling of SlipChip Evaluated Theoretically and Experimentally as a Function of the Surface Chemistry and the Gap Size between the Plates for Lubricated and Dry SlipChips.” *Langmuir*, 26(14), 12465–12471.
Lin, B.-C., and Su, Y.-C. (2008). “On-demand liquid-in-liquid droplet metering and fusion utilizing pneumatically actuated membrane valves.” *J. Micromech. Microeng.*, 18(11), 115005.
Lin, R., Fisher, J. S., Simon, M. G., and Lee, A. P. (2012). “Novel on-demand droplet generation for selective fluid sample extraction.” *Biomicrofluidics*, 6(2), 024103.

Liu, H., and Zhang, Y. (2009). “Droplet formation in a T-shaped microfluidic junction.” *Journal of Applied Physics*, 106(3), 034906.
Liu, H., and Zhang, Y. (2017). “Lattice Boltzmann simulation of the trapping of a microdroplet in a well of surface energy.” *Computers & Fluids*, ICMMES2015, 155, 68–75.
Liu, K., and Qin, J. (2013). “Droplet-fused microreactors for room temperature synthesis of nanoscale needle-like hydroxyapatite.” *Nanotechnology*, 24(12), 125602.
Menech, M. D., Garstecki, P., Jousse, F., and Stone, H. A. (2008). “Transition from squeezing to dripping in a microfluidic T-shaped junction.” *Journal of Fluid Mechanics*, 595, 141–161.
Ménétrier-Deremble, L., and Tabeling, P. (2006). “Droplet breakup in microfluidic junctions of arbitrary angles.” *Phys. Rev. E*, 74(3), 035303.
Milliken, W. J., Stone, H. A., and Leal, L. G. (1993). “The effect of surfactant on the transient motion of Newtonian drops.” *Physics of Fluids A: Fluid Dynamics*, 5(1), 69–79.
“Minimal Energy and Stability Rubrics.” (2012). *The Physics of Microdroplets*, John Wiley & Sons, Ltd, 65–82.
Nagel, M., Brun, P.-T., and Gallaire, F. (2014). “A numerical study of droplet trapping in microfluidic devices.” *Physics of Fluids*, 26(3), 032002.
Nekouei, M., and Vanapalli, S. A. (2017). “Volume-of-fluid simulations in microfluidic T-junction devices: Influence of viscosity ratio on droplet size.” *Physics of Fluids*, 29(3), 032007.
Ngo, I.-L., Dang, T.-D., Byon, C., and Joo, S. W. (2015). “A numerical study on the dynamics of droplet formation in a microfluidic double T-junction.” *Biomicrofluidics*, 9(2), 024107.
Nguyen, M.-A., and Sarles, S. A. (2016). “Microfluidic Generation, Encapsulation and Characterization of Asymmetric Droplet Interface Bilayers.” American Society of Mechanical Engineers Digital Collection.
Nguyen, N.-T., Wang, C., Wong, T. N., Low, L. N., and Ho, S. S. (2006). “A Silicon/glass-based microfluidic device for invetigation of Lagrangian velocity field in microdroplets.” *J. Phys.: Conf. Ser.*, 34, 130–135.
Nisisako, T., Okushima, S., and Torii, T. (2005). “Controlled formulation of monodisperse double emulsions in a multiple-phase microfluidic system.” *Soft Matter*, 1(1), 23–27.
Nisisako, T., Torii, T., and Higuchi, T. (2002). “Preparation of Picoliter-Sized Reaction / Analysis Chambers for Droplet-Based Chemical and Biochemical Systems.” *Micro Total Analysis Systems 2002*, Y. Baba, S. Shoji, and A. van den Berg, eds., Dordrecht: Springer Netherlands, 362–364.
Nisisako, T., Torii, T., and Higuchi, T. (2004). “Novel microreactors for functional polymer beads.” *Chemical Engineering Journal*, 7th International Conference on Microreaction Technology, 101(1), 23–29.
Noh, W. F., and Woodward, P. (1976). “SLIC (Simple Line Interface Calculation).” *Proceedings of the Fifth International Conference on Numerical Methods in Fluid Dynamics June 28 – July 2, 1976 Twente University, Enschede*, Lecture Notes in Physics, A. I. van de Vooren and P. J. Zandbergen, eds., Berlin, Heidelberg: Springer, 330–340.

O'Brien, C. M., Rood, K. D., Bhattacharyya, K., DeSouza, T. Q., Sengupta, S., Gupta, S. K., Mosley, J. D., Goldschmidt, B. S., Sharma, N., and Viator, J. A. (2012). "Capture of circulating tumor cells using photoacoustic flowmetry and two phase flow." *JBO*, 17(6), 061221.
Osher, S., and Sethian, J. A. (1988). "Fronts propagating with curvature-dependent speed: Algorithms based on Hamilton-Jacobi formulations." *Journal of Computational Physics*, 79(1), 12–49.
Pasternack, L., Fleming, J. W., and Owrutsky, J. C. (1996). "Optically seeded stimulated Raman scattering of aqueous sulfate microdroplets." *J. Opt. Soc. Am. B, JOSAB*, 13(7), 1510–1516.
Peng, L., Yang, M., Guo, S., Liu, W., and Zhao, X. (2011). "The effect of interfacial tension on droplet formation in flow-focusing microfluidic device." *Biomed Microdevices*, 13(3), 559–564.
Piccin, E., Ferraro, D., Sartori, P., Chiarello, E., Pierno, M., and Mistura, G. (2014). "Generation of water-in-oil and oil-in-water microdroplets in polyester-toner microfluidic devices." *Sensors and Actuators B: Chemical*, 196, 525–531.
Qian, J. Y., Chen, M., Wu, Z., Jin, Z., and Sunden, B. (2019). "Effects of a dynamic injection flow rate on slug generation in a cross-junction square microchannel." *Processes*, 7(10), 765.
Rallison, J. M. (1984). "The Deformation of Small Viscous Drops and Bubbles in Shear Flows." *Annual Review of Fluid Mechanics*, 16(1), 45–66.
Ray, A. K., and Bhanti, D. D. (1997). "Effect of optical resonances on photochemical reactions in microdroplets." *Appl. Opt., AO*, 36(12), 2663–2674.
Riaud, A., Zhang, H., Wang, X., Wang, K., and Luo, G. (2018). "Numerical Study of Surfactant Dynamics during Emulsification in a T-Junction Microchannel." *Langmuir*, 34(17), 4980–4990.
Rothschild, M., and Forte, A. (1995). "Methods for the fabrication of microstructure arrays."
Rowan, S. M., McHale, G., Newton, M. I., and Toorneman, M. (1997). "Evaporation of Microdroplets of Three Alcohols." *J. Phys. Chem. B*, 101(8), 1265–1267.
Rowan, S. M., Newton, M. I., and McHale, G. (1995). "Evaporation of Microdroplets and the Wetting of Solid Surfaces." *J. Phys. Chem.*, 99(35), 13268–13271.
Saqib, M., Şahinoğlu, O. B., and Erdem, E. Y. (2018). "Alternating Droplet Formation by using Tapered Channel Geometry." *Scientific Reports*, 8(1), 1–9.
Schlicht, B., and Zagnoni, M. (2015). "Droplet-interface-bilayer assays in microfluidic passive networks." *Sci Rep*, 5(1), 1–8.
Schramm, L. L., Stasiuk, E. N., and Marangoni, D. G. (2003). "2 Surfactants and their applications." *Annu. Rep. Prog. Chem., Sect. C: Phys. Chem.*, 99(0), 3–48.
Shi, Y., Gao, X., Chen, L., Zhang, M., Ma, J., Zhang, X., and Qin, J. (2013). "High throughput generation and trapping of individual agarose microgel using microfluidic approach." *Microfluid Nanofluid*, 15(4), 467–474.
Shi, Y., Tang, G. H., and Xia, H. H. (2014). "Lattice Boltzmann simulation of droplet formation in T-junction and flow focusing devices." *Computers & Fluids*, 90, 155–163.
Shui, L., Berg, A. van den, and Eijkel, J. C. T. (2009). "Capillary instability, squeezing, and shearing in head-on microfluidic devices." *Journal of Applied Physics*, 106(12), 124305.

Simon, M. G., Lin, R., Fisher, J. S., and Lee, A. P. (2012). "A Laplace pressure based microfluidic trap for passive droplet trapping and controlled release." *Biomicrofluidics*, 6(1), 014110.
Sohrabi, S., Kassir, N., and Moraveji, M. K. (2020). "Droplet microfluidics: fundamentals and its advanced applications." *RSC Adv.*, 10(46), 27560–27574.
Solvas, X. C. i, and deMello, A. (2011). "Droplet microfluidics: recent developments and future applications." *Chem. Commun.*, 47(7), 1936–1942.
Sontti, S. G., and Atta, A. (2019). "CFD study on Taylor bubble characteristics in Carreau-Yasuda shear thinning liquids." *The Canadian Journal of Chemical Engineering*, 97(2), 616–624.
Squires, T. M., and Quake, S. R. (2005). "Microfluidics: Fluid physics at the nanoliter scale." *Rev. Mod. Phys.*, 77(3), 977–1026.
Sripadaraja, K., Umesh, G., and Satyanarayan, M. N. (2020). "Simulation studies on picolitre volume droplets generation and trapping in T-junction microchannels." *SN Appl. Sci.*, 2(8), 1413.
Steegmans, M. L. J., Schroën, K. G. P. H., and Boom, R. M. (2009). "Characterization of Emulsification at Flat Microchannel Y Junctions." *Langmuir*, 25(6), 3396–3401.
Steijn, V. van, Kleijn, C. R., and Kreutzer, M. T. (2010). "Predictive model for the size of bubbles and droplets created in microfluidic T-junctions." *Lab Chip*, 10(19), 2513–2518.
Steven Abbott. (2018). "Surfactant Science, Principles & Practice." *DEStech Publications, Inc.*
Stone, H. A., Bentley, B. J., and Leal, L. G. (1986). "An experimental study of transient effects in the breakup of viscous drops." *Journal of Fluid Mechanics*, 173, 131–158.
Stone, H. A., and Leal, L. G. (1989). "Relaxation and breakup of an initially extended drop in an otherwise quiescent fluid." *Journal of Fluid Mechanics*, 198, 399–427.
Stone, H. A., and Leal, L. G. (1990). "The effects of surfactants on drop deformation and breakup." *Journal of Fluid Mechanics*, 220, 161–186.
Stone, H. A., Stroock, A. D., and Ajdari, A. (2004). "Engineering Flows in Small Devices: Microfluidics Toward a Lab-on-a-Chip." *Annual Review of Fluid Mechanics*, 36(1), 381–411.
Sun, X., Tang, K., Smith, R. D., and Kelly, R. T. (2013). "Controlled dispensing and mixing of pico- to nanoliter volumes using on-demand droplet-based microfluidics." *Microfluid Nanofluid*, 15(1), 117–126.
Surya, H. P. N., Parayil, S., Banerjee, U., Chander, S., and Sen, A. K. (2015). "Alternating and merged droplets in a double T-junction microchannel." *BioChip J*, 9(1), 16–26.
Tadros, T. F. (2013). "Emulsion Formation, Stability, and Rheology." *Emulsion Formation and Stability*, John Wiley & Sons, Ltd, 1–75.
Tangen, U., Sharma, A., Wagler, P., and McCaskill, J. S. (2015). "On demand nanoliter-scale microfluidic droplet generation, injection, and mixing using a passive microfluidic device." *Biomicrofluidics*, 9(1), 014119.
Taylor, G. I. (1932). "The viscosity of a fluid containing small drops of another fluid." *Proceedings of the Royal Society of London. Series A, Containing Papers of a Mathematical and Physical Character*, 138(834), 41–48.

Taylor, G. I. (1934). “The formation of emulsions in definable fields of flow.” *Proceedings of the Royal Society of London. Series A, Containing Papers of a Mathematical and Physical Character*, 146(858), 501–523.
Thorsen, T., Roberts, R. W., Arnold, F. H., and Quake, S. R. (2001). “Dynamic Pattern Formation in a Vesicle-Generating Microfluidic Device.” *Phys. Rev. Lett.*, 86(18), 4163–4166.
Tomas, A., Paquet, D., Courthaudon, J.-L., and Lorient, D. (1994). “Effect of Fat and Protein Contents on Droplet Size and Surface Protein Coverage in Dairy Emulsions.” *Journal of Dairy Science*, 77(2), 413–417.
Totlani, K., Hurkmans, J.-W., Gulik, W. M. van, Kreutzer, M. T., and Steijn, V. van. (2020). “Scalable microfluidic droplet on-demand generator for non-steady operation of droplet-based assays.” *Lab Chip*, 20(8), 1398–1409.
Um, E., Lee, D.-S., Pyo, H.-B., and Park, J.-K. (2008). “Continuous generation of hydrogel beads and encapsulation of biological materials using a microfluidic droplet-merging channel.” *Microfluid Nanofluid*, 5(4), 541–549.
Umbanhowar, P. B., Prasad, V., and Weitz, D. A. (2000). “Monodisperse Emulsion Generation via Drop Break Off in a Coflowing Stream.” *Langmuir*, 16(2), 347–351.
Veniamin Grigor′evich Levich. (1962). *Physicochemical hydrodynamics.* Englewood Cliffs, N.J.: Prentice-Hall international series in the physical and chemical engineering sciences.
Vivek Ranade. (2002a). “2 Mathematical modeling of flow processes.” *Process Systems Engineering*, Elsevier, 35–55.
Vivek Ranade. (2002b). “4 Multiphase flow processes.” *Process Systems Engineering*, Elsevier, 85–122.
Vowell, S. (2009). *Microfluidics: The Effects of Surface Tension*.
Wang, K., Lu, Y. C., Xu, J. H., and Luo, G. S. (2009a). “Determination of Dynamic Interfacial Tension and Its Effect on Droplet Formation in the T-Shaped Microdispersion Process.” *Langmuir*, 25(4), 2153–2158.
Wang, K., Zhang, L., Zhang, W., and Luo, G. (2016). “Mass-Transfer-Controlled Dynamic Interfacial Tension in Microfluidic Emulsification Processes.” *Langmuir*, 32(13), 3174–3185.
Wang, R. (2013). “Nanoparticles influence droplet formation in a T-shaped microfluidic.” *J Nanopart Res*, 15(12), 2128.
Wang, W., Yang, C., and Li, C. M. (2009b). “On-demand microfluidic droplet trapping and fusion for on-chip static droplet assays.” *Lab Chip*, 9(11), 1504–1506.
Weaver, J. C., Williams, G. B., and Bliss, J. G. (1991). “Process for chemical manipulation of non-aqueous surrounded microdroplets.”
Wehking, J. D., Gabany, M., Chew, L., and Kumar, R. (2014). “Effects of viscosity, interfacial tension, and flow geometry on droplet formation in a microfluidic T-junction.” *Microfluid Nanofluid*, 16(3), 441–453.
Xu, J. H., Li, S. W., Tan, J., and Luo, G. S. (2008). “Correlations of droplet formation in T-junction microfluidic devices: from squeezing to dripping.” *Microfluid Nanofluid*, 5(6), 711–717.
Xu, J. H., Li, S. W., Tan, J., Wang, Y. J., and Luo, G. S. (2006). “Preparation of highly monodisperse droplet in a T-junction microfluidic device.” *AIChE Journal*, 52(9), 3005–3010.

Yakhshi-Tafti, E., Kumar, R., and Cho, H. J. (2011). “Measurement of Surface Interfacial Tension as a Function of Temperature Using Pendant Drop Images.” *International Journal of Optomechatronics*, 5(4), 393–403.
Yan, Y., Guo, D., and Wen, S. Z. (2012). “Numerical simulation of junction point pressure during droplet formation in a microfluidic T-junction.” *Chemical Engineering Science*, 84, 591–601.
Yesiloz, G., Boybay, M. S., and Ren, C. L. (2015). “Label-free high-throughput detection and content sensing of individual droplets in microfluidic systems.” *Lab Chip*, 15(20), 4008–4019.
Zec, H., Rane, T. D., and Wang, T.-H. (2012). “Microfluidic platform for on-demand generation of spatially indexed combinatorial droplets.” *Lab Chip*, 12(17), 3055–3062.
Zhang, Y., and Liu, H. (2012). “Physics of Multiphase Microflows and Microdroplets.” *Microdroplet Technology: Principles and Emerging Applications in Biology and Chemistry*, Integrated Analytical Systems, P. Day, A. Manz, and Y. Zhang, eds., New York, NY: Springer, 1–21.
Zhang, Z., Xu, J., Hong, B., and Chen, X. (2014). “The effects of 3D channel geometry on CTC passing pressure – towards deformability-based cancer cell separation.” *Lab Chip*, 14(14), 2576–2584.
Zheng, B., Tice, J. D., and Ismagilov, R. F. (2004a). “Formation of Droplets of Alternating Composition in Microfluidic Channels and Applications to Indexing of Concentrations in Droplet-Based Assays.” *Anal. Chem.*, 76(17), 4977–4982.
Zheng, B., Tice, J. D., Roach, L. S., and Ismagilov, R. F. (2004b). “A Droplet-Based, Composite PDMS/Glass Capillary Microfluidic System for Evaluating Protein Crystallization Conditions by Microbatch and Vapor-Diffusion Methods with On-Chip X-Ray Diffraction.” *Angewandte Chemie International Edition*, 43(19), 2508–2511.
Zhu, P., and Wang, L. (2017). “Passive and active droplet generation with microfluidics: a review.” *Lab on a Chip*, 17(1), 34–75.

PUBLICATIONS

8.1. Papers published in international journals

- Sripadaraja, K., Umesh, G. & Satyanarayan, M.N. Simulation studies on picolitre volume droplets generation and trapping in T-junction microchannels. *SN Appl. Sci.* **2,** 1413 (2020). https://doi.org/10.1007/s42452-020-03198-9.

- Sripadaraja, K., Satyanarayan, M.N. & Umesh, G. Generation of microdroplets in T-junction devices by pulsed fluid flow: Simulation studies. *ISSS J Micro Smart Syst* **10,** 103–117 (2021). https://doi.org/10.1007/s41683-021-00073-6

- Raja, S., Satyanarayan, M.N., Umesh, G. *et al.* Numerical Investigations on Alternate Droplet Formation in Microfluidic Devices. *Microgravity Sci. Technol.* **33,** 71 (2021). https://doi.org/10.1007/s12217-021-09917-0.

8.2. Papers presented in National/International Conferences

1. Sripadaraja.K, Ichcha Manipur, Ashwin Lal, Umesh. G. (2017). "Optimising operating parameters of open droplet microfluidic devices" Poster presented in "Eighth ISSS International Conference on Smart Materials, Structures & Systems" July 05-07, Indian Institute of Science, Bangalore.

2. Sripadaraja K, Umesh G, Satyanarayan M. N. (2019) "Influence of surfactant on droplet generation and trapping efficiency of picolitre droplets in microchannels". Paper presented in "Tenth ISSS National Conference on Smart Materials, Structures & Systems" Oct 21-23, NMAM Institute of Technology, Nitte.